IOWA STATE UNIVERSITY
Digital Repository

Graduate Theses and Dissertations

Iowa State University Capstones, Theses and Dissertations

2015

Performance-based design of reinforced concrete bridge piers subjected to vehicle collisions

Steven Joseph AuYeung
Iowa State University

Follow this and additional works at: https://lib.dr.iastate.edu/etd

 Part of the Civil Engineering Commons

Recommended Citation
AuYeung, Steven Joseph, "Performance-based design of reinforced concrete bridge piers subjected to vehicle collisions" (2015). *Graduate Theses and Dissertations*. 14763.
https://lib.dr.iastate.edu/etd/14763

This Thesis is brought to you for free and open access by the Iowa State University Capstones, Theses and Dissertations at Iowa State University Digital Repository. It has been accepted for inclusion in Graduate Theses and Dissertations by an authorized administrator of Iowa State University Digital Repository. For more information, please contact digirep@iastate.edu.

www.manaraa.com

Performance-based design of reinforced concrete bridge piers subjected to vehicle collisions

by

Steven Joseph AuYeung

A thesis submitted to the graduate faculty

in partial fulfillment of the requirements for the degree of

MASTER OF SCIENCE

Major: Civil Engineering (Structural Engineering)

Program of Study Committee:
Alice Alipour, Major Professor
Behrouz Shafei
Ming- Chen Hsu

Iowa State University

Ames, Iowa

2015

Copyright © Steven Joseph AuYeung, 2015 All rights reserved.

www.manaraa.com

TABLE OF CONTENTS

www.manaraa.com

www.manaraa.com

LIST OF FIGURES

Chapter I.

www.manaraa.com

Chapter II.

www.manaraa.com

www.manaraa.com

www.manaraa.com

LIST OF TABLES

Chapter I.

Chapter II.

www.manaraa.com

ACKNOWLEDGMENTS

I would like to thank my advisor Alice for providing me with the opportunity to work and learn under her both as an undergraduate and graduate student. I have developed substantially academically and personally through this experience. Also, if it were not for her, I would have never been able to experience the great state of Iowa and all of the joys it has to offer; truly a once in a lifetime opportunity. I would also like to thank my committee members Behrouz Shafei and Ming-Chen Hsu for all their support and help; I am truly grateful. In addition, I would like to thank everyone at Ames Alliance Brazilian Jiu-Jitsu for allowing me to be a part of their community during my brief time here. Thanks to them, I was able to work through the frustrations and stress that accompanies graduate school.

www.manaraa.com

ABSTRACT

One of the leading causes of bridge failures within the United States is accidental vehicle collisions with the bridge pier. The focus of this research is to analyze the response of reinforced concrete bridge piers when subjected to a vehicle collision. A parametric study is performed to observe the different degrees of shear and flexure failure in a pier with respect to pier diameter, transverse reinforcement spacing and vehicle impact velocity.

The finite element software LS-DYNA was used to conduct the performed work. Material models, contact algorithms and modeling methods were first validated by recreating reinforced concrete beam impact experiments. In addition, an in depth analysis was performed investigating the internal forces generated within the impact beams with respect to differential steel reinforcement layouts. Once the models were calibrated and validated, the reinforced concrete bridge piers were constructed. The Ford F800 reduced vehicle model obtained from the National Crash Analysis Center and the National Transportation Research Center, Inc. was used in the study. The bridge pier collision models were then validated once more by comparing vehicle damage and impact forces with published experimental and numerical research results. In order to ensure stability within the impact simulations, the conservation of energy of the systems were closely monitored.

This study shows that the overall failure mode of the pier was dependent on the pier diameter and the transverse reinforcement ratio governed the extent of localized damage experienced within the pier. The impacting vehicles kinetic energy had the most profound effects on the magnitude of internal forces generated within the pier. A performance-based design approach is proposed which allows a designer to design a bridge pier in a simplistic manner with the use of damage ratios that relate to certain amounts of damage.

www.manaraa.com

CHAPTER I GENERAL INTRODUCTION

Vulnerability of Bridge Piers to Vehicle Collisions

Accidents involving vehicle collisions could severely affect the safety of the users as well as the overall functionality of the infrastructure. While vehicle collisions with bridge piers are a rare extreme loading event that can occur during a bridges life cycle, the amount of damage as a result of it can be catastrophic. Out of all the causes for a bridge failure such as flood, scour, deterioration, overloading and seismic loads, vehicle collisions were the second leading cause for failure (Agrawal and Chen, 2008). Another study conducted by Cook (2012) found a similar conclusion from investigating the bridge failure rates and trends from bridge collapse data collected over a period of 25 years for the state of New York. Out of the 92 bridge failures analyzed, 19.6% were caused by impact making it the second leading cause of bridge failures after hydraulic causes. Significant damage to the pier, bent cap, foundation system and superstructure has been observed in previous accidents. In some cases, a total collapse of the bridge may occur. A bridge failure would result in detrimental economic impacts, impose danger to the user's safety, with a possibility of loss of life. Direct economic impacts would consist of immediate repair costs or even costs associated with replacing the entire bridge. Indirect costs associated with the bridge repair are significant as well. If the failed bridge is an important component of a transportation network, the disruption of the traffic circulation due to the added detours would be major. The lost time associated with this would affect the commerce of businesses of all sizes. Due to the severe consequences of a bridge collapse, the satisfactory design of piers to withstand the expected loadings without failure is of great importance.

www.manaraa.com

Current design standards provided by the American Association of State Highway and Transportation Officials (AASHTO) *Load and Resistance Factor Design (LRFD) Bridge Design Specifications* (2012) requires that abutments and piers within 9.144 m of the roadway to be considered for the extreme event of a vehicle collision. Those bridge structures found susceptible to vehicle collisions must be designed to either redirect or absorb the impact force or provide structural resistance. The required equivalent static force (ESF) that the structure must be designed for is a 2,669 kN single point load applied to the pier at a height of 1.524 m above the ground and at an angle of incidence from 0 to 15 degrees with the edge of pavement in a horizontal plane. This recommendation however is based on experimental testing involving a single semi-tractor-trailer colliding into a rigid pier at 50 mph. This leaves a large room for uncertainty when designing a bridge pier with different design specifications that could possibly undergo different loading conditions such as varying vehicle mass and velocity. Past research has shown that AASHTO's design specifications underestimate the demand expected on the bridge pier from collision loadings (e.g. Agrawal et al., 2013 and Gomez and Alipour, 2014). This raises a concern of safety in regards to the current bridges in service today.

Research Objectives

The objective of this research is to create a new design process for bridge piers subjected to impact loadings. A performance-based design method that is typically used to design structures undergoing seismic loadings will be tailored to this vehicle to pier impact event. A similar impact event will be modeled to ensure the material models and finite element controls are working properly. Then a bridge pier will be modeled using the validated controls and material models. Both the bridge pier and vehicle model are then validated with analytical published results. A set of parametric studies and sensitivity analyses will be conducted to

www.manaraa.com

observe the effects of pier diameter, superstructure, hoop spacing, vehicle impact velocity and multi-pier bents with respect to the response of the pier itself.

Thesis Organization

Chapter II discusses the validation of the finite element material models and modeling techniques used to conduct the vehicle impact simulations. There is a void in the literature involving experimental data on vehicle collisions with bridge piers so a similar impact event was modeled in order to ensure that the material models and modeling techniques are accurate and reliable. Two experiments involving reinforced concrete beams being impacted by a drop hammer were replicated for validation. Results from the analysis were compared to experimental results with respect to mid-span displacement, impact forces and reaction forces.

Chapter III consists of validating the bridge pier collision models by comparing maximum impact forces with published research results and monitoring the energy balance of the simulations. Once the model was validated, two parametric studies were conducted. One was to determine whether modeling an idealized superstructure on top of the pier as opposed to a lumped mass would affect the response of the pier when subjected to vehicle collisions. The second parametric study involved a response comparison between a one pier bent system and a multi-pier bent system. Then a sensitivity analysis is performed to evaluate the significance of different pier design parameters such as diameter, hoop spacing, and vehicle impact velocity. A performance based analysis is conducted to classify the different damage states observed which are quantified through damage ratios. This proposed performance-based analysis could be used to replace the current design standards required by AASHTO for vehicle collisions on bridge piers.

www.manaraa.com

References

1. AASHTO, *AASHTO LRFD Bridge Design Specifications,* Sixth Edition, American Association of State Highway and Transportation Officials, Washington, D.C., 2012.

2. Agrawal, A. K., and Chen, C. (2008). "Bridge Vehicle Impact Assessment." Project #C-07-10, University Transportation Research Consortium, New York Department of Transportation.

3. Agrawal, A. K., Liu, G. Y., & Alampalli, S. (2013, March). Effects of truck impacts on bridge piers. In *Advanced Materials Research* (Vol. 639, pp. 13-25).

4. ASCE. (2013). "Report Card for America's Infrastructure." American Society of Civil Engineers. <http:// http://www.infrastructurereportcard.org/executive-summary> (June 6, 2015)

5. Cook, W. (2014). Bridge Failure Rates, Consequences, and Predictive Trends.

6. Gomez, N. L., & Alipour, A. (2014, April). Study of Circular Reinforced Concrete Bridge Piers Subjected to Vehicular Collisions. In *Structures Congress 2014*(pp. 577-587). ASCE.

www.manaraa.com

CHAPTER II IMPACT ANALYSIS ON REINFORCED CONCRETE BEAMS

A paper to be submitted to the *International Journal of Impact Engineering*

Steven AuYeung and Alice Alipour

Abstract

The design of the nation's infrastructure to extreme load cases is crucial to preserve human life and structures. Such load cases may involve impact loads whether it be accidental vehicular collisions, debris from extreme weather events or malicious attacks. With the rising terror levels and increasingly violent extreme weather events, the importance of impact resistant structures has increased. In response to this increased demand, a various amount of experimental and numerical studies have been performed to gain a better understanding of the behavior of reinforced concrete (RC) structures under impact loading. Past research has shown that RC structures are known to behave differently under impact loads in comparison to being loaded in static loading conditions. Structures have shown to experience a change in failure mode, crack patterns and an increase in apparent strength. Strain rate effects and inertial forces are responsible for this behavior. Experimental work has been performed studying the crack patterns, contact and reaction forces as well as mid-span displacement of RC beams under drop hammer testing. Many researchers have produced methods to accurately replicate the experimental results with the use of finite element analyses. The finite element analyses reported in the literature have primarily involved validating modeling methods and material models. The validation procedure involves matching reaction forces, maximum displacements, and crack patterns.

The present work presents a more in depth analysis of a RC beams subjected to impact loads with finite element testing. Two different beam impact experiments were modeled using the FE software. The beams were designed to account for the effects of longitudinal and

www.manaraa.com

transverse reinforcement ratios. The distribution of shear, moments, plastic strain and internal energy was analyzed with respect to different reinforcement layouts. Results reported that having different amounts of compressive and tensile longitudinal reinforcement greatly effects the energy distribution throughout the beam. The longitudinal reinforcement governs how well the beam can stabilize and respond against the impact loads. Different amounts of transverse reinforcement ratios have shown to greatly affect the distribution of plastic straining and damage throughout the beam. Larger amounts of transverse reinforcement allowed for a better distribution of shear cracks as well as decreasing the severity of them.

Introduction

With the civil infrastructure being the backbone of our society, it has a large impact on our personal and economic well-being. Our nation's infrastructure is the foundation for our workforce and provides safety for the public. It is crucial to create structures that are more resilient under extreme load cases. Such load cases may involve impact loads whether it is accidental vehicular collisions, debris from extreme weather events or malicious attacks. Reinforced concrete (RC) components have been typically used for protective applications against impact loads. However, there is a limited amount of information in regards to the analysis and behavior of RC elements undergoing impact due to the complex nature of the loading event. Additional information is needed in regards to this topic in order to employ more efficient, economical and safe designs of protective structures.

There has been published experimental and numerical work studying the behavior of RC beams impacted by steel drop hammers (e.g. Fujikake et al. 2009, Saatchi and Vecchio 2009, Ozbolt and Sharma 2011, Jian et al. 2012). Experimental work performed by Fujikake et al. (2009) and Saatchi and Vecchio (2009) consisted of analyzing a beams behavior under impact

www.manaraa.com

with varying levels of reinforcement detailing. The work by Fujikake et al. (2009) consisted of three RC beams having varying longitudinal reinforcement ratio subjected to impact from a drop hammer. The 400 kg hammer was dropped from heights ranging from 0.15 to 1.20 m. Flexural failure was observed throughout all three specimens however the amount of local damage varied. The study concluded that varying amounts of longitudinal reinforcement governs the amount of localized damage that can accumulate within a member. Testing has shown that localized damage in RC beams increases with higher amounts of tensile reinforcement due to the increase in stiffness. It was also found that the amount of localized failure can be reduced by providing more reinforcement in the compressive face of the beam.

In the study performed by Saatchi and Vecchio (2009), it was found that under the impact, shear mechanisms were the dominating factors in the primary behavior of beams. Even in beams that were statically flexure-critical, shear failure was still of a main concern under impact loading. Adequate transverse reinforcement in the shear critical sections of the beam prevented a portion of the beam from being punched out. The study consisted of four RC beams with identical longitudinal reinforcement and varying transverse ratios ranging from 0 – 0.3%. Two types of drop hammers were used: a 211 kg hammer for light impacts and a 600 kg hammer for heavy impacts. Both hammers were dropped from a height of 3.26 m. All specimens were subjected to multiple impacts in order to observe the impact response with respect to pre-existing damage. The (a) test series consisted of an impact test with the light hammer followed by two more subsequent impacts with the heavy hammer. The (b) test series consisted of two subsequent impact tests from the heavy hammer followed by an impact test with the light hammer.

Using numerical simulations to study the response of RC structures undergoing impact loads has been an increasing preferred method in the past decade as they are a more efficient way

www.manaraa.com

of testing the behavior of members with different characteristics. Various researchers have used commercial finite element software to replicate these experiments in order to create a validated numerical method for future design procedures. Ozbolt and Sharma (2011) studied concrete models that could accurately capture the rate and erosion effects of concrete under these loading situations. Jian et al. (2012) has performed studies in testing different concrete material models to predict peak impact forces, mid-span deflections and crack patterns of a numerically modeled beam subjected to impact loads. While it is crucial to develop validated models that can accurately capture a member's response under impact, it is equally important for in depth analyses to be performed as well.

More specifically, the work done so far fails to address the generated internal forces and distribution of stresses that dominate design parameters of the beam. The aim of this work is to study beam resisting mechanisms under impact loads by analyzing the internal shear, moments and energy distribution with the use of LS-DYNA. For this purpose, a series of parametric analyses studying the effects of different variables have been conducted. To ensure the validation of results from the parametric numerical analyses, the analytical models have been calibrated with the experimental test results of Fujikake et al. (2009) and then validated by the test results from Saatchi and Vecchio (2009). By developing a numerical model that can accurately predict an impact response and studying the internal actions with respect to steel reinforcement layouts followed by extensive set of parametric studies, improved design recommendations can be achieved from the work.

www.manaraa.com

Model Validation

The study performed by Fujikake et. al. (2009) consisted of a 400 kg drop hammer impacting on a reinforced concrete beam. The test setup is shown in Figure 1. The purpose of this experiment was to investigate the response of the beam to impact loads with respect to varying amounts of longitudinal reinforcement. The simply supported 1400 mm long RC beam had cross sectional dimensions of 150×250mm. The compressive strength of 42 MPa concrete with a maximum aggregate size of 10 mm was used throughout all three test specimens. All three specimens were reinforced with four longitudinal bars, two in compression and two in tension. Three different types of reinforcing bars which included D13, D16 and D22 deformed bars were used to represent the different longitudinal steel ratios. The D10 bars were used as transverse reinforcement spaced at 75 mm. The D10, D13, D16, and D22 reinforcing bars had yield strengths of 295, 397, 426, and 418 MPa, respectively. The experiment consisted of three beam specimens: S1616 series, S1322 series and S2222 series; the longitudinal bar arrangements are shown in Table 1. The beams were supported by two specially designed support devices which allowed free rotation of the beam but prevented the beam from displacing longitudinally and vertically. The hammer used throughout the experiment had a hemispherical head with a radius of 90mm and mass of 400kg (Figure 1). For the S1616 series, the hammer was dropped at heights of 0.15 m, 0.3 m, 0.6 m, and 1.2 m; for the S1322 and S222 series, the hammer was dropped from heights of 0.3 m, 0.6 m, 1.2 m, and 2.4 m. The peak contact force between the hammer and RC beam was measured through a load cell attached to the hammer and the mid-span displacement was recorded with a laser displacement sensor.

The finite element model beam impact test setup is presented in Figure 2 with a breakdown of the model showing the steel reinforcement cage, the concrete core, concrete cover,

www.manaraa.com

and drop hammer. The concrete section of the beam was generated using eight node, constant stress, and single-point integration solid hexahedron elements. Single-point integration, constant stress solid elements were selected because they are computationally efficient and combat the issues regarding overly stiff behavior that is normally associated with fully integrated elements. The steel reinforcement was created using two node, Hughes-Liu with cross section integration, 2×2 Gauss quadrature, tubular beam elements. These beam elements were chosen because they allow finite element strains to occur, are simple and computationally efficient, are compatible with solid elements, and include finite transverse shear strains (LSCT 2006). Since no deterioration or slip was mentioned in the experiments, a perfect bond between the steel reinforcement and concrete was assumed. Single point constraints were assigned to specific nodes to create simply supported boundary conditions for the beam.

Contact algorithm

While material modeling and boundary conditions can greatly affect the accuracy of numerical results, the contact algorithms would greatly affect the accuracy of the results as well. The accuracy of the forces and stresses generated within elements of a finite element model are highly dependent on the algorithms employed. Two sets of contact schemes can be defined: nodal-based and segment-based. The nodal-based contact algorithms detect the penetration of nodes into segments and penalty forces are then applied to the penetration and segment nodes. Segment-based contact algorithms however detect penetrations of one segment into another segment and penalty forces are applied to the nodes of each corresponding segment. A penalty method is used when calculating contact forces; this method is made up of springs placed normal to the penetrating nodes and contact surfaces. The resulting penetrations are detected and forces are applied to them based on the maximum of the two penalty stiffness values:

www.manaraa.com

$$k = \frac{\alpha K A^2}{V} \quad (1)$$

$$k = S_F \frac{m}{\Delta t^2} \quad (2)$$

where α is the penalty scale factor, $K$is the material bulk modulus, A is the segment area and V is the element volume. S_F is the force constrain scale factor, m is the nodal mass and Δt is the global time step.

The automatic surface to surface contact algorithm is the most recommended and validated type for impact simulations and was used in this study to model beam impacts (Tabiei, 2014). Within the automatic surface to surface contact algorithm settings, the SOFT formulation was implemented; this is recommended when two bodies with dissimilar materials and mesh densities come into contact with one another. A dynamic coefficient of friction of 0.3 validated by El-Tawil et al. (2005) was used during the analyses.

Hourglass controls

While the use of single point integrated elements is computationally efficient, hour glassing of elements is of concern. Hour glassing refers to zero-energy modes of deformation in solid, shell, and thick shell elements with a single integration point. It is called a zero-energy mode because no strain or strain energy is resulted from the element deformation. Figure 3 (b) shows a severe case of hour glassing that is detectable through visual inspection. Note that not all hour glassing can be identified though individual inspection; for example rotational hourglass modes are not visible in the deformed mesh. Hourglass energies must be inspected in the energy balance of the system and should be kept under 10% as a rule of thumb (Bala and Day, 2013).

To combat this issue, the use of hour glass controls are implemented which adds stresses to the local element level to resist the hour glassing deformations. Adding too much hour glass resisting stresses may over stiffen elements that are working well so the use of these controls

www.manaraa.com

must be fine-tuned. The hour glass coefficient, C_{HG}, is used to apply stiffening stresses to counteract the hour glass effect. Mesh refinement can also help eliminate this problem to an extent by allowing a more uniform force distribution between contacting segments. For this study, the Type 5 Flanagan-Belytschko with exact volume integration hourglass control and a C_{HG} of 0.021 was u sed. This method is known to be the most stable under collision simulations (Tabiei, 2014)

Material modeling

Concrete

RC structures are known to have a complex behavior when subjected to impact loads. The individual behavior of both the concrete and steel under these conditions differ from a static loading condition. Past research has shown that all materials are known to exhibit a certain degree of strength increase when under high rates of loading (e.g. Greene 1964, Cowell 1966, Atchley and Howard 1967, Schuler 2006, and Asprone 2009). Results have been compiled from several researchers as an example and are shown in Table 2. One observation made by Grote et al. (2001) that explained this strength enhancement had to do with the growth of micro cracks within the concrete. During static loading, micro-cracks form at the aggregate interface and propagate into larger cracks eventually leading to failure. Under dynamic loading, there is not enough time for these micro-cracks to form and propagate because the loading is so abrupt.

Another governing factor contributing to this dynamic strength increase is the "strain rate effect." When the strain rate of a material is extremely rapid due to a sudden impact, the specimen may behave in a more brittle manner. Due to this phenomenon, high strain rates have the ability to make a specimen that normally has ductile properties respond in a brittle manner under high impact forces, also known as the ductile to brittle transition (DBT) (Askeland, 2002).

www.manaraa.com

An example that illustrates this phenomenon elementarily would be a silly putty; when stretched at a slow rate it will deform by a large amount but when stretched abruptly the putty will break in a brittle manner. This is because when stretched slowly, the molecules have time to disentangle to cause large plastic deformations, but when pulled suddenly the molecules do not have time to respond as they normally would.

In order to accurately predict the impact response of a RC beam, the concrete material model used would have to include strain rate effects, post yield behavior, damage parameters and aggregate properties. Among the material models available in the LS-DYNA material library, material model 159 was used to accurately model the behavior of concrete for the RC beam analyses. Material model 159 is a continuous surface cap model and was chosen because it was developed, evaluated, and validated for use by the Federal Highway Administration to model the dynamic performance of concrete used in roadside safety structures subjected to vehicle collisions (Murray, 2007). The input system allows the user to choose unconfined compressive strength, aggregate size, density, rate effects, pre-existing damage, modulus of recovery, and erosion criteria. The material model defined the required strengths, stiffness, hardening, softening, and rate effect parameters as a function of concrete density, compressive strength, and maximum aggregate size. A visco-plastic formulation is used to model an increase in strength of the elements with an increasing strain rate.

Damage effects are governed by the accumulation of strain energy and when a certain threshold is exceeded, damage begins to initiate. The damage thresholds are based on formulations for brittle and ductile damage during plasticity. Brittle damage occurs in areas where there is tensile pressure and depends on the maximum principle strain. Ductile damage occurs in compressive pressure areas and is controlled by the total strain. Both the bulk and shear

www.manaraa.com

moduli are simultaneously and proportionally reduced as a function of the damage threshold. Damage is initiated when strain-based energy terms exceed a specified damage threshold resulting in the loss of strength and stiffness of the respective elements. The concrete that was used in the model had a mass density of 2,274 kg/m^3, an unconfined compressive strength of 42 MPa, and a maximum aggregate size of 10 mm.

Steel

Similar to concrete, the mechanical characteristics of steel under high rates of loading differs from those under static loading. Past researchers such as Keenan (1960), Cowell (1965), Mainstone (1975), Malvar et al. (1998) and Asprone (2010) have all concluded that the yield strength of steel is strain rate dependent. The general observations from experimental testing have shown a reduction in ductility and more rate sensitivity in lower grade steels. It has been shown that ultimate strength does not show much rate sensitivity when compared to the yield strength (Cowell, 1965). The strain rate effects on steel have to do with the microstructure of the material. Plastic deformations up to failure within a steel specimen are due to the microscopic slips within the individual iron crystals. A required yield stress is then needed to free the dislocations of these crystals resulting in micro slips that generate the plastic deformations. Mainstone (1975) found that under high loading rates, a higher stress is needed for these slips within the crystals to occur. An example of steel exhibiting apparent increase in strength can be seen in Figure 4 which shows the percent strength increase of three sizes of reinforcing bars underdoing varying strain rates obtained by Keenan and Feldman (1960).

The material models used for the steel reinforcement must capture the strain rate sensitivity for the materials yield strength. Cowell (1965) showed that the yield strength was the most sensitive material characteristic to strain rates so it is conservative to assume only the yield

www.manaraa.com

strength must be scaled. The steel reinforcing bars were modeled using an elasto-plastic material model that accounts for a stress-strain curve and strain rate dependency. The material properties that had to be input for each reinforcement bar include mass density, modulus of elasticity, Poisson's ratio, yield stress, stress-strain curve, and the strain rate scaling effect on the yield stress curve. In order to account for the dynamic increase factors (DIF) due to strain rate sensitivity of the steel reinforcement, the proposed equations developed by Malvar and Crawford (1998) have been used. The DIF is calculated based on the strain rate ($\dot{\varepsilon}$) and the α factor.

$$DIF = \left(\frac{\dot{\varepsilon}}{10^{-4}}\right)^{\alpha} \qquad \begin{cases} \alpha_{fy} = 0.074 - 0.040\dfrac{f_y}{414} \\ \alpha_{fu} = 0.019 - 0.009\dfrac{f_y}{414} \end{cases} \tag{3}$$

where f_y is the bar yield strength in Mpa, α_{fy} is the factor when scaling the yield stress, and α_{fu} is the factor used when scaling the ultimate stress. These equations are only valid for yield stresses between 290 and 710 Mpa, and for strain rates between 10^{-4} and 225 s^{-1}.The strain rate curves implemented in the steel material model are shown in Figure 5. Steel reinforcing bars were modeled with a mass density of 7850 kg/m^3, Poisson's ratio of 0.3, Young's modulus of 200 GPa and a tangent modulus of 1.5 GPa. The yield stress of the D10, D13, D16 and D22 bars were 295, 397, 426 and 418 MPa.

Numerical Results

Plastic strain profiles of the numerical model were compared to the crack patterns exhibited in the experiments, shown in Figure 6-8. The numerical model captured the flexural and shear cracking observed in the experiment. Some models did experience more flexural failure indicated by the erosion of elements in the tensile face of the beam which is associated with the erosion parameters used. The model also was calibrated by matching contact forces and maximum mid-span deflection obtained from experimental results. The S1616, S1322, and S222

www.manaraa.com

specimens' numerical and experimental time histories are presented in Figure **9**-11. The S1616 models did well in predicting the peak contact force caused by the initial impact of the drop hammer at low drop heights of 0.15 and 0.3 m. The post peak contact force behavior however was not captured as accurately as seen in Figure 9 (a) and (b). The experimental results show an oscillatory behavior while the numerical models display a flat behavior which is believed to be caused by the simplified boundary conditions used. Maximum mid-span displacement of the beam was accurately predicted by the models at these drop heights.

As the hammer drop height increased to 0.6 and 1.2 m, the models began to better capture the post peak oscillatory behavior of the contact force time histories which is better shown in Figure 9 (c) and (d). This is due to the fact that as beams undergo impacts with higher velocities, only a localized portion of it is able to respond due to the short duration of loading. This means that the importance of the boundary conditions diminish because they don't contribute to the response as much. When comparing the mid-span displacement time histories at these drop heights, the numerical simulations predicted slightly lower peak displacements. At a hammer drop height of 0.6m, the peak displacements occur at 18ms and when analyzing the contact force time history at this instance in time, the numerical results reports slightly higher contact forces. At a hammer drop height of 1.2m, maximum displacement occurs at 20ms and during this time, the numerical results also report slightly larger contact forces. This indicates that the numerical models have a marginally stiffer behavior than the experimental specimen.

Simulation results for test specimen S1322 report the same behavioral observation made from the S1616 impact simulations at hammer drop heights of 0.3 – 1.2m which can be seen in in Figure 10 (a-c). At a hammer drop height of 2.4m, the model appears to have trouble capturing the initial spike in force seen in the time history in Figure 10 (d). The simulation shows the

www.manaraa.com

hammer causing major localized damage resulting in element erosion which explains this behavioral discrepancy at this instance in time. The numerical models for the S2222 specimen proved to provide the most accurate results in terms of capturing peak contact forces, maximum mid-span displacement and post peak behavior as seen in Figure 11.

Monitoring the energy balance of the system was another method that was used to ensure that there were no issues with the model. The conservation of energy is an important indicator that assures the models' stability and that the kinetic energy of the hammer is transferred effectively to internal energy within the beam. In a stable reliable model, the energy balance should show a smooth transfer of the kinetic energy to internal energy all while having a constant total system energy. The hourglass energy of the system should also be kept within 10% of the total system energy to ensure the accuracy of results (Bala and Day, 2013).

Specimen S2222 at a hammer drop height of 2.4 m experienced the most damage out of all the simulations and is used as an example to analyze the energy balance. The progression of the different energy quantities with respect to time is shown in Figure 12. During the time 5 ms, the peak contact force occurred and this is when the maximum energy exchange between the hammer and the beam occurs. The system then shows to have the most hourglass energy between the time of 8 and 10ms. During this time frame, the beam experienced very high stresses resulting in local element deformations and distortions. This is believed to be the cause of the rise in hourglass energies. Before any additional hour glassing could develop, the respective elements have been deleted due to the erosion criteria of the concrete material model. The maximum recorded hourglass energy was calculated to be 6% of the systems total energy ensuring the accuracy and reliability of the simulation results were not adversely affected. At time 13 ms, there is a change in the rate of transfer between the kinetic and internal energies and

www.manaraa.com

continues throughout the rest of the simulation indicating some instability. This is believed to be caused from the erosion of elements as seen in Figure 8 (d).

From here on, the instance in time when the drop hammer makes contact with the beam will be considered the starting reference point in time. In order to study the response of RC beams with respect to varying longitudinal reinforcement ratios, first the contact force and mid-span displacement of all three specimens were compared in Figure 13 under a drop height of 1.2m. This drop height was chosen because the contact force and mid-span displacement time histories matched the best with the experimentally recorded data. In the displacement time history, the general response of all three specimens is described by a linear increase followed by a gradual peak and residual displacements. Specimen S1616 was shown to exhibit the largest peak and residual displacement out of all the beams.

The force-time history response exhibits characteristics of an impulse loading response. The recorded contact force initially spikes followed by a dampened wave response with decreased amplitudes. Although the peak impact forces are fairly similar, specimen S1616 was shown to have a longer duration of residual forces than the other two specimens. The large displacements and residual forces exhibited by specimen S1616 can be attributed to its relatively lower flexural rigidity. Fujikake et al. (2009) stated that the flexural rigidities affects the duration of impact load, maximum displacement, and time for the maximum displacement to occur. The flexural rigidities (*EI*) of the cracked sections for specimens S1616, S1322 and S222 are calculated to be 4×10^3, 6.1×10^3, and 6.8×10^3 kN.m^3. Specimen S1322 and S2222 time histories did not differ significantly and can be attributed to the small differences in their flexural rigidities.

www.manaraa.com

Internal shear and moment response

Figure 14-16 displays the internal shear forces and moments that were obtained from these tests to study the stress distribution along the length of the beam for different conditions. During the experimental work, specimen S1616 experienced impact loads from hammer drop heights of 0.15–1.2m. For the sake of the behavioral analyses between specimens, an additional impact test was run for specimen S1616 with a hammer drop height set at 2.4 m. The internal forces generated were recorded every 100 mm and obtained at intervals of 2 ms during the first 7 ms when the hammer has made contact with the beam. Data was only obtained during this time frame because this was when the peak contact forces were recorded for all tests. Time steps of 2 ms were chosen because the fluctuations and progression in shear and moments during the time frame could be clearly distinguished.

The general behavior of all three test specimens is that as time progresses, the shear and moment diagrams converge toward a static behavior of a simply supported beam with a point load acting at mid-span. Simulation results for specimen S1616 shown in Figure 14 (a) provide a very well presentation of this behavior at a hammer drop height set to 0.3 m. It was observed under these drop heights that no significant shear or moment is generated within the beam at time 1.0 ms. At time 3.0 ms, shear forces are mainly concentrated at the location of impact indicating that a localized portion of the beam is actively resisting the impact. This portion of the beam will be referred to as the "effective length". The effective length was established by Costovos (2009) from viewing the response of RC beams undergoing concentrated, high rate loading. It was concluded that under loadings with short durations, only localized regions of the beam where the load was applied could provide resistance. As time progresses, the effective length of the beam continue to develop until it is equal to the true length of the beam. This can be seen between the

www.manaraa.com

time steps of 5.0–7.0 ms where the maximum shear forces have occurred and the entire beam is actively resisting the impact load. This is indicated by the even distribution of shear forces along the length of the beam. When the entire beam has been engaged in the loading, maximum moments were then able to fully develop.

At a drop height of 0.6 m shown in Figure 14 (b), maximum shear forces occurring at location of impact were observed to occur at a time step of 3.0 ms. Following this, the shear forces slightly decrease and are distributed throughout the entire beam. The reason why the shear forces were highest at this time was due to the fact that flexural failure had occurred in the beam preventing any additional shear forces to occur at later time steps. This observation is in parallel with the fact that maximum moments are generated at this instance in time. At a hammer drop height of 1.2 m, the development of shear forces is very unstable. At time of 1.0 ms, peak shear occurs at mid-span but at the next time step, shear at this location reduces by a noticeable amount; maximum shear now occurs near the supports of the beam. The shear then jumps to an overall maximum at the beams mid-span at time 5.0 ms then exhibits a rapid decrease at 7.0 ms. Simulation and experimental visual results show flexural failure at this hammer drop height which can explain for the erratic behavior in the shear diagram.

Shear diagrams of specimen S1322 resembled similar behavior to those from S1616. At low hammer drop heights, maximum shear forces developed during the time frame of 5.0–7.0 ms. Under hammer drop heights of 1.2 and 2.4 m, shear forces were a maximum at 3.0 ms and then slightly decreased at the later time steps due to the initiation of failure within the beam. However, failure occurring within this specimen was observed to be caused by localized failure. Another observation made was that specimen S1322 did a better job than S1616 at evenly distributing the shear forces along the length of the beam. Higher stiffness due to the larger

www.manaraa.com

amounts of tensile reinforcement was believed to be responsible for this behavior in specimen S1322. This increase in stiffness is also responsible for the points of inflection in the moment's diagram. Using Figure 15 (c) as an example, at time 1.0 ms, the shear diagram indicated that a localized portion of the beam is actively resisting the impact. This effective length of the beam is observed to undergo positive bending moments. Due to the high stiffness, the effective length of the beam behaves as if it has fixed boundary conditions at both ends. As a result, negative moments are generated in areas of the beam that are located outside of the effective length. At the following time step of 5.0 ms, there still seems to be a point of inflection located near the left support even though the entire beam has been engaged to the loading. The restricted translational degrees of freedom at the left support in combination to high stiffness of the beam are believed to be responsible for this behavior.

An anomaly was also observed in the moment diagram for the test involving the 2.4 m hammer drop height. This test showed a lower maximum moment than the preceding simulations involving lower hammer drop heights. As shown in Figure 15 (d), time of maximum moment occurs at 3.0 ms and slightly decreases at later time steps. When analyzing the shear diagram, there also seems to be a relatively large decrease in shear between time steps of 3.0 and 7.0 ms. This specimen was shown to undergo local failure which explains this drop in shear and relatively low bending moments generated within the beam.

By comparing the internal shear forces, it can be observed that the compressive reinforcement ratio affects the amount of local failure as shown in specimens S1322 and S2222. It can be seen that the shear within specimens S2222 appears to be more stable between time steps than that of specimen S1322. This can be clearly seen at a hammer drop height of 2.4 m shown in Figure 15 (d) and Figure 16 (d). For specimen S2222, the shear forces in the beam stay

www.manaraa.com

relatively constant after 1.0 ms. However for specimen S1322, shear forces are shown to fluctuate between each of the time steps. This increase in compressive reinforcement prevented local failure allowing for the beam to stabilize after impact.

Reinforcement energy distribution

An additional analysis was performed to determine the effects of ratio of compressive and tensile reinforcement on the performance of RC beams under impact loads. The energy absorbed by the tensile and compressive reinforcement was measured in order to determine the extent of energy that was absorbed by the reinforcement under varying drop heights. The internal energy can be defined as the elastic strain energy and the work done in permanent deformation in LS-DYNA. Time history data for the compressive reinforcements internal energy normalized by the systems total energy is presented in the left side of Figure 17 (a-d). Impact simulations involving hammer drop heights of 0.3 and 0.6 m report very low energy in the compressive reinforcement. At a drop height of 1.2 m, Figure 17 (c) shows very little internal energy for specimens S1616 and S2222 while the ratio of absorbed energy for specimen S1322 has increased to 11.9%. This abrupt spike in the internal energy time history indicates a sudden engagement of the compressive reinforcement due to the localized damage in the compressive face of the beam. For a hammer drop height of 2.4 m, no significant differences are observed in the energy distribution.

The normalized internal energy time histories of the tensile reinforcement are presented in the right column of Figure 17 (a-d). At hammer drop heights of 0.3 and 0.6 m, the general behavior for all three test specimens show a linear increase in energy followed by a post peak decline and plateau. Within the first 7 ms in the linear portion of the time histories, the specimens have experienced the full impact of the hammer. The hammer proceeds to rebound off

www.manaraa.com

the beam allowing for the beam to return to its original position which can be seen through the post peak decline in energy. Large amounts of plastic straining and damage have occurred due to the impact which causes the post peak plateau behavior. S1616's tensile reinforcement shows the most energy absorbed by the compressive reinforcement while specimens S1322 and S2222 show identical amounts of energy absorbed.

At a hammer drop height of 1.2 m, tensile reinforcement of S1616 continues to show the largest amounts of absorbed energy. Due to the smaller reinforcement ratio, this member's relatively low flexural rigidity and increased ductility causes large deflections which is responsible for such high ratios of energy. Specimen S2222 energy time history shows the same behavior as the 0.6 m time history. The internal energy in the compressive reinforcement is shown to increase by a relatively noticeable amount while the energy within the tensile reinforcement decreases for specimen S1322. Due to the low stiffness in the compressive region of the beam, the impact forces cannot be properly absorbed. When the compressive region is unable to transfer the forces of the impact within the initial stage of impact, more energy will be dissipated through localized damage and straining in the compressive reinforcement which explains the change in energy distribution. This behavior is more severe at hammer drop heights of 2.4 m. All specimens show a loss in internal energy due to increased amount of localized damage but specimen S1322 shows the largest loss. The maximum internal energy generated has dropped below 20% and this is a clear indication that the entire beam is not being engaged in the impact load.

Longitudinal reinforcement concluding remarks

During impact loading events, the kinetic energy of the projectile is dissipated through straining, fracture, plastic deformation and friction of the target member. If the member being

www.manaraa.com

impacted is very stiff, it will not experience much deformation when loaded. As a result, the kinetic energy from the projectile will be dissipated through localized straining, fracture and friction. This means that increasing the tensile reinforcement results in more localized damage due to the increase in the stiffness which is in agreement with the Fujikake et al. (2009) studies. This is clearer when comparing the impact response of beam S1616 and S1322, as the larger amounts of tensile reinforcement in S1322 results in localized damage. It was also found that increasing the compressive longitudinal reinforcement, increased the beams resistance to localized failure. This was seen when comparing the impact response between specimen S1322 and S2222 where both beams had identical amounts of tensile reinforcement but beam S2222 had more compressive reinforcement.

The analytical results conclude that local failure in S1322 was due to the lack of local stiffness in the compressive region of the beam. During the initial impact, only the compressive face of the beam is able to respond to the load. This localized area of the beam was not strong enough to redistribute the forces throughout the rest of the beam and the energy from impact was dissipated through spalling of the concrete and straining of the compressive reinforcement. It is crucial for design that an adequate amount of compressive reinforcement be provided in order to allow for the distribution of impact forces.

Effect of Transverse Reinforcement

While Fujikake et al. (2009) has concluded that the longitudinal reinforcement governed a beams resistant to localized failure, past experimental work has concluded that a RC member's behavior to impact loads is largely influenced by shear mechanisms. Chen et al. (2002) and Kishi et al. (2002) have both reported significant shear cracks forming in specimens that were statically flexural-critical. This emphasizes a great importance on the detailing of the transverse

www.manaraa.com

reinforcement. Saatchi et al. (2009) performed experimental work that consisted of RC beams with varying amounts of transverse reinforcement subjected to impact loads from a drop hammer. In order to better design RC members for impact, an impact analysis must be performed in regards to internal shear propagation of RC specimens with varying levels of transverse reinforcement detailing. Using the same material models and modeling techniques implemented in the previous section, the experiment performed by Saatchi et al. (2009) will be used to study the effects of transverse reinforcement on the performance of RC members subjected to impact loads. Crack profiles, reaction force time histories and mid-span displacement time histories recorded from the experiment will be used as the basis for validation. An analysis will then be performed regarding the relationship between amounts of transverse reinforcement, damage modes, and propagation of internal forces. The model used to conduct the Fujikake et al. (2009) analysis will then be tested with respect to varying amounts of transverse reinforcement to determine if consistent conclusions are made with this simulation.

Test setup

Saatchi and Vecchio (2009) test setup and numerical model are shown in Figure 18 and 19. The 4880 mm long RC specimens had cross sectional dimensions of 250 mm × 410 mm. The experiment consisted of a 212 kg steel hammer dropped from a height of 3.26 m onto the beam. The beam was simply supported with supports located at 940 mm from the ends of the beam.

Table 3 reports the differential spacing of transverse reinforcement for each test series. Test series SS1a, SS2a and SS3a were replicated. The concrete had a maximum aggregate size of 10 mm and the unconfined compression strength ranged from 44.7- 47 MPa. All specimens were longitudinally doubly reinforced with No. 30 deformed bars and transversely reinforced with closed stirrups. The longitudinal and transverse reinforcement had reported yield strengths of

www.manaraa.com

464 MPa and 605 MPa. The 212 kg drop hammer was placed 1mm away from the face of the beam with an assigned initial velocity corresponding to the drop height of 3.26 m.

Analytical results

In order to ensure the model was reporting correct results, the peak reaction force and mid-span displacement as well as the crack profiles were compared to those reported from the experiment (Figure 20-21). As it can be seen, the mid-span displacements correlated very well with the experimental data. The reaction forces obtained from the FE model was acquired from a single support with the restrained translational DOF in the X, Y and Z direction. The peak force from the numerical results was precise when compared to the experimental results with the percent error of all three tests ranging from 0.74 – 6.78%. The numerical model, however, could not capture the fluctuations in the later stages of the time history. These fluctuations recorded in the experiment were most likely due to the oscillations of the specimen during the free vibration period. With simplified boundary conditions applied in the numerical model, this would affect the post impact vibrations occurring throughout the specimen which would explain the differences in the post peak response. Another behavior the finite model was unable to capture was the initial pre-stressing force of the restraints shown within the first 5 ms of the time history data. The error shown in the mid-span displacement results can be due to deformations caused by large shear forces. The numerical model could not capture the large shear deformations occurring in the actual experiment which helped account for the mid-span deflection. While the largest deviation of the numerical results from the experimental results was 10%, the displacements varied by a mere 2 mm indicating a good agreement with the experimental results.

When comparing the plastic strain contours of the numerical model with the experimental crack profiles (Figure 20), the distribution of the 45 degree shear cracks were able to be

www.manaraa.com

accurately predicted. However, the element erosion depicted in the numerical analysis portrays the opposite visual results seen from the experiments. Crack profiles obtained from the experiment show localized failure and large shear cracks. The model was not able to capture this failure mode and instead exhibits flexural failure to some degree indicated by the eroded elements at the bottom face. This discrepancy in behavior is believed to be caused by the hourglass controls slightly overstiffening the elements at the flexural face of the beam. Time history results for the reaction force and mid-span displacements were not shown to be significantly affected by the models over stiff behavior so the model was considered reliable.

Shear and moment analysis

Internal shear forces and moments were obtained for each test specimen to understand the difference in behavior with respect to the varying degrees of transverse reinforcement. Section cuts were made every 160-200 mm. Data was obtained from the time frame of 2.3 - 2.9 ms at intervals of 2 ms because the maximum shear and moments were sufficiently captured within this time frame (Figure 22). Note that the reaction force time histories report maximum forces at 5 ms however due to the nature of this impulsive load, the supports will experience the initial peak force later than the portion of the beam that has been impacted by the hammer. Internal forces were obtained at time intervals of 0.2 ms because the fluctuations in the change in behavior could be clearly distinguished.

Figure 22 shows the shear and moment diagrams for specimens (a) SS1, (b) SS2, and (c) SS3. When analyzing the shear diagram for specimen SS1, it can be seen that as the effective length of the beam grows larger, the magnitude of the shear decreases because it is able to be distributed along the length of the beam. At time 2.3 ms, the effective length is relatively small to the true length of the beam resulting in very high concentrated shear forces. As time progresses

www.manaraa.com

forward, the effective length grows slightly larger and the severity of the shear in the beam decreases. When observing the moment diagram, it appears that as the effective length grows, the negative moments induced at mid-span and the positive moments located near the ends of the effective length both slightly increase from time 2.3 – 2.5 ms. At the following time steps of 2.7 and 2.9 ms, the negative and positive moments are shown to continually decrease in conjunction to the increasing effective length.

Specimen SS2's shear diagram shows a larger effective length at time 2.3 ms when compared to SS1. As a result of a larger effective length, the intensity of the shear was lower and bending moments were significantly larger. The shear behavior between the two specimens begin to converge however at later time steps of 2.7 and 2.9 ms. It appears that by increasing the transverse reinforcement ratio of a member, only the shear behavior during initial contact is affected. Saatchi and Veccio (2009) reported that with lightly transverse reinforced specimens, the drop weight would punch out a segment of the beam creating large shear deformations at mid-span; this explains why specimens SS1 experienced the largest peak shear forces and lowest bending moments. The increased amount of transverse reinforcement in SS2 allowed the beam to resist the initial punching shear during initial impact by being able to redistribute these force along the length of the beam better and as a result, bending moments were able to fully develop.

There appears to be a point of diminishing returns when increasing the amount of transverse reinforcement ratio beyond 0.2%. This can be clearly seen when comparing the shear and moment diagrams as well as the strain profiles for specimen SS2 and SS3 provided in Figure 23. Strain profiles were taken for all three specimens at the time of maximum shear. Major forty five degree shear cracks had started to initialize from the point of impact and propagate down to the bottom face of the beams. The edges of the beams effective length were shown to be the

www.manaraa.com

areas with the highest amount of shear making this area the most vulnerable for failure. The amount of transverse reinforcement within this high shear region for specimen SS2 was adequate to resist the diagonal tension. The severity and distribution of straining within the beam didn't significantly change when increasing the transverse reinforcement ratio, as seen in specimen SS3. This plastic strain behavior matches well with Costovos's (2009) observation that the cracking occurring in the beams is limited within the effective length.

Another key observation to be made is that the effective length of all three specimens is approximately the same. This can be linked to the fact that the effective length of the beam is dependent on the inertial properties of the specimen such as mass, geometry and support conditions. While the inertial properties govern the portion of the specimen that responds to the impact force, the steel reinforcement governs how the impact forces are distributed throughout the beam. In such cases, although the shear forces tend to govern the failure during testing, bending moments can pose a threat as secondary effect as well. For instance, Figure 23 shows large pockets of plastic strain occurring above supports due to these secondary effects. This underlines the importance to properly reinforce the RC member for possible large negative bending moments occurring in the initial stages of impact loading.

Figure 24 and 25 show a visual representation of specimens SS1's effective length and mode of failure during each time step. Below the shear and moment diagrams are Von-Mises stress contours of the beam with a displaced shape magnified to a higher level for visualization purposes. The displacements were magnified to clearly display the effective length of the beam. At time step of 0.5 ms (Figure 24 (a)), the peak shear forces at the ends of the beams effective length as well as the distribution of Von-Mises stresses suggest a punching shear type of actions occurring. During the next time step of 0.7 ms shown in Figure 24 (b), the shear forces decrease

www.manaraa.com

and begin to distribute outwards and allows for bending actions to occur. The dominating actions occurring within the specimen transition from punching shear to shear. At time of 1.0 ms, the support systems are engaged in resisting the impact and shear forces have decreased by 50%. The Von-Mises stress contours show that stress concentrations have dissipated. A shear-bending type of action begins to dominate once the support system gains the ability to resist the loading. It is recommended that the mid-span of the beam be heavily reinforced against shear to resist the punching shear forces in the initial stages of loading. Additional longitudinal reinforcement should be added at locations near supports to resist against negative bending moments during the later stages of loading.

Parametric study

The numerical analysis by Saatchi and Vecchio (2009) revealed that increased amounts of transverse reinforcement prevented a localized portion of the beam from being punched out during the initial stages of impact due to the very high and concentrated shear forces. The transverse reinforcement located within the areas of high shear concentrations were able to redistribute the forces throughout the rest of the beam resulting in less severe shear cracking. Fujikake's S2222 numerical model went through additional testing in regards to the specimen's impact response with varying amounts of transverse reinforcement to check whether consistent conclusions could be made. Specimen S2222 with transverse reinforcement spacing's of 75, 150, and 300 mm underwent impacts from a drop hammer initially placed 2.4 m above the top face of the beam.

When viewing the final damage states of all the beams in Figure 26, the amount of the localized shear failure observed within a beam increases as the amount of transverse reinforcement decreases. As seen in Figure 26 (a), there is a large concentration of strain

www.manaraa.com

propagating from the point of impact downward at a forty five degree angle representing the cracking due to shear for the specimen with a reinforcement spacing of 75 mm. There is also some local and flexural failure observed indicated by the eroded elements at the top and bottom face of the beam. At a reinforcement spacing of 150 mm, the beam shown in Figure 26 (b) exhibits more localized failure and more severe straining throughout the entire beam. There is also a larger degree of flexural failure indicated by the large number of eroded elements at the bottom face of the beam. The beam with a reinforcement spacing of 300 mm, shown in Figure 26 (c), exhibited similar amounts of flexural failure as the previous beam. However, this beam exhibited a remarkably larger degree of localized failure due to shear at mid-span. The drop hammer has essentially punched out a localized segment of the beam which correlates well with conclusions made in Saatchi and Vecchio's (2009) numerical study.

Transverse reinforcement concluding remarks

It can be concluded that the transverse reinforcement plays a significant role in the beam's ability to resist the initial highly concentrated punching shear actions induced by the drop hammer. The impact force from the hammer is transferred through the beam by shear mechanisms so it is crucial that there is an adequate amount of transverse reinforcement to withstand and redistribute the forces throughout the rest of the beam. When adequate shear reinforcement is provided, the bending moments fully develop within the beam. Additionally, negative bending moments located near the beam's supports are considered a possible major concern so it is crucial to properly reinforce these sections as well.

Beam Impact Study Conclusions

The finite element software LS-DYNA along with the material models, contact algorithms and modeling methods chosen were shown to successfully replicate multiple RC

www.manaraa.com

beam impact events. The models were able to accurately capture the peak contact forces, maximum mid-span displacements and crack propagation which are the main design parameters for structural members undergoing impact. It was found that increasing a member's tensile longitudinal reinforcement resulted in an increased amount of localized failure because it stiffened up the beam. During impact loading events, the kinetic energy of the projectile is dissipated through straining, fracture, plastic deformation and friction of the target member. If the member being impacted is very stiff, it will not experience much deformations when loaded. As a result, the kinetic energy from the projectile will be dissipated through localized straining, fracture and friction. If the member is not adequately reinforced in the compressive region of the beam, the kinetic energy from the projectile will cause large amounts of localized failure. It was also concluded that large shear forces develop in localized portions of the beam during the initial stages of impact. If the beam is not adequately reinforced in the transverse direction, there is a high chance that the drop hammer will punch out a segment of the beam under a punching shear failure. It is recommended that great care should be applied toward the detailing of the transverse reinforcement in beams resisting impact loads in addition to negative bending moments at locations near the supports in the later stages of loading that requires adequate longitudinal reinforcement in the compressive face.

www.manaraa.com

Table 1. *Steel reinforcement specifications for Fujikake et al. (2010) drop hammer tests*

	Compression Side		Tension Side	
Test Series	Number and Size (mm)	Area (mm^2)	Number and Size (mm)	Area (mm^2)
S1616	(2) D16	397	(2) D16	397
S1322	(2) D13	167	(2) D22	774
S2222	(2) D22	774	(2) D22	774

Table 2. *Experimental results for concrete strength under varying strain rates*

Author	**Green (1964)**		**Cowell (1966)**	
# of Test Specimens **Specimen Geometry** **Test Type**	24 Cube Ballistic Pendulum		102 Cylinder Pneumatic Hydraulict Test	
Concrete Type	3.9 ksi 7.4 ksi	28 Day Cure	5 ksi	Wet Specimen
	4.8 ksi 8.7 ksi	49 Day Cure	5 ksi	Dry Specimen
Strain Rate	0.3 s^{-1}		0.3 s^{-1}	
Results	**Test Specimen**	**% Strength Increase**	**Test Specimen**	**% Strength Increase**
	3.9 ksi	37%	Wet Specimen	35%
	7.4 ksi	34%		
	4.8 ksi	28%	Dry Specimen	24%
	8.7 ksi	20%		

Table 3*. Saatci and Vecchio (2009) transverse reinforcement ratios for different test series*

Specimen	Transverse Reinforcement Ratio (%)	Stirrup Spacing (mm)
SS1	0.1	300
SS2	0.2	150
SS3	0.3	100

www.manaraa.com

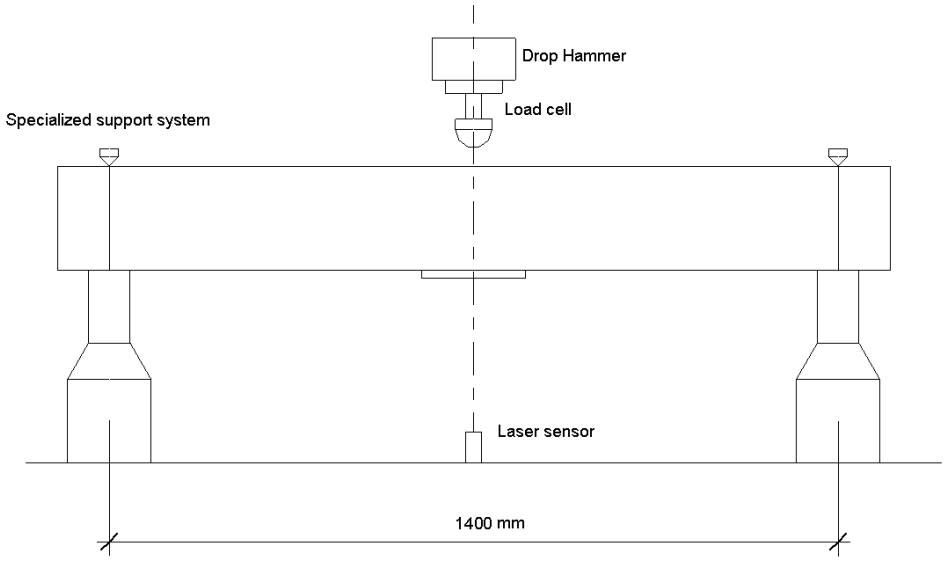

Figure 1. *Drop hammer test setup (Fujikake et al. 2009)*

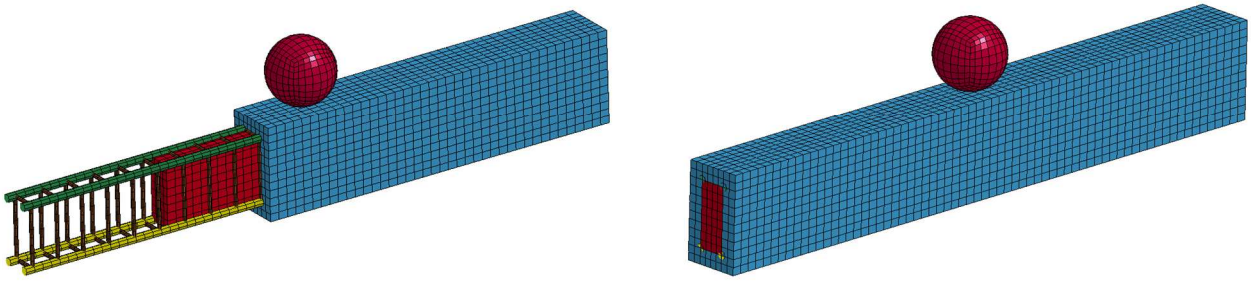

Figure 2. *Finite element models of the case study beams*

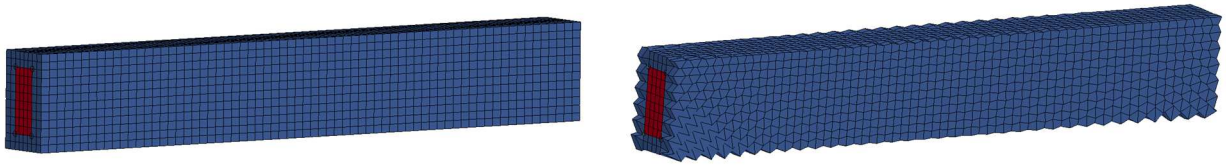

(a) (b)

Figure 3. *Specimen (a) without hour glassing (b) and with hour glassing*

www.manaraa.com

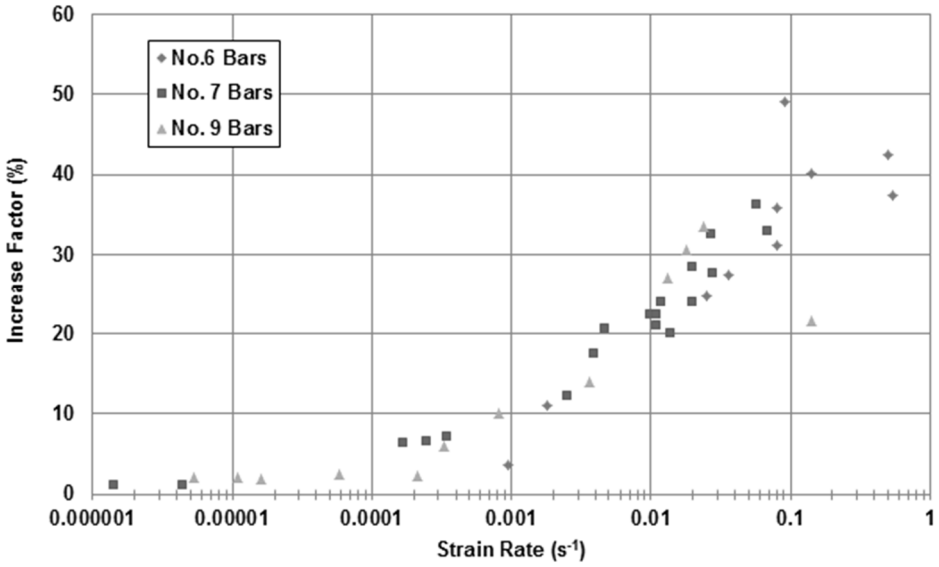

Figure 4. *Steel dynamic strength increase (Kennan et al. 1960)*

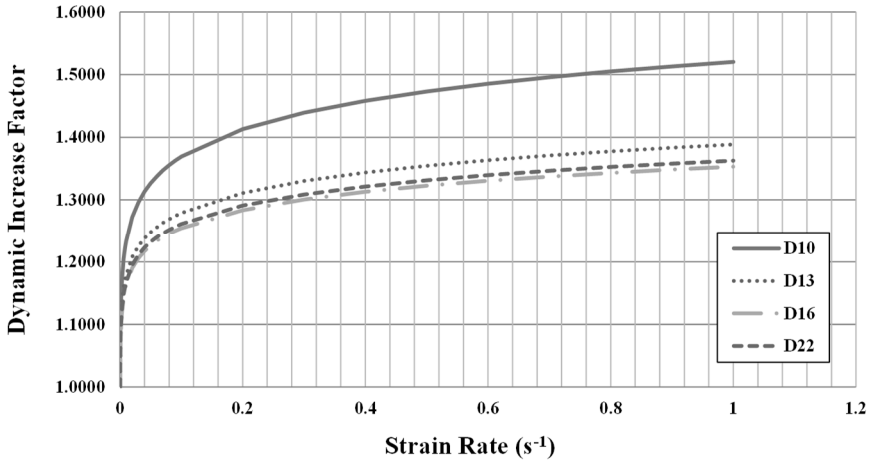

Figure 5. *Steel dynamic increase factor (DIF) for the case study beams*

www.manaraa.com

(a)

(b)

(c)

(d)

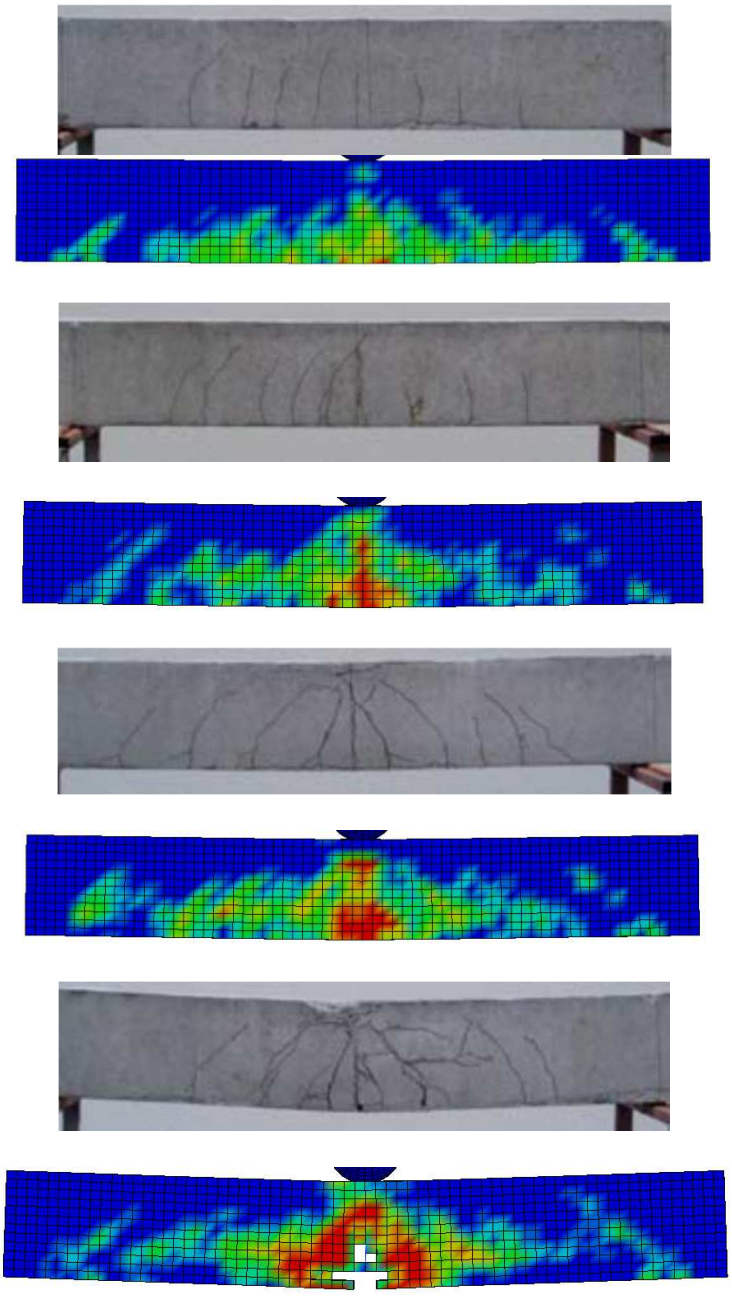

Figure 6. *Comparison of the S1616 cracking pattern in the experiments and the finite element model at drop heights (a) 0.15, (b) 0.30, (c) 0.6 m and (d) 1.2m*

www.manaraa.com

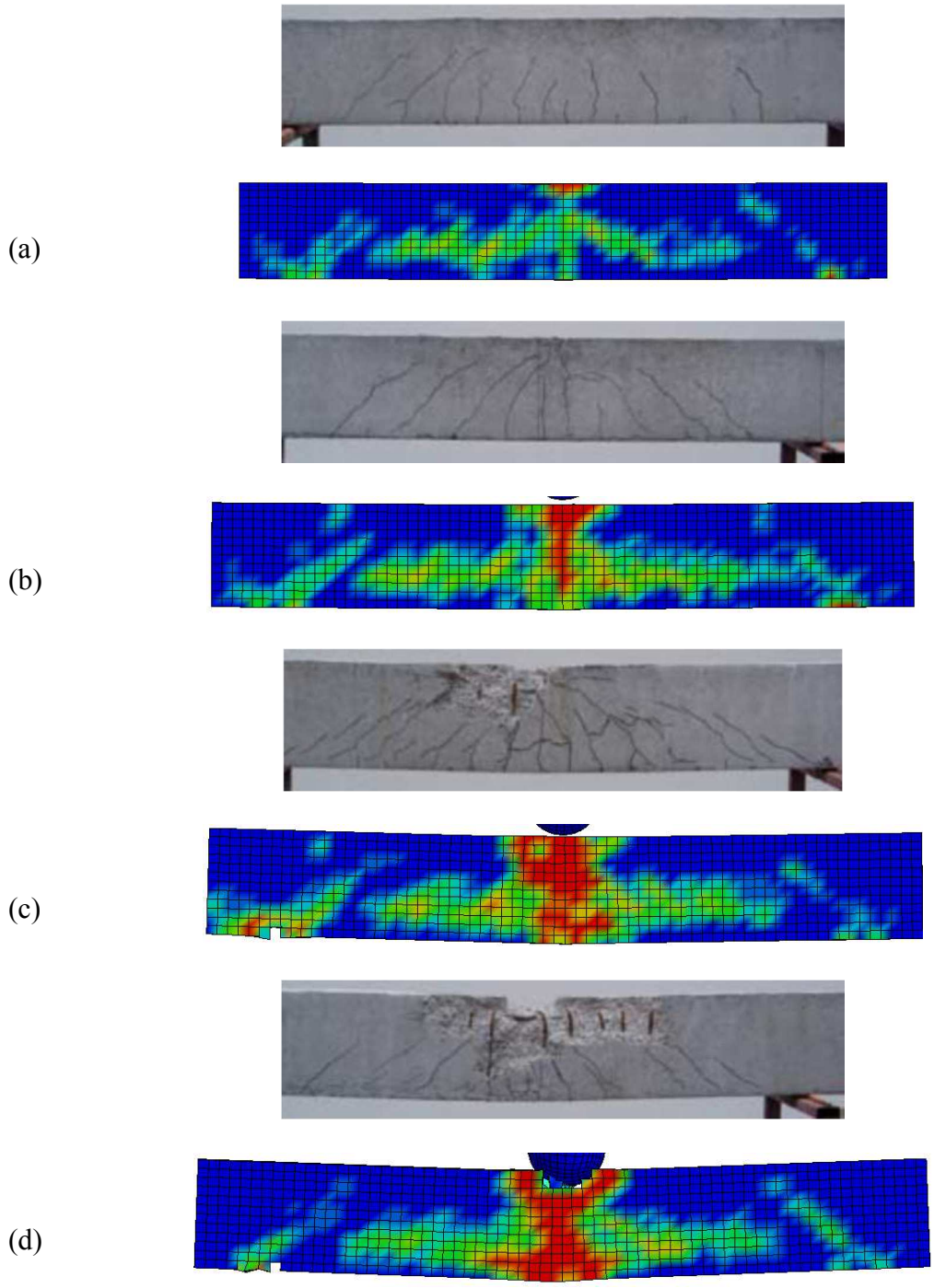

Figure 7. *Comparison of the S1322 cracking pattern in the experiments and the finite element model at drop heights (a) 0.15, (b) 0.30, (c) 0.6 m and (d) 1.2m*

www.manaraa.com

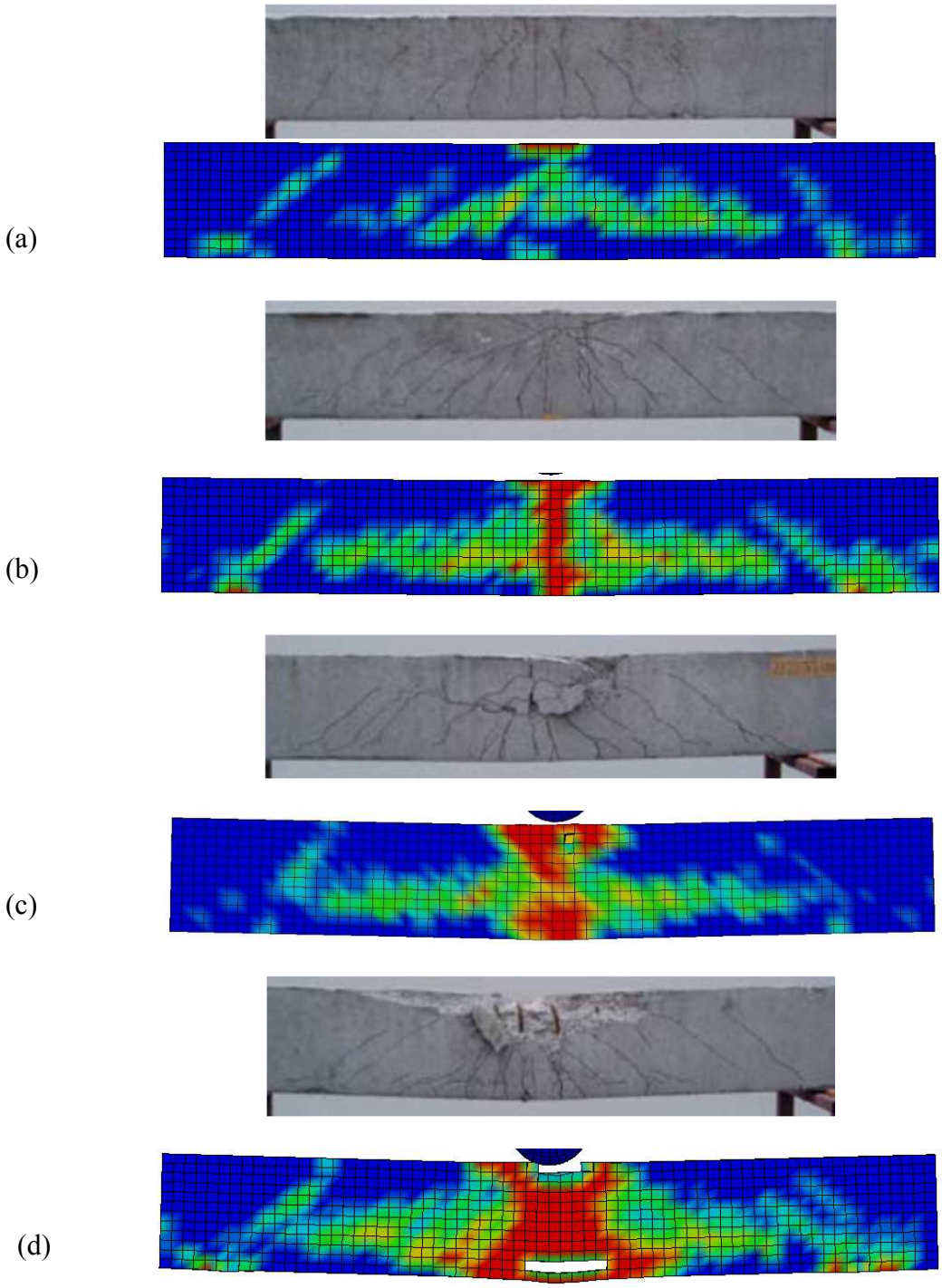

Figure 8. *Comparison of the S2222 cracking pattern in the experiments and the finite element model at drop heights (a) 0.15, (b) 0.30, (c) 0.6 m and (d) 1.2m*

www.manaraa.com

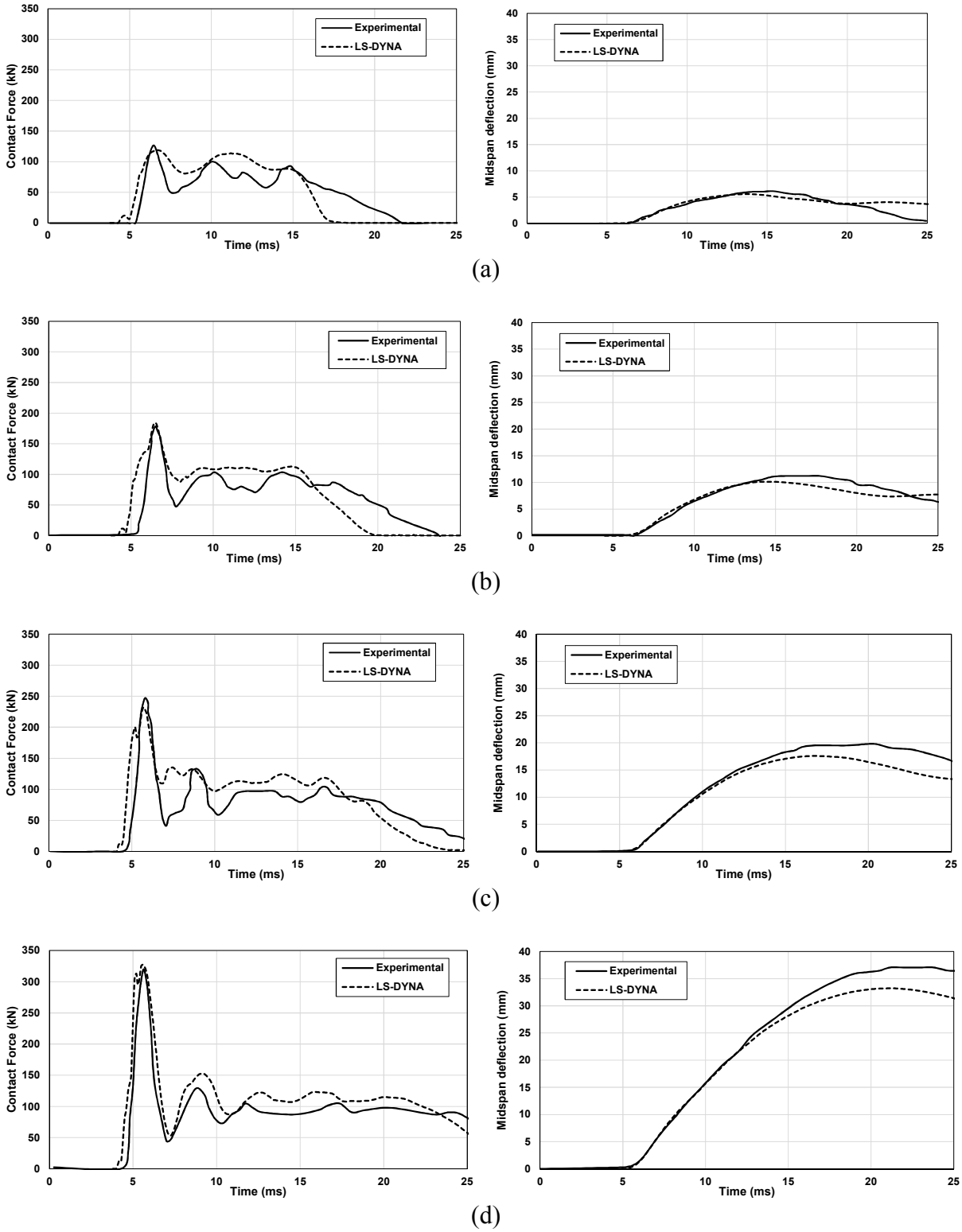

Figure 9. *Impact force and mid-span deflection for beam S1616 for drop heights of (a) 0.15, (b) 0.3, (c) 0.6, and (d) 1.2 m*

www.manaraa.com

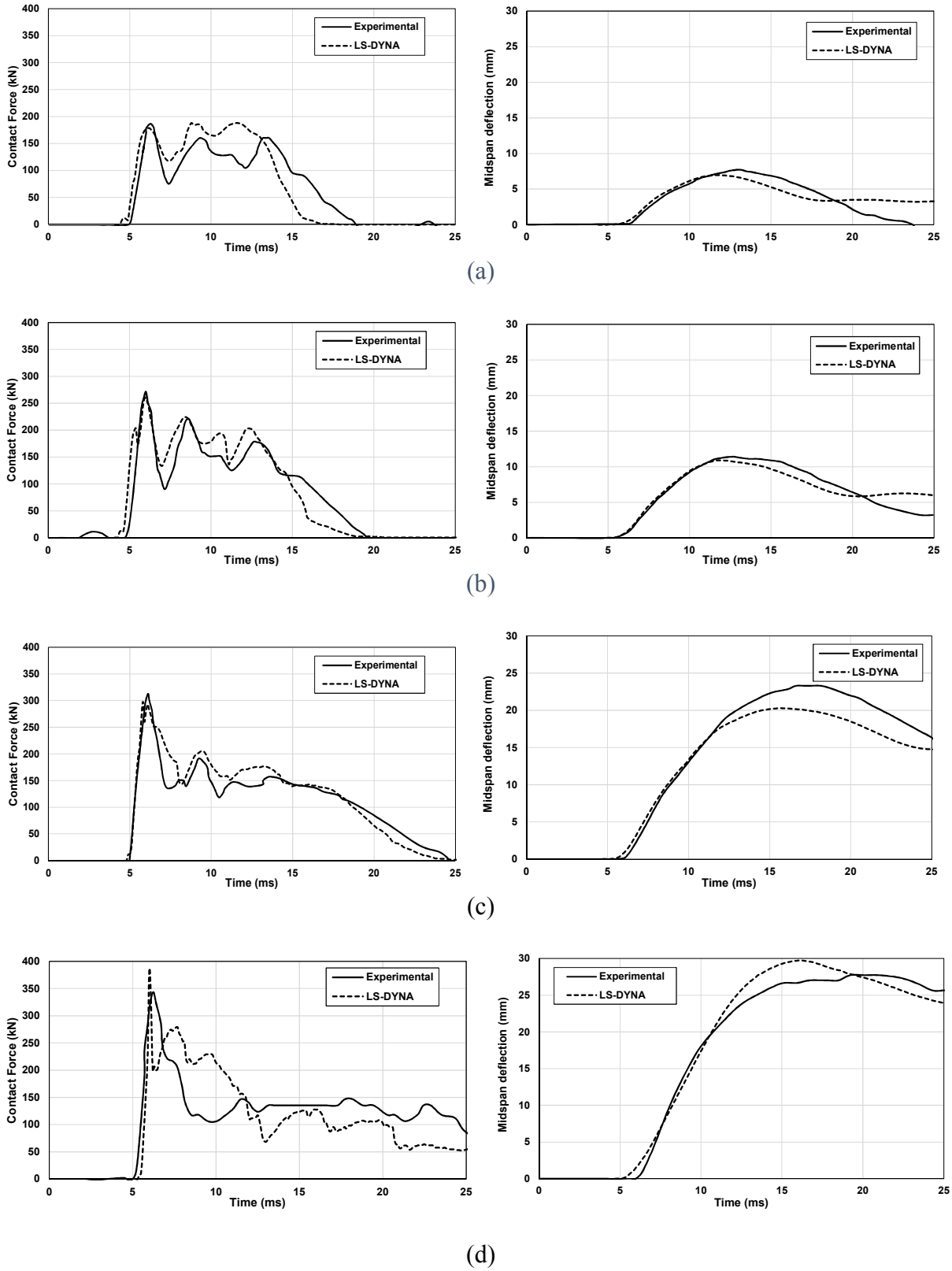

Figure 10. *Impact force and mid-span deflection for beam S1322 for drop heights of (a) 0.3, (b) 0.6, (c) 1.2, and (d) 2.4 m*

www.manaraa.com

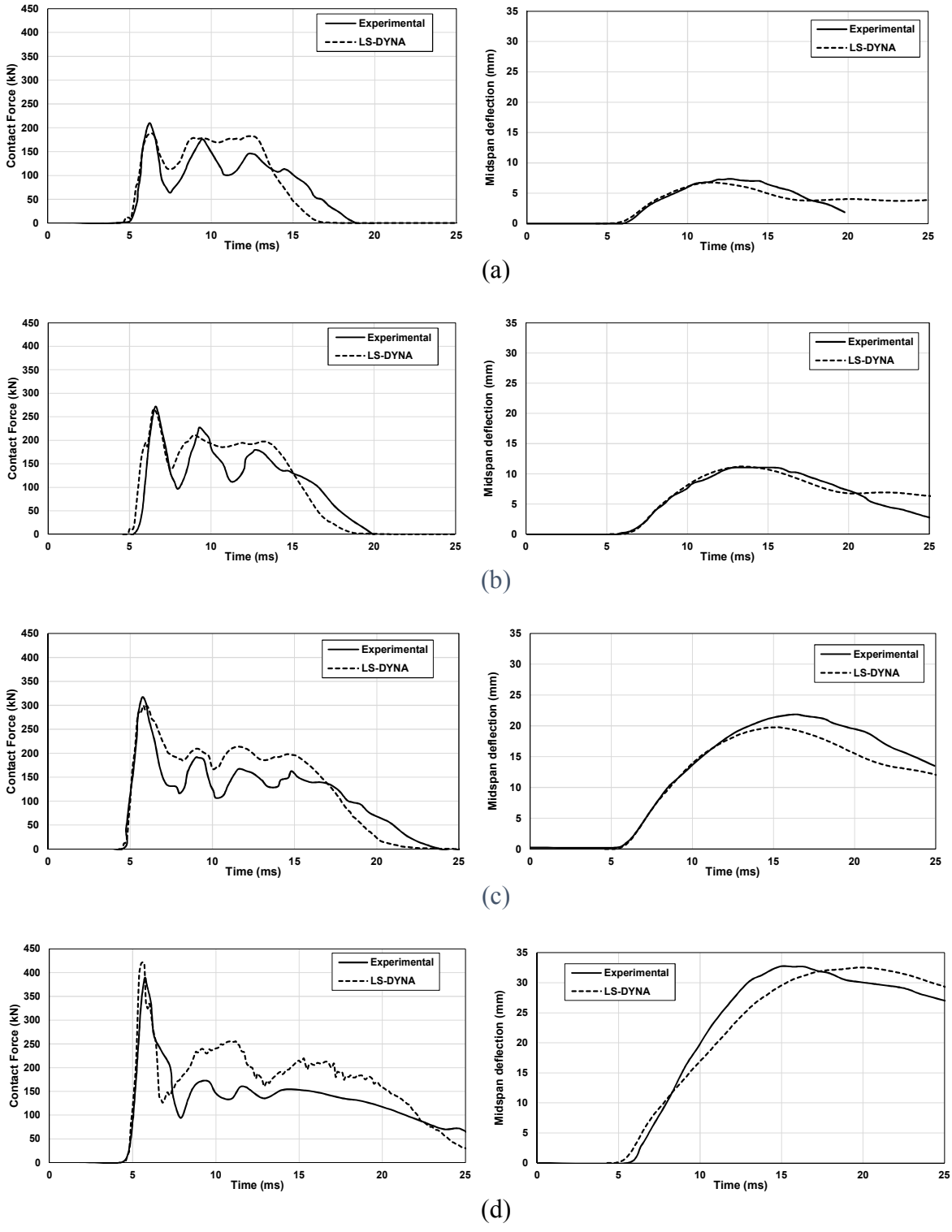

Figure 11. *Impact force and mid-span deflection for beam S2222 for drop heights of (a) 0.3, (b) 0.6, (c) 1.2, and (d) 2.4 m*

www.manaraa.com

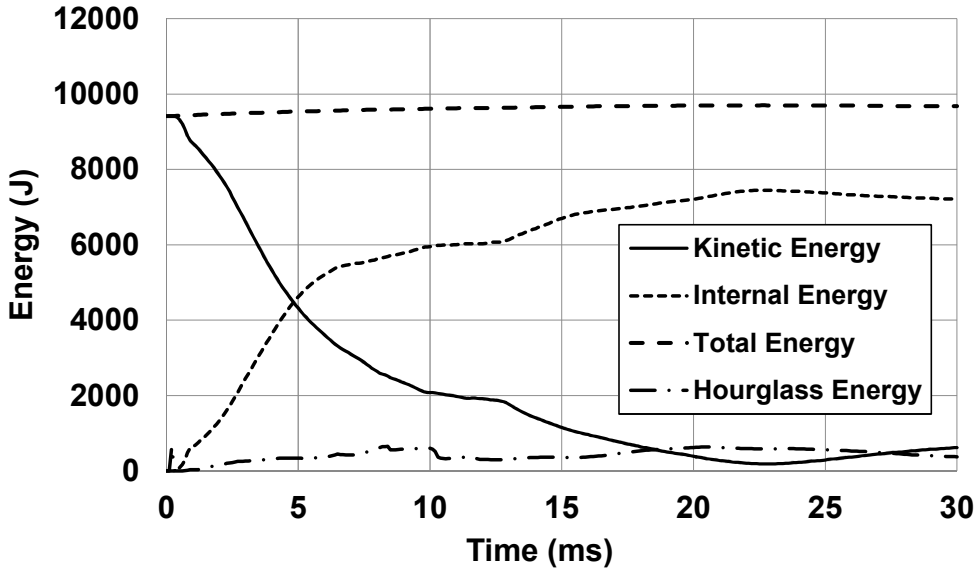

***Figure 12**. Energy balance analysis of specimen S2222 under a hammer drop height of 2.4 m*

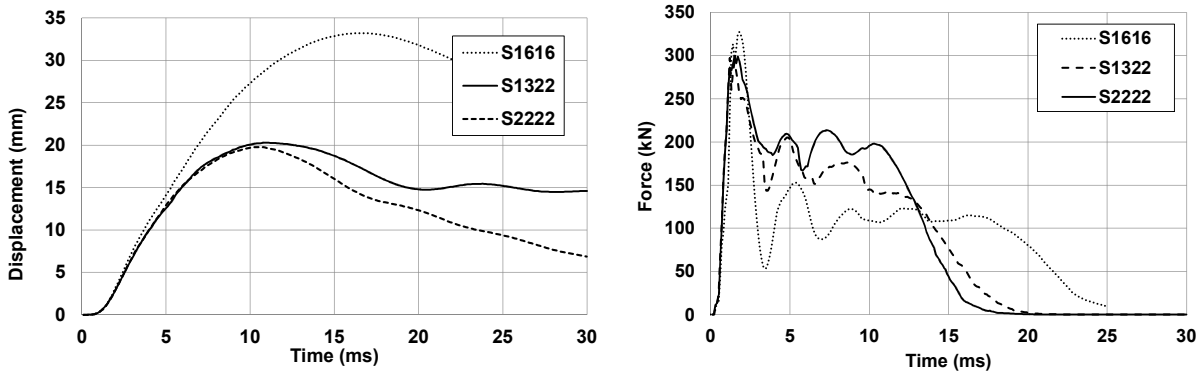

(a) (b)

***Figure 13.** (a) Displacement time history and (b) force time history for test specimens at drop height of 0.6 m*

www.manaraa.com

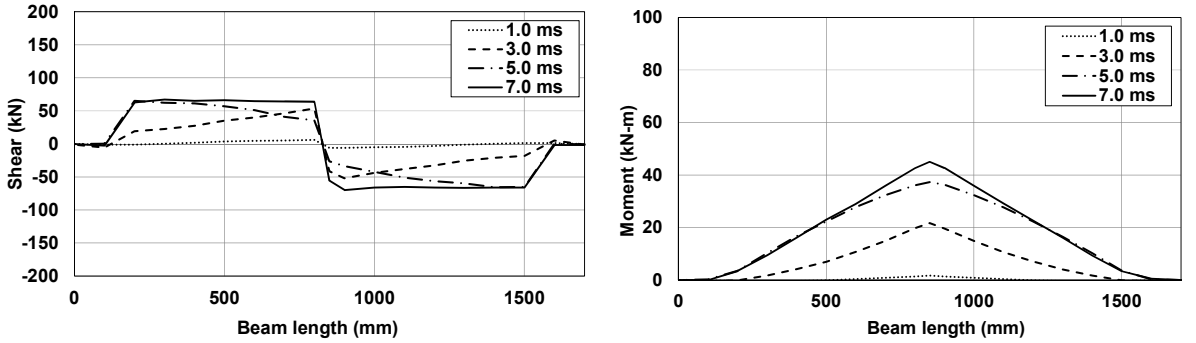

(a)

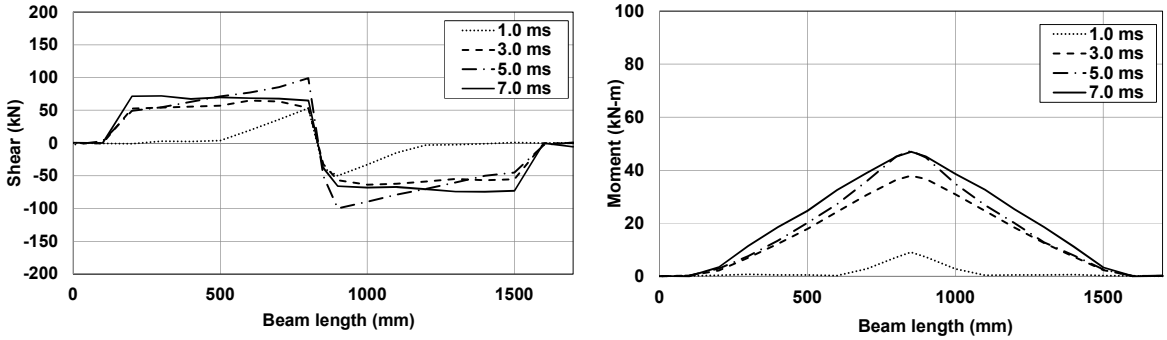

(b)

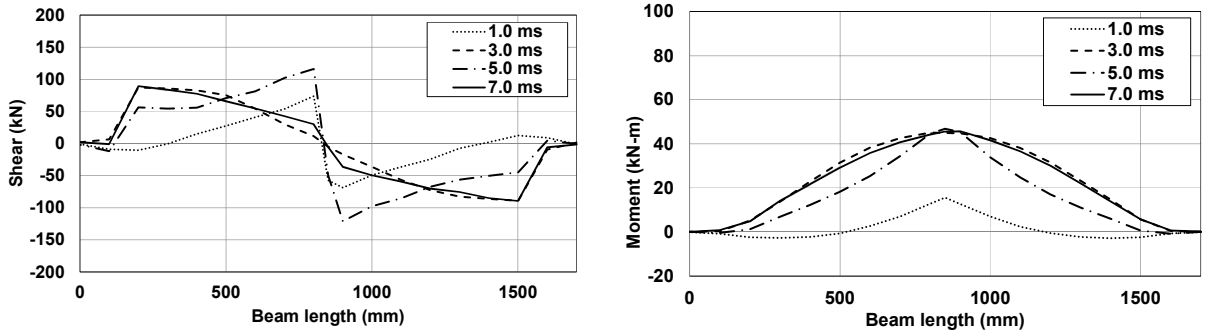

(c)

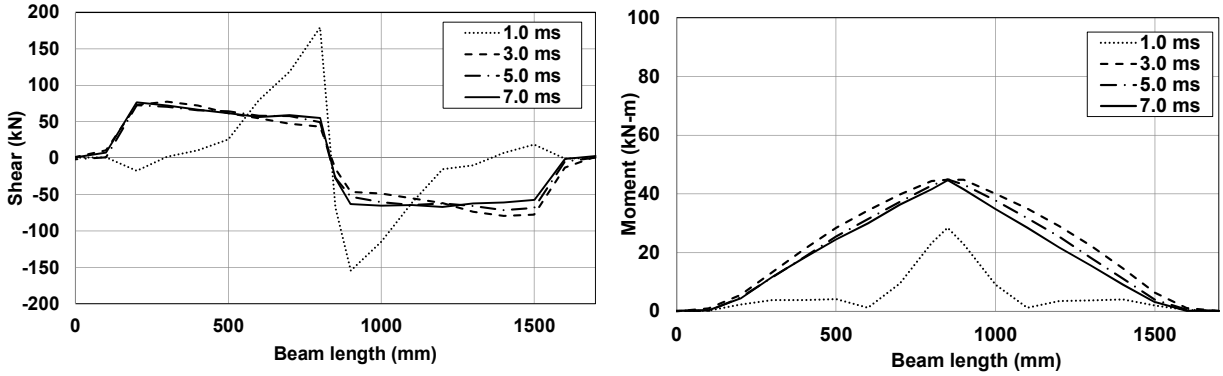

(d)

Figure 14. *Internal shear and moment forces for S1616 for drop heights (a) 0.30 (b) 0.6 (c) 1.2 and (d) 2.4 m*

www.manaraa.com

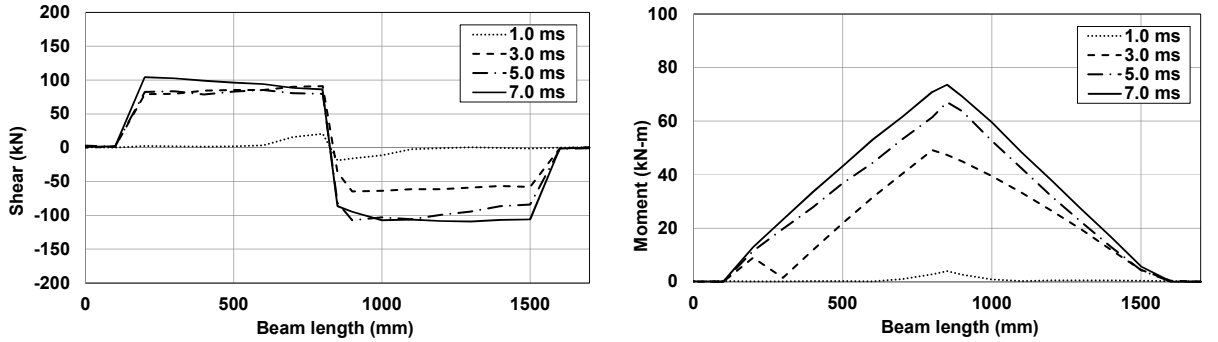

(a)

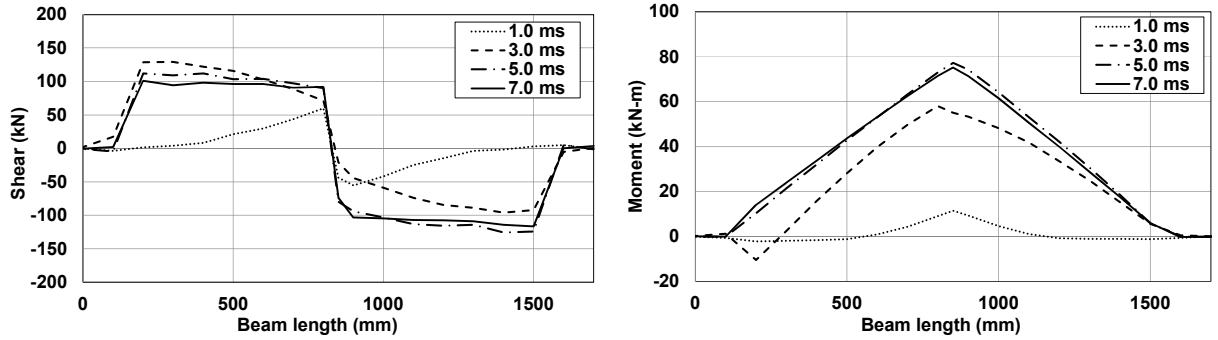

(b)

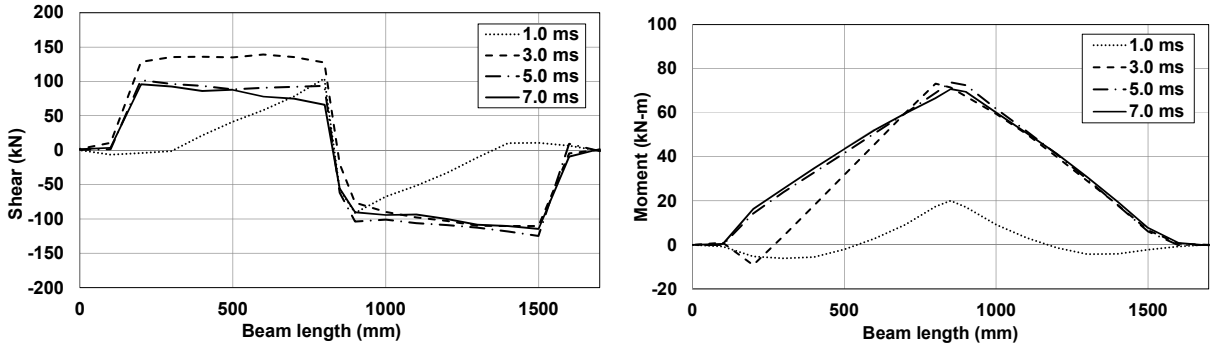

(c)

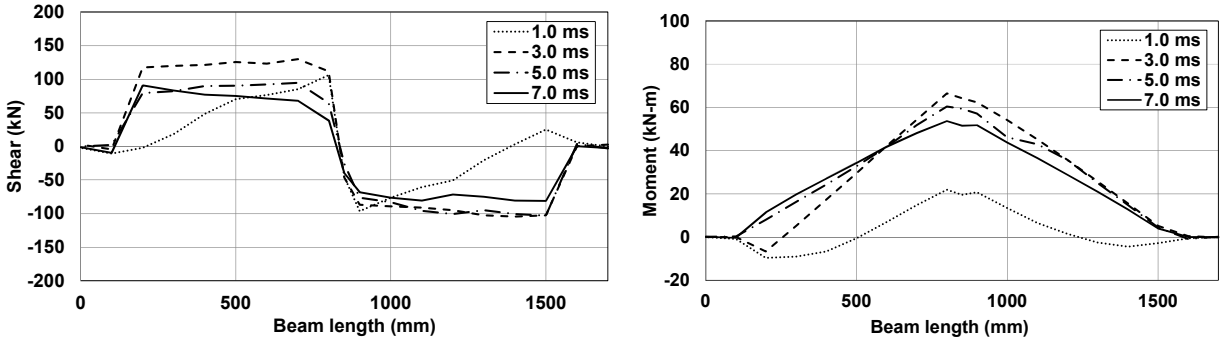

(d)

Figure 15. *Internal shear and moment forces for S1322 for drop heights (a) 0.3 m (b) 0.6 m (c) 1.2 m and (d) 2.4 m*

www.manaraa.com

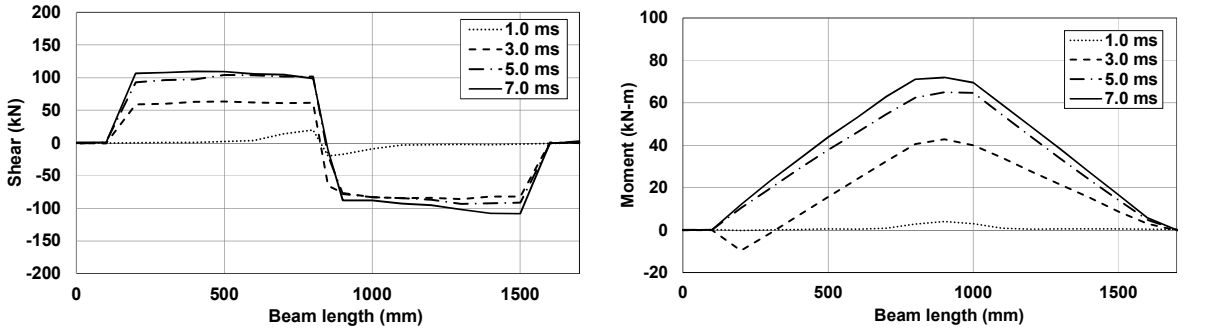

(a)

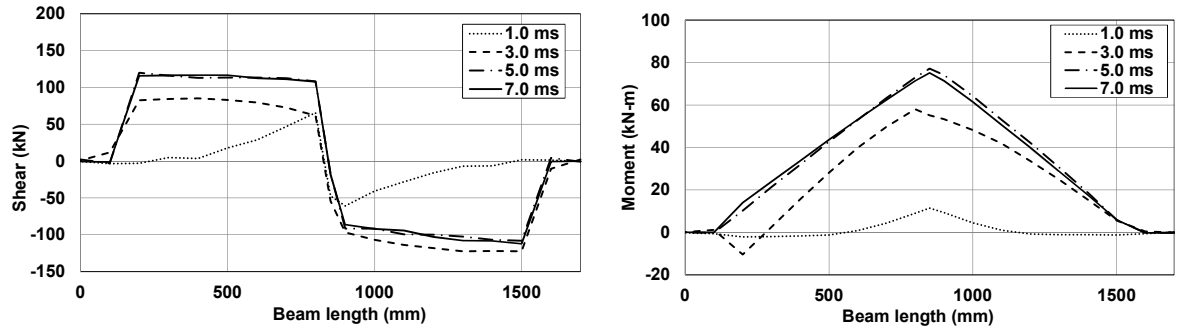

(b)

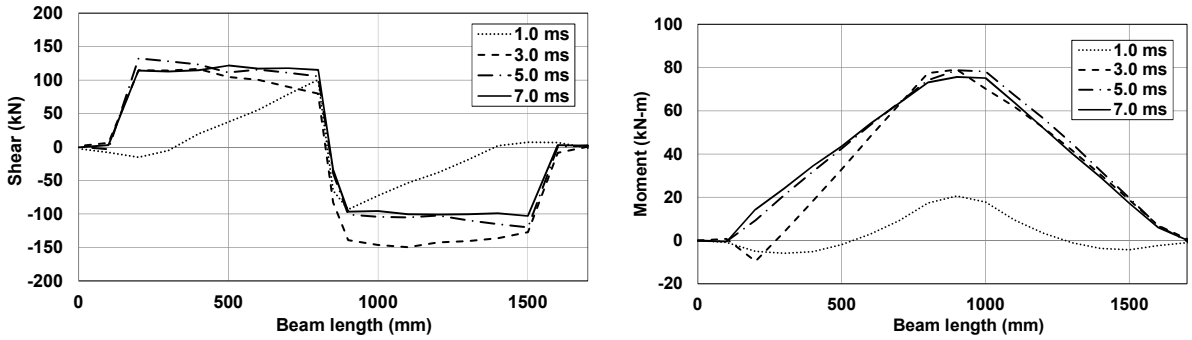

(c)

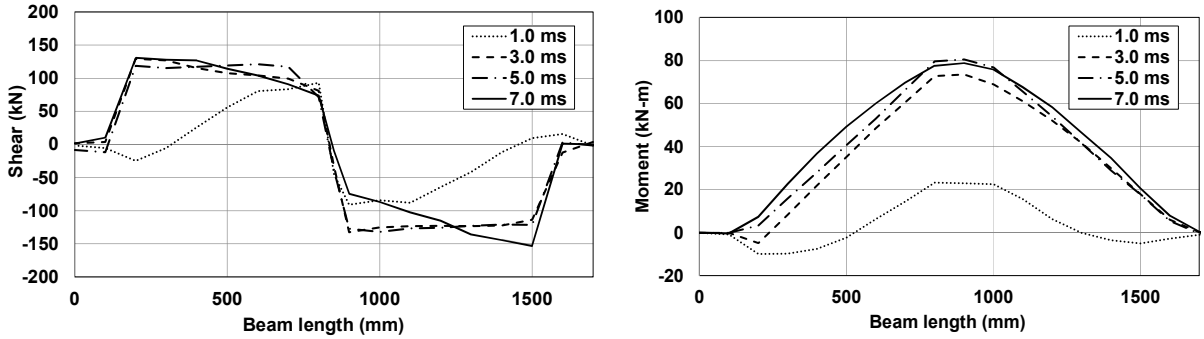

(d)

Figure 16. *Internal shear and moment forces for S2222 for drop heights (a) 0.3 m (b) 0.6 m (c) 1.2 m and (d) 2.4 m*

www.manaraa.com

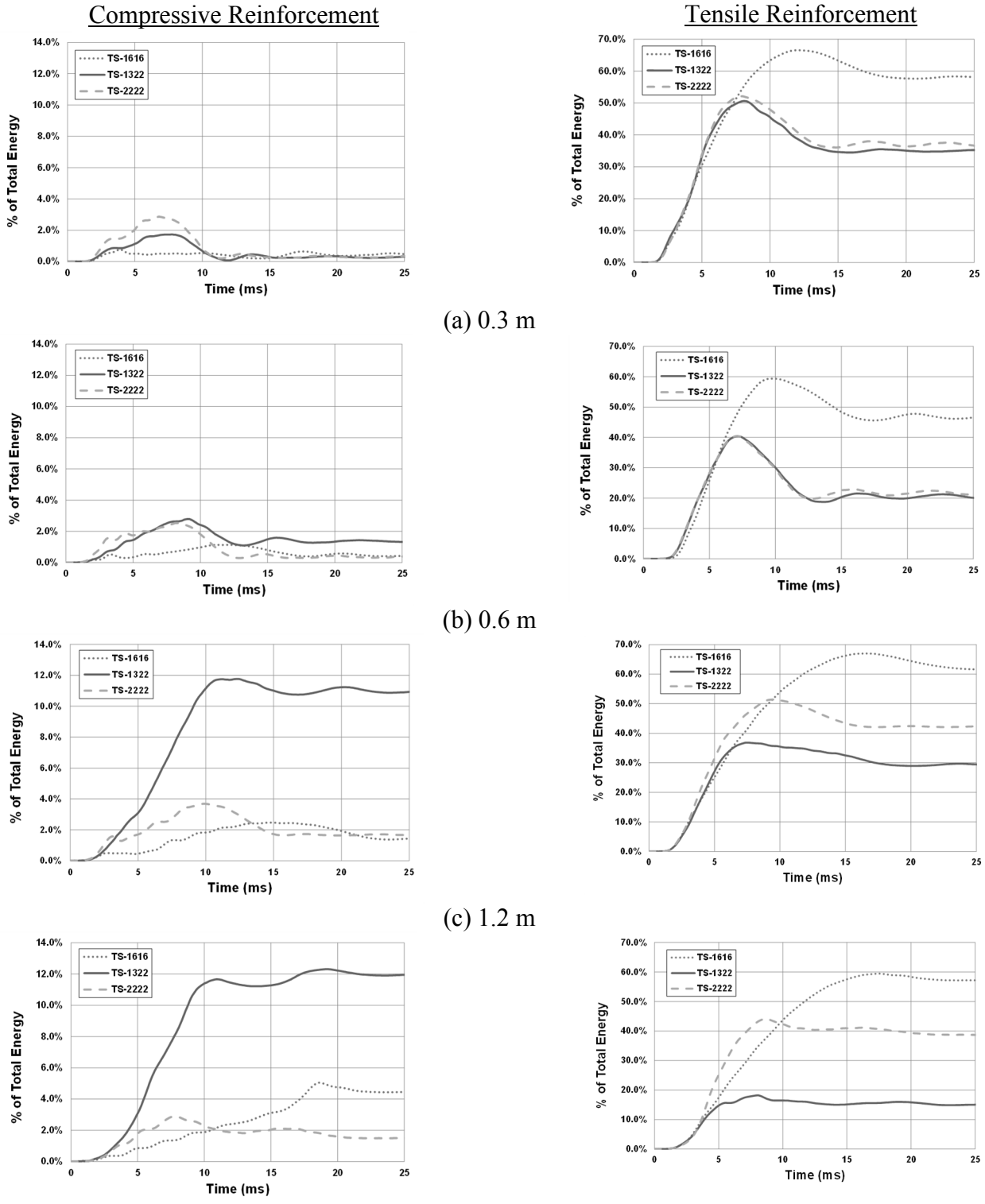

Figure 17. *Compressive (left) and tensile (right) longitudinal reinforcement normalized internal energy*

www.manaraa.com

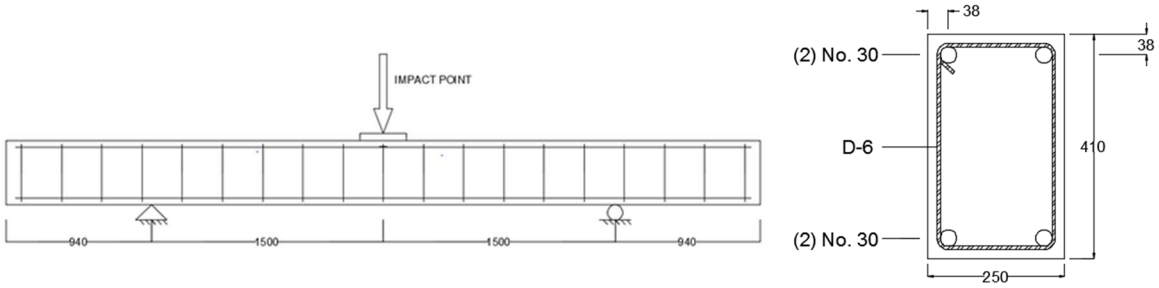

Figure 18. *Specimen properties for the transverse reinforcement analysis*

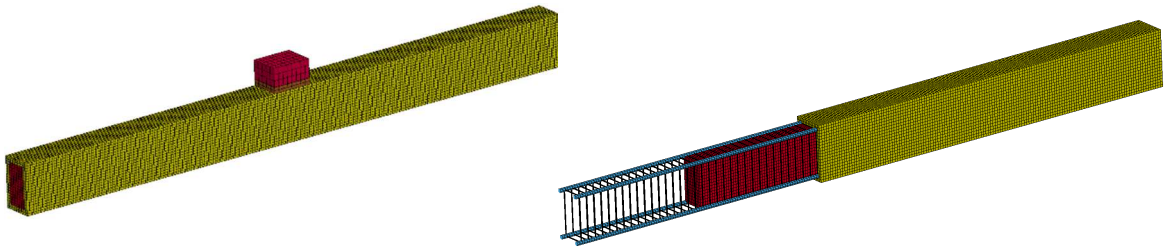

Figure 19. *Isometric view of finite element model for the transverse reinforcement analysis*

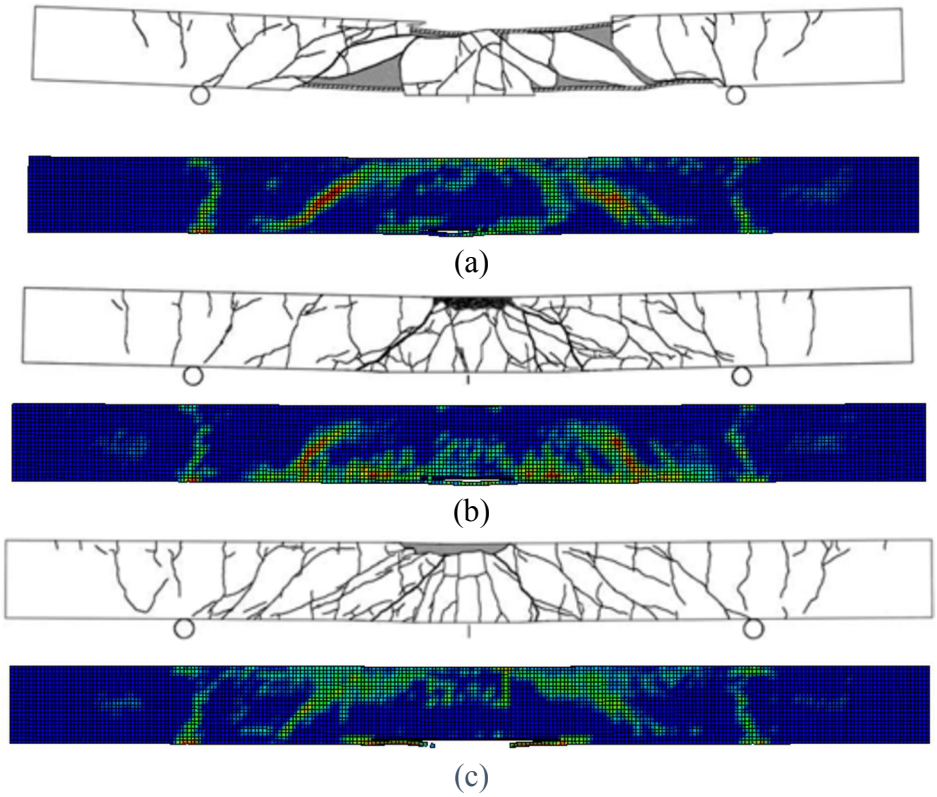

Figure 20. *Comparison of crack pattern between experiments and finite element models for specimens (a) SS1, (b) SS2, and (c) SS3*

www.manaraa.com

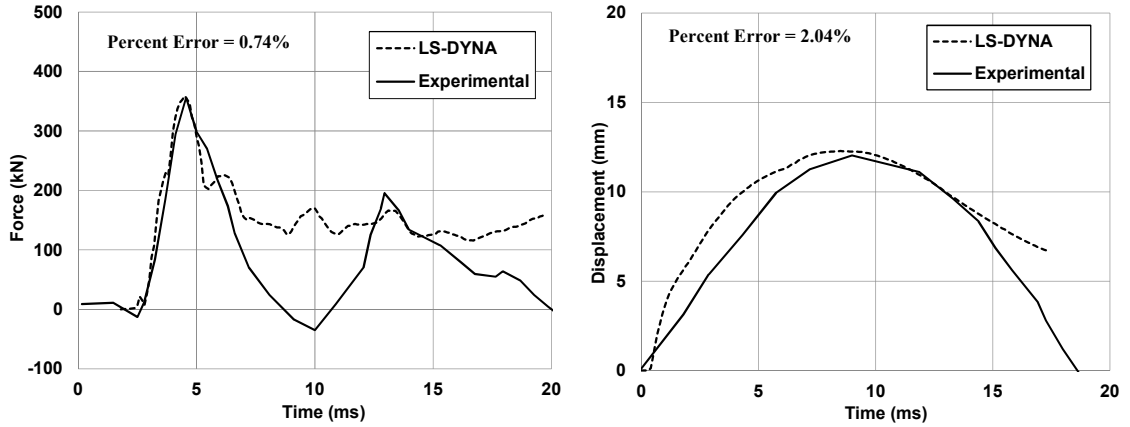

(a)

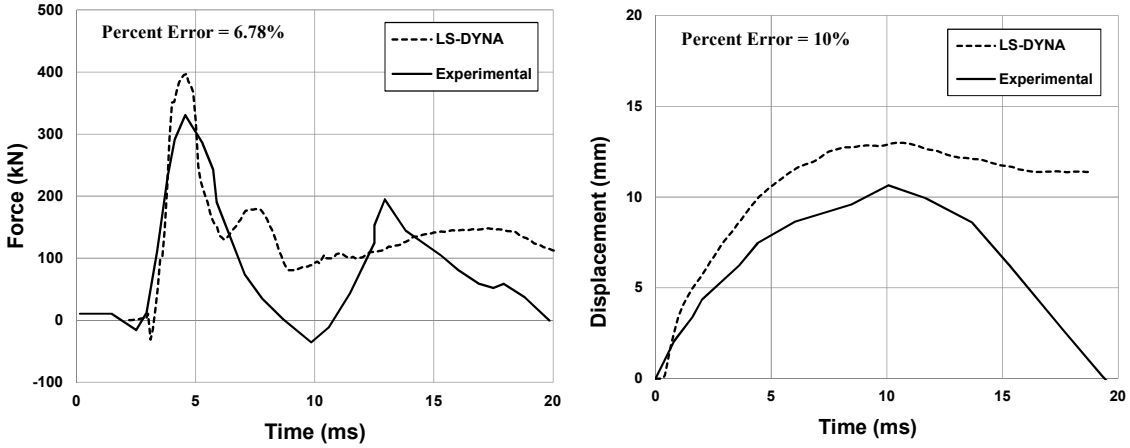

(b)

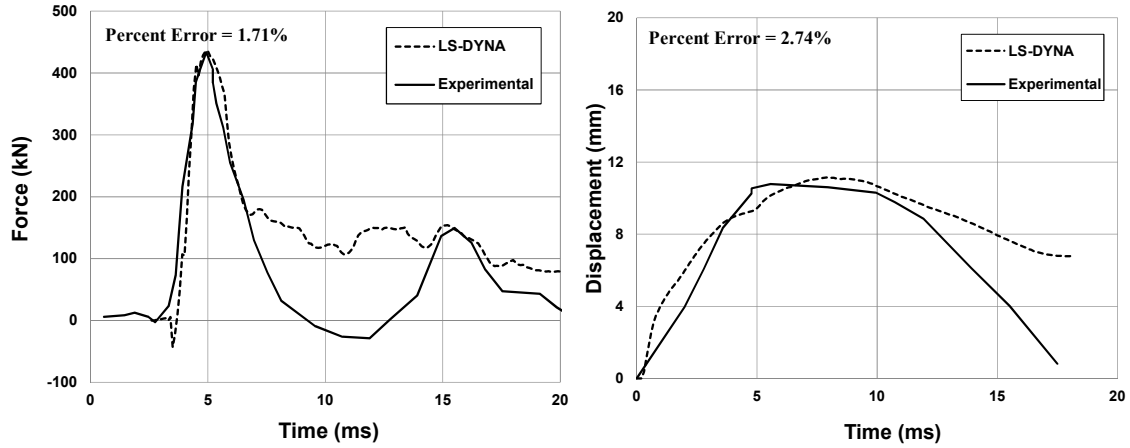

(c)

Figure 21. *Impact force and mid-span deflection for specimen's (a) SS1 (b) SS2 and (c) SS3*

www.manaraa.com

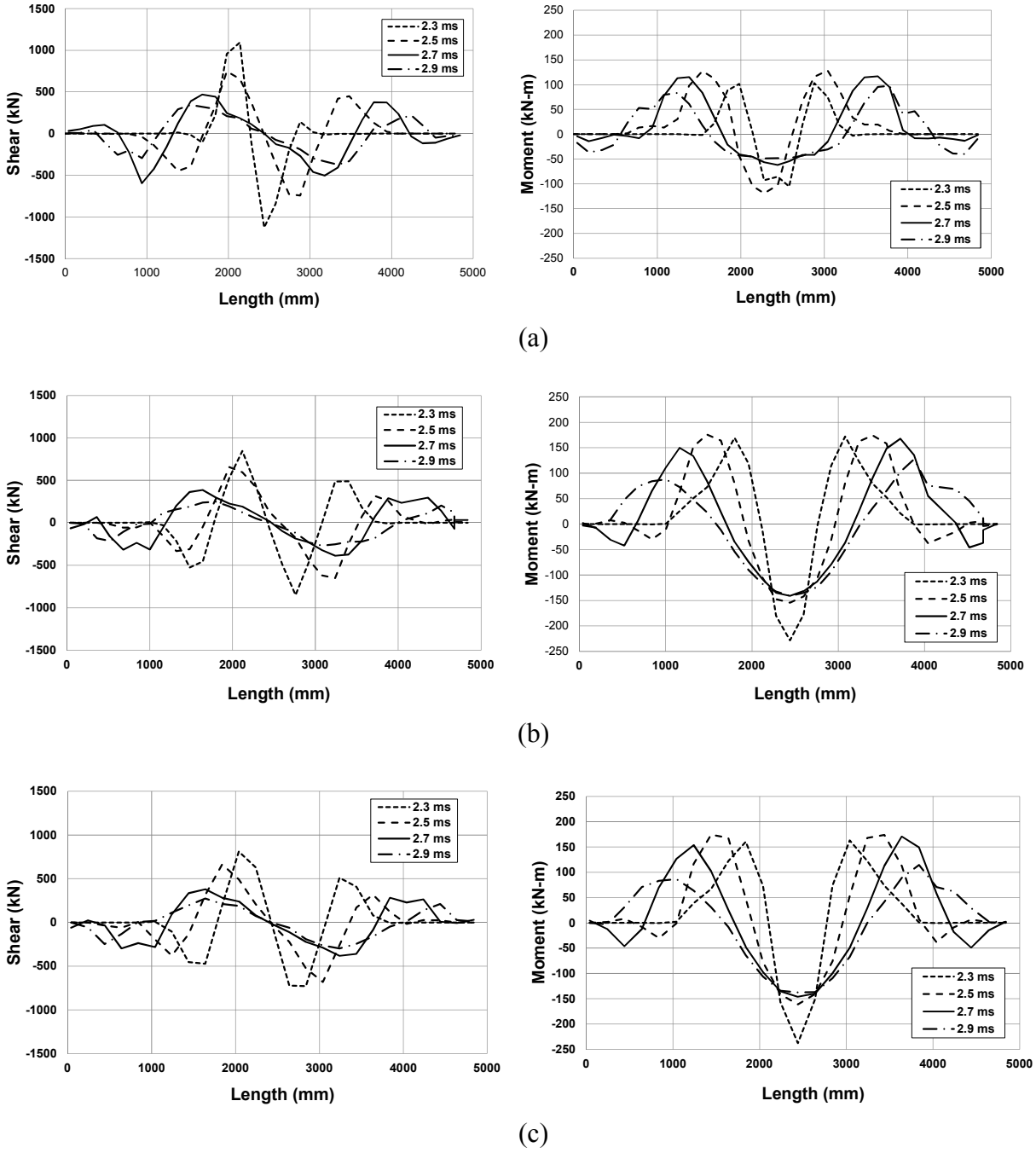

Figure 22. *Internal shear and moments for specimen's SS1, SS2 and SS3 at time steps (a) 0.5 ms, (b) 0.7 ms, (c) 1.0 ms and (d) 1.2 ms*

www.manaraa.com

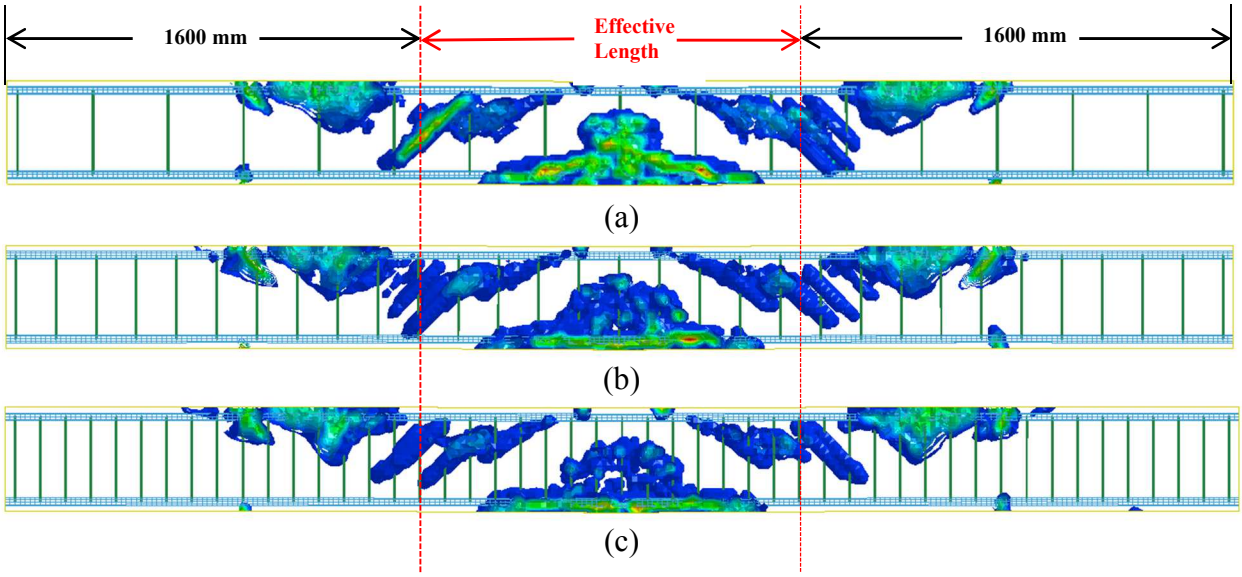

Figure 23. *Plastic strain contours at time of 2.3 ms for specimen's (a) SS1 (b) SS2 and (c) SS3*

www.manaraa.com

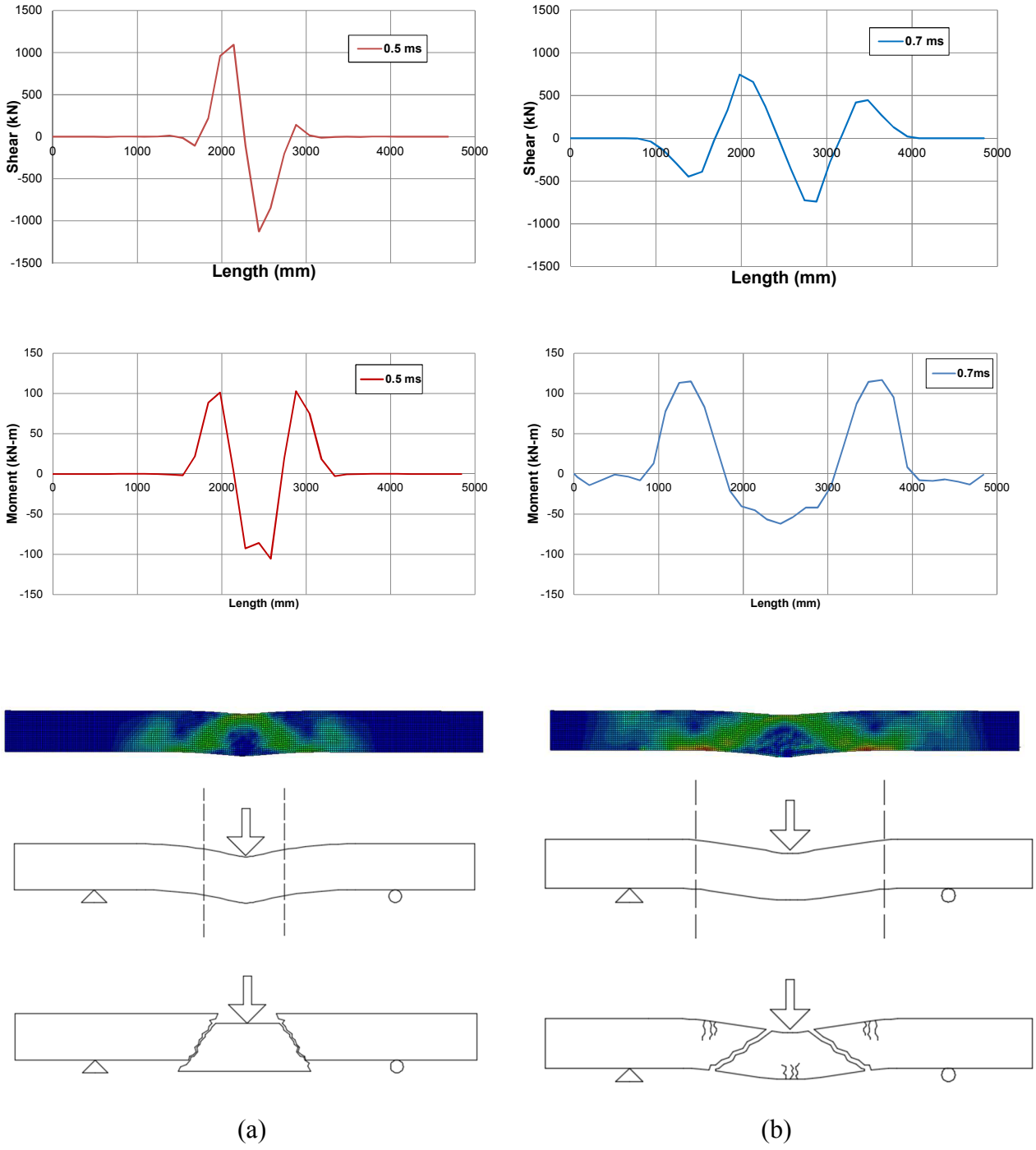

Figure 24. *Shear and moment Analysis for specimen SS1 at Time Steps (a) 0.5 ms and (b) 0.7 ms*

www.manaraa.com

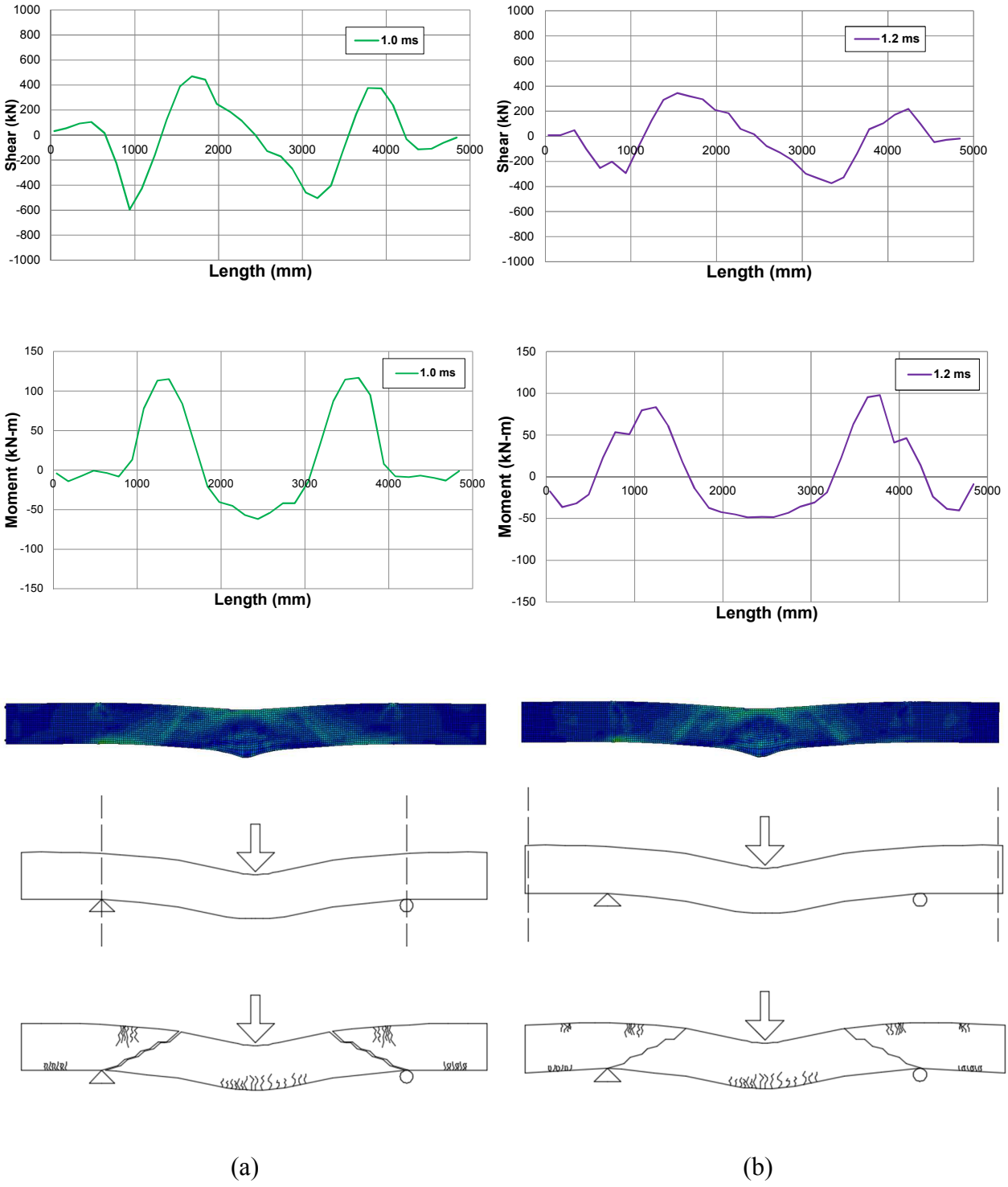

Figure 25. *Shear and moment analysis for Specimen SS1 at time Steps (a) 1.0 ms and (b) 1.2 ms*

www.manaraa.com

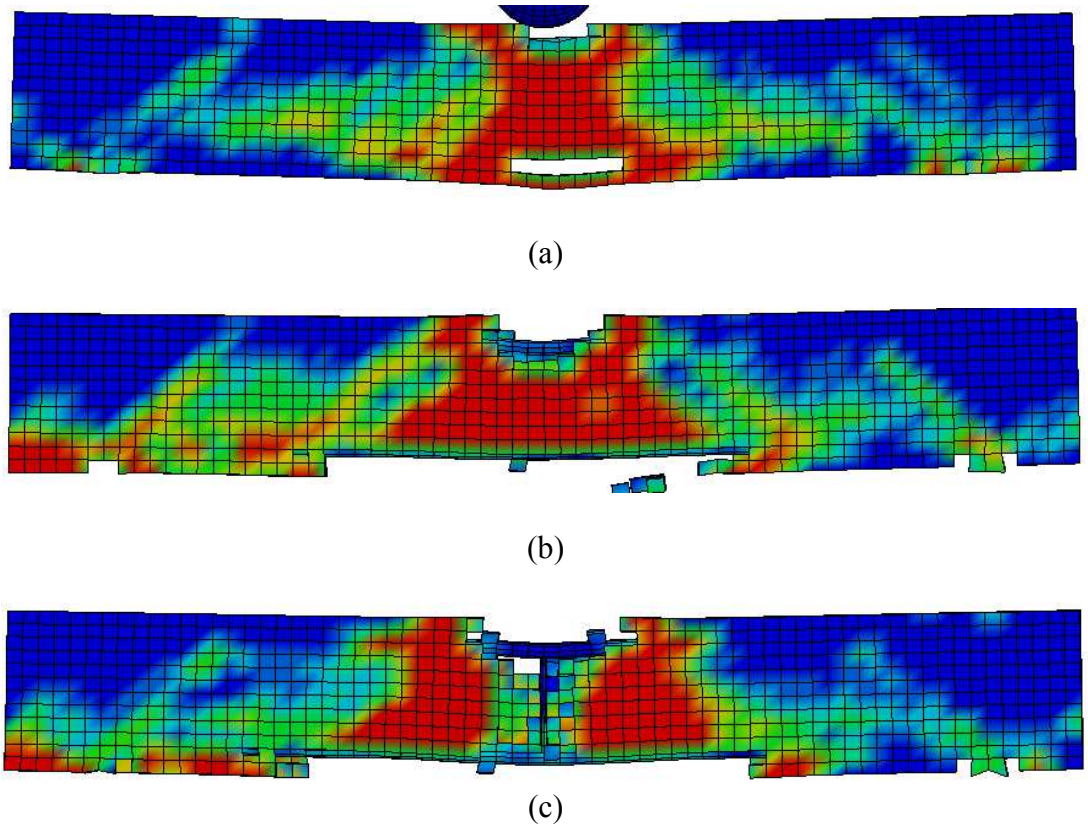

(a)

(b)

(c)

Figure 26. *Post impact damage states of specimen S2222 with a hoop spacing of (a) 75, (b) 150, and (c) 300 mm under a hammer impact from a drop height of 2.4m*

www.manaraa.com

References

1. Askeland, D. R., & Phulé, P. P. (2003). The science and engineering of materials. Asprone, D., Cadoni, E., & Prota, A. (2009). Experimental analysis on tensile dynamic behavior of existing concrete under high strain rates. *ACI Structural Journal*, *106*(1), 106-113.

2. Asprone, D., Cadoni, E., & Prota, A. (2009). Tensile high strain-rate behavior of reinforcing steel from an existing bridge. *ACI Structural Journal*, *106*(4).

3. Atchley, B. L., & Furr, H. L. (1967, November). Strength and energy absorption capablities of plain concrete under dynamic and static loadings. In *ACI Journal Proceedings* (Vol. 64, No. 11). ACI.

4. Tabiei, A. (2014) "Contact in LSDYNA", course notes.

5. Cowell, W. L. (1965). *Dynamic tests of concrete reinforcing steels* (No. NCEL-TR-394). NAVAL CIVIL ENGINEERING LAB PORT HUENEME CALIF.

6. Cowell, W. L. (1966). *DYNAMIC PROPERTIES OF PLAIN PORTLAND CEMENT CONCRETE* (No. NCEL-TR-447). NAVAL CIVIL ENGINEERING LAB PORT HUENEME CALIF..

7. Cotsovos, D. M., Stathopoulos, N. D., & Zeris, C. A. (2008). Behavior of RC beams subjected to high rates of concentrated loading. *Journal of structural engineering*, *134*(12), 1839-1851.

8. Fujikake, K., Li, B., & Soeun, S. (2009). Impact response of reinforced concrete beam and its analytical evaluation. *Journal of structural engineering*.

9. Green, H. (1964, July). IMPACT STRENGTH OF CONCRETE. In *ICE Proceedings* (Vol. 28, No. 3, pp. 383-396). Thomas Telford.

10. Keenan, W. A. (1959). *The Yield Strength of Intermediate Grade Reinforcing Bars Under Rapid Loading* (Doctoral dissertation, University of Illinois at Urbana-Champaign).

11. Li, Q. M., & Meng, H. (2003). About the dynamic strength enhancement of concrete-like materials in a split Hopkinson pressure bar test. *International Journal of solids and structures*, *40*(2), 343-360.

12. Mainstone, R. J. (1975). Properties of materials at high rates of straining or loading. *Matériaux et Construction*, *8*(2), 102-116.

www.manaraa.com

13. Malvar, L. J., & Crawford, J. E. (1998). *Dynamic increase factors for concrete*. NAVAL FACILITIES ENGINEERING SERVICE CENTER PORT HUENEME CA.

14. Malvar, L. J., & Crawford, J. E. (1998). Dynamic increase factors for steel reinforcing bars [C]. In *28th DDESB Seminar. Orlando, USA*.

15. Murray, Y. D. (2007). *Users manual for LS-DYNA concrete material model 159* (No. FHWA-HRT-05-062).

16. Ožbolt, J., Sharma, A., İrhan, B., & Sola, E. (2014). Tensile behavior of concrete under high loading rates. *International Journal of Impact Engineering*,*69*, 55-68.

17. Saatci, S., & Vecchio, F. J. (2009). Effects of shear mechanisms on impact behavior of reinforced concrete beams. *ACI structural Journal*, *106*(1), 78-86.

www.manaraa.com

CHAPTER III PERFORMANCE-BASED DESIGN APPROACH FOR REINFORCED CONCRETE BRIDGE PIERS

A paper to be submitted to the *ASCE Journal of Structural Engineering*

Steven AuYeung, Alice Alipour

Abstract

Vehicle collisions with bridge piers result in major damage to the supporting pier and could lead to total collapse. The ASCE annual report card for America's infrastructure (2013) rated the United States bridges a C+; this makes many of the bridges vulnerable to failure when subjected to extreme loading events. Past work has shown that current design standards underestimate the forces that actually occur in a vehicle collision scenario. A parametric study was performed to study the internal actions within a pier such as shear and moment with respect to pier diameter, transverse reinforcement spacing and vehicle impact velocity.

LS-DYNA, a popular finite element software used in the vehicle collision testing community was used to conduct the research. Validated models produced from past research were used to ensure accurate and realistic results. The vehicle models offered by the National Crash Analysis Center and the National Transportation Research Center, Inc. are used to conduct this research. Material models and modeling techniques were validated by replicating experimental work involving drop hammer impacts on reinforced concrete beams. The obtained bridge pier collision models were validated again by comparing vehicle damage and impact forces with published experimental and numerical research results. The conservation of energy of the systems were closely monitored in order to ensure stability within the impact simulations,.

This study shows that the pier diameter governed the overall failure mode and the amount of transverse reinforcement dictated the amount of localized damage the pier experienced. Kinetic energy of the impacting vehicle governed the magnitude of internal forces generated

www.manaraa.com

within the pier. The proposed performance-based design approach resulting from this work allows a one to design a bridge pier for a vehicle collision event in a simplistic manner without the use of extensive finite element modeling.

Introduction

Vehicle collisions with bridge piers are one of the rare extreme loading events that can occur during a bridges life cycle, however the amount of damage resulting from them can be catastrophic. Studies conducted by Wardhana and Hadipriono (2003) and Cook (2014) investigated the bridge failure rates and trends within the United States. Both studies concluded that failures due to impact were the second leading cause next to hydraulic causes. Previous vehicle collisions have resulted in significant damage to the pier, bent cap, foundation system as well as the superstructure with the possibility of total collapse of the bridge. The result of a bridge failure would cause detrimental economic impacts, impose danger to the public safety, and loss of human life. Direct costs would include cost of closure, immediate emergency repairs and major traffic disruptions. Indirect costs associated with the bridge repair can even be higher especially if the failed bridge forms an important component where the disruption of the traffic circulation due to detours would result in major traffic delays elongating freight routes (Furtado and Alipour, 2014). The lost time associated with this would affect the commerce of businesses of all sizes. Due to the severe consequences of a bridge collapse, the design of these piers is of great importance.

Several examples of vehicles collision with bridge pier events have caused significant amounts of damage to the bridge resulting in traffic disruptions in major metropolitan areas. A bridge located in Grand Junction, CO on I-70 was struck by a tractor trailer on August 15, 2007 (Gallegos and McPhee, 2007). Force from the impact caused a shear failure in the column

www.manaraa.com

located at the bent cap connection as seen in Figure 1. On May 22, 2011, a tractor trailer collided with a bridge pier located on the SC Highway 150 overpass (Kudelka 2011). The collision destroyed the impacted column and half of the bent cap resulting in the sagging of the superstructure spans as shown in Figure 2. Damage was so severe that the whole overpass was later replaced with an entirely new bridge that took four months to construct. Figure 3 shows the resulting damage from a tractor trailer collision with a bridge support pier of the Dolphin Road overpass located in Dallas, Texas on June 11, 2012 (Vega 2012). Shear failure was observed at the top of the pier near the bent cap. Resulting damage caused the bridge to be shut down for a week in order for the repairs to be made.

AASHTO (2012) LRFD Design Requirements

The American Association of State Highway and Transportation Officials (AASHTO) *Load and Resistance Factor Design (LRFD) Bridge Design Specifications* (2012) requires that abutments and piers within 9.144 m of the roadway to be considered for the extreme event of a vehicle collision. Bridge structures prone to vehicle collision forces must be designed to either redirect or absorb the impact force or provide structural resistance. According to AASHTO, the required 2,669 kN ESF that the structure must be designed for must be applied as a single point load at a height of 1.524 m above the ground and at an angle of incidence from zero to 15 degrees with the edge of pavement in a horizontal plane (3.6.5.1 AASHTO 2012).

This recommendation is based on a single experimental test performed by Buth et al. (2011) involving a 36.3 metric ton semi-tractor-trailer colliding into a pier at 80 kph. The pier used for testing was made of reinforced concrete and had an outer steel layer encasing the pier. An extensive bracing system was used making the pier rigid in order to estimate the contact force during the collision. These testing conditions do not provide a realistic representation of the

www.manaraa.com

relatively flexible piers of actual bridges that are vulnerable to these collision events. By also encasing the RC pier with a protective steel layer, resulting damage modes and erosion effects could not be properly assessed post impact. This is crucial for the designer to make a safety and risk assessment based on how important the bridge is to the transportation network it's a part of. The fact that this design recommendation fails to take into consideration the variability of vehicle speeds, mass and the columns characteristics leaves the designer with a large amount of uncertainty in the safety of the design.

Currently collapse prevention is the only design criteria for bridge piers (Sharma et al., 2012). This manner of design is not sufficient due to the fact that some bridges are considered a vital part of major transportation networks for freight and commerce. These bridges that are of great importance may need to be designed for full operation post impact. Desired post impact performances of the bridges should be established by importance of the bridge, bridge owner and state departments. This study investigates the damage effects that truck collisions have on RC bridge piers based on impact velocity, pier diameter and reinforcement detailing through the use of finite element methods. By gaining a better understanding of a piers response to these parameters, an adaptive design approach can be established. The following work comprises of an extensive literature review on the characterization of an impact loading event, overview of current design standards, finite element modeling and validation, impact analysis of the piers and a suggested performance-based design approach.

Impact Event Characterization

An impact event is normally characterized using the peak dynamic force (PDF) and equivalent static force (ESF) (El-Tawil et al., 2005). The PDF is defined as the largest impact force occurring throughout a single experiment. The ESF is defined by a static external force

www.manaraa.com

applied at any time to the structure that produces the same deformation from a dynamic analysis (Chopra, 2011). This method is based on equating the deformation resulting from a static loading of a structure to the deformations associated with the structure under dynamic loading (i.e mass, stiffness and damping). The PDF is not an accurate representation of structural demands when designing because during the time of the PDF, the entire structure has not had enough time to respond to the loading. Another reason why the use of an ESF is preferred is that the results are not as susceptible to issues associated with hour glassing that is expected in finite element analyses. (El-tawil et al., 2005). Hour glassing refers to local element distortions that have no associated strains or strain energy. This issue is discussed in a more extensive manner later on in the finite element modeling section of this chapter.

This stiffness based ESF method however will not provide an accurate estimate of the members undergoing plastic deformations under impact because it is based on the assumption of an elastic response or behavior. Another method of calculating ESF is provided by the Eurocode in Part 1-7, section 4 (EN, B. 1991). The code states that the design of a structure for impact can be represented by an equivalent static force providing equal action occurring during impact. For soft impacts where the structures are designed to absorb energies through plastic/elastic deformations, the ESF method is defined by:

$$\frac{1}{2}mv^2 \leq F_o\, y_o \qquad (1)$$

where m, v, F_o, y_o represent the vehicle mass, velocity, plastic strength of the structure, and the deformation capacity respectively. This equation is based on the assumption that the structure is ductile enough to undergo plastic deformations in order to absorb the kinetic energy of the colliding object.

www.manaraa.com

A peak 50 ms moving average has been implemented by researchers in the automotive crash community to represent the ESF. This technique has been used by other researchers to obtain a design ESF when testing vehicle redirection impacts on longitudinal barriers. The use of moving averages is used to filter out spikes in the data occurring over a short time period which can be associated with unusable noise in the signal. If the time interval for the moving average is too large, useful peaks in the data can be filtered out as well resulting in lower calculated forces than that of actually occurring. Buth et al. (2011) filtered the raw data of the force-time histories obtained from the full scale impact experimentation through a 50-ms moving average. A 25-ms moving average was also used to filter the force-time histories; this method was able to capture the peak contact force better than the 50-ms moving average filter and was used to establish the 2,669 kN ESF requirement that was later introduced in the AASHTO LRFD bridge specifications (LRFD-2012).

All three methods of obtaining an ESF for the design of bridge piers subjected to vehicle collisions are shown to have limitations. The stiffness based method introduced by Chopra (2011) only considers the elastic response of the structure. If the pier were to resist the impact load elastically, it would have an impractically large mass. In reality, the majority of the kinetic energy of the impacting vehicle is absorbed by the pier through plastic deformations so taking material plasticity into account is crucial for design. The method recommended by the Eurocode 1: Actions on Structures: Part 1-7 (2006) does follow the assumption that the pier will undergo plastic deformations to absorb the kinetic energy of the vehicle. However, it fails to take into account the inertial effects which play a large role in the load resisting mechanisms of a structure undergoing dynamic loads. Lastly, the ESF obtained through filtering the contact force time history data by moving averages fails to take into account the structural properties of the pier by

www.manaraa.com

any means. As such it has no logical basis in determining a piers capacity to vehicle collision loading events.

Concerns of Current Design Standards

The issue with the current standard is that it implements an ESF method that does not accurately capture the imposing demands that must be resisted by the pier during impact loads. The ESF established by Buth et al. (2011) raises the concern that the methods employed to obtain this ESF are too simplistic. The design ESF resulted from the filtering of force-time history data and neglects the structural characteristics of the pier. Also, design standards require that the 2,669 kN force obtained from Buth et al. (2011) filtered data be applied as a static point load to the bridge pier. An issue with this is that a 2,669 kN static load applied to a bridge pier is much different than a 2,669 kN dynamic impulsive load caused by a collision. Under static loading, the forces imposed on a member have the time to be transferred throughout the structure and finally to the support systems; as such both the member and supports are actively resisting the imposed forces. Time histories of the contact forces recorded under Buth et al. (2011) experiment reveal that a vehicle impact load can be characterized as an impulse load. When a pier is subjected to an impulse load caused by a vehicle collision, the whole structure, including the supports, is not able to immediately respond to the loading because of the short duration of the excitation. This means that the location of impact needs to be strong enough to resist the initial shock and transfer these forces to the support systems without failing.

Agrawal et al. (2013) performed a numerical analysis which consisted of applying a 2,669 kN static load recommended by AASHTO to a pier and compared it's behavior to the same pier undergoing a vehicle collision. The pier that underwent the dynamic collision load reported much larger displacements and damage levels. The ESF recommended by AASHTO

www.manaraa.com

was only able to produce the same displacements and contact forces for a truck traveling less than 50 kph. The static analysis greatly underestimated the displacement and force demand that a bridge pier would actually undergo for vehicle speeds greater than 50 kph.

Another issue with designing a pier according to current provisions is that the ESF is based on a single vehicle traveling at 80 kph. Potential impact conditions are dependent on local traffic conditions. Current design provisions could result in an over design for piers located in areas with generally low vehicle speeds which would prove to be uneconomical. An under design is possible as well if the bridge pier is located in an area with high vehicle velocities and a high population of heavy commercial vehicles.

Finite Element Model Generation

The previous work shows that AASHTO's design requirement can't accurately capture the piers response to vehicle impacts with different kinetic energies (Gomez et al. 2015) which creates a need for additional work to be done. Full scale experimental work involving vehicle collisions is extremely expensive and difficult to perform. Alternatively, the uses of finite element software to conduct these tests are an attractive method due to the relatively lower associated costs. The use of finite element models allows the user to create numerous amounts of different test cases at no additional costs and gives the ability to perform more extensive analyses. The finite element models used in this paper are based on those developed and validated by Gomez and Alipour (2014).

The models consist of the full representation of a bridge bent including the superstructure tributary mass, pier(s), pile cap, and piles with the soil-pile-structure interaction captured using the soil p-y curves. An elastic material layer, 50 mm thick was applied on top of the pile cap to represent the weight of the 1 m deep soil layer that's supported by the foundation. The bridge

www.manaraa.com

piers are circular reinforced concrete sections with 5 m height above the ground surface. It was put into question whether the addition of a superstructure imposed on top of the pier would affect the results as opposed to testing done to a pier without a superstructure. Due to the short duration of loading during an impact event relative to the natural period of the structure, it is hypothesized that the change in boundary conditions on top of the pier caused by the addition of the superstructure will not significantly affect the results.

To investigate this, an additional model was created that included a superstructure shown in Figure 4. The bridge piers consisted of a 900 mm circular reinforced concrete column with 5 m in height above the ground surface. For both piers, a 1% longitudinal reinforcement ratio was used and was reinforced with twelve No.25 longitudinal bars. This fulfilled the design guidelines according to Section 5.10.11.4.1a (AASHTO, 2012) where the area of longitudinal reinforcement must be between 1 – 4 % times the gross cross sectional area of the column. No. 10 hoop bars spaced at 150 mm were used to capture the effect of transverse reinforcement on the shear capacity of the piers. This fulfilled the maximum spacing requirements for transverse reinforcement in compression members stated in Section 5.10.6 (AASHTO 2012) where the spacing's shall not exceed the pier diameter or 300 mm. A concrete cover of 65 mm was provided for all the piers. An example layout for the pier cross sections is shown in Figure **5**.

The superstructure is comprised of a 5.5 m × 5 m × 1 m thick concrete slab. Discreet springs were placed at all four corners of the slab in order to represent the lateral and longitudinal stiffness of the bridge which was assumed to be governed by the abutments. The longitudinal and transverse abutment response was calculated in accordance to Caltrans Seismic Design Criteria (SDC-2013). A bilinear demand model was used to represent the backfill passive pressure forces that are used to resist abutment displacement which is shown in Figure 6 . A deep

www.manaraa.com

pile foundation was implemented to support the bridge piers. The foundation consisted of a pile cap with nine PP360×11.12 pipe piles. The tops of the pile caps are placed 1 m below the assumed ground surface. Load displacement curves for laterally loaded sand were calculated in accordance to the American Petroleum Institute (API) to effectively capture the interaction that occurs between the deep pile foundation and the surrounding soil (API, 2005). These curves shown in Figure 7 represent the stiffness of the surrounding soil at varying depths along the length of the piles and are modeled using compressive inelastic springs. Springs were placed every 0.5 m along the length of the piles in the X and Y axes. A 50 mm thick elastic material layer was applied on top of the pile cap to represent the weight of the 1 m deep soil layer that is supported by the foundation.

All models were preloaded under gravitational forces before the vehicle impact simulations were performed. Since bridge piers carry large loads imposed by the self-weight of the superstructure, a pier exposed to gravitational forces will have a higher compressive strength due to confinement effects as opposed to an unstressed pier. Imposing initial gravity loads can be done in three ways: quasi-static transient analysis with mass damping, explicit dynamic relaxation, and implicit dynamic relaxation. Considering the high computational efficiency, the implicit dynamic relaxation was used to apply the gravity loads.

The Ford F800 model obtained from the NCAC was collided with the piers at impact velocities of 55, 80 and 120 kph. The vehicle type and impact velocity of 80 kph was chosen due to regulatory crash testing guidelines. Crash testing guidelines of permanent or temporary highway features are provided by the "Recommended Procedures for the safety performance of Evaluation of Highway Safety Appurtenances" (NCHRP-350, 1993). In accordance to this document, a roadside feature may be tested for one to six test levels. Test level 1 is required for

www.manaraa.com

local streets with low volume and traffic speeds. A level 2 test is required for structures located in collector roadways and a level 3 test is needed for structures situated in high-speed arterial roadways. Structures located in areas with heavy vehicle traffic require test levels 4-6. A study performed by Agrawal and Chen (2008) found that 95% of vehicle collisions with bridges were tractor trailers and trucks; this would require a test level of at least 4. Test level 4 would require a single unit truck with a mass of at least 5.5 metric tons and an impact velocity of 80 kph. The other two impact velocities of 55 and 120 kph were chosen to observe the effects of different impact velocities on the response of the pier.

The following proceeding sections will include a discussion on the material models, hourglass controls, and contact algorithms used. When performing explicit dynamic finite element collision analyses, the accuracy and reliability of the results are heavily dependent on these four factors. Methods used to validate and ensure the models are operating correctly are discussed in depth as well.

Material modeling

Concrete sections of the FE model had an assigned compressive strength of 28 MPa, maximum aggregate size of 24 mm, and a mass density of 2,325 kg/m^3. The concrete elements are eight node, constant stress, and single-point integration solid hexahedron elements. Single-point integration, constant stress solid elements were selected due to their computational efficiency. Among the material models available in the LS-DYNA, material model 159 was chosen for its ability to accurately model the behavior of concrete under impact loads.

Material model 159 is a continuous surface cap model and was developed, evaluated, and validated for use by the Federal Highway Administration to model the dynamic performance of concrete used in roadside safety structures subjected to vehicle collisions (Murray, 2007). The

www.manaraa.com

user is allowed to choose the unconfined compressive strength, aggregate size, density, rate effects, pre-existing damage, modulus of recovery and erosion criteria. The material model defines the required strengths, stiffness's, hardening, softening, and rate effect parameters as a function of concrete density, compressive strength, and maximum aggregate size. A visco-plastic formulation is used to model an increase in strength of the elements with an increasing strain rate. Damage to the concrete elements is tracked through ductile and brittle damage parameters. Damage effects are governed by the accumulation of strain energy and when a certain threshold is exceeded, damage begins to initiate. The damage thresholds are based on formulations for brittle and ductile damage during plasticity. Brittle damage occurs in regimes where there is a tensile pressure and is dependent on the maximum principle strain. Ductile damage occurs in compressive pressure regimes and is controlled by the amount of total strain. Both the bulk and shear moduli are simultaneously and proportionally reduced as a function of the damage threshold.

Material model 24, which is an elasto-plastic material model takes into account strain rate sensitivity, and was used to model the steel reinforcement. The steel bars used for reinforcement were assumed to have a yield strength of 420 MPa, modulus of elasticity of 200 GPa, tangent modulus of 1,500 MPa, and a mass density of 7,850 kg/m^3. Two node, Hughes-Liu with cross section integration, 2×2 Gauss quadrature, tubular beam elements were used to model the longitudinal and transverse reinforcement. These beam elements were chosen because they allow finite element strains to occur, are simple and computationally efficient, compatible with solid elements, and include finite transverse shear strains (Hallquiest, 2006). Rate effects on yield stress for the steel reinforcement were modeled using the dynamic increases factor formulas established by Malvar et al. (1998) which are discussed later on. The method used to numerically

www.manaraa.com

model the steel reinforcement embedded into the concrete was done by having the steel beam elements share common nodes with the concrete solid elements. This method follows the assumption that there is a perfect bond between the concrete and steel interface.

Hourglass controls

Single-point integrated elements were used in the model due to their relative computational efficiency when compared to using fully integrated elements. The use of these particular elements however is associated with hour glass effects. Hour glassing is defined by local deformations occurring within the single-point integrated elements that have no associated strain or strain energy. Since there is no strain energy associated with such deformed elements, the corresponding stiffness matrix will have no resistance to such deformations. In order to counteract this, hourglass stiffening forces are added at the local element level. The stiffness based controls were used because it is more stable in controlling the hourglass energies and it is the preferred method in auto crash simulations. More specifically, Type 5 Flanagan-Belytschko with exact volume integration hourglass control was used with a recommended hourglass coefficient of 0.05 (Hallquiest, 2007).

Contact algorithm

In order for the truck and the pier to interact during the collision, contact algorithms must be employed. Choosing appropriate contact algorithms can greatly affect the reliability and accuracy of the results. LS-DYNA uses nodal-based and segment-based contact methods. Node-based contact methods detect the penetration of nodes into segments and penalty forces are then applied to the penetration and segment nodes. Segment-based contacts however detect penetrations of one segment into another and penalty forces are applied to the nodes of each

www.manaraa.com

segment. A penalty method is used when calculating contact forces; this method is made up of springs placed normal to the penetrating nodes and contact surfaces.

The automatic surface to surface contact algorithm was used throughout testing because it was known to decreases the mesh hour glassing when compared to other contact methods and was the recommended contact method for crash simulations (Tabiei, 2014). Within this contact method, the nodal-based contact algorithm was used as it is most suitable for two colliding bodies with dissimilar materials and mesh densities coming into contact with one another. This card detects the penetrations of nodes of the contacting segments and applies forces to the penetrating nodes based on the maximum of the two penalty stiffness values, k:

$$k = \frac{\alpha K A^2}{V} \tag{2}$$

$$k = SOFSCL\frac{m}{\Delta t^2} \tag{3}$$

where α is the penalty scale factor, $K$is the material bulk modulus, A is the segment area and V is the element volume. $SOFSCL$ is the force constrain scale factor, m is the nodal mass and Δt is the global time step. A dynamic coefficient of friction value of 0.3 verified by El-Tawil et al. (2005) for vehicle collision analyses was used in the contact card as well.

Model Validation

The chosen material models, hourglass controls, and contact algorithms used for the pier and vehicle models must be validated to ensure reliability and confidence in the results. Concrete is a complex material to model, especially when loaded in dynamic conditions. Choosing a material model that can accurately simulate the actual strain rate sensitivity, stiffness degradation and post-peak softening response is crucial. Also, ensuring that the modeling of the steel reinforcement embedded in the concrete is another vital aspect. To validate the methods used, a

www.manaraa.com

RC beam impact experimental study performed by Fujikake et al. (2009) was successfully replicated. Resulting crack profiles, contact forces, reaction force and mid-span displacement time histories were used as criteria for comparison. Figure 8 and 9 show the crack profile and time history comparison for one of the test specimens. Discrepancy between the quantitative and qualitative results was minimal so the resulting finite element controls were deemed validated.

In order to verify the Ford F800 reduced model and contact algorithms used, the truck was crashed into the bridge pier at 55, 80, 120 and 140 kph. These impact velocities were chosen in order to compare peak contact forces from the results to peak forces recorded from El-Tawil et al. (2005), Mohammed (2011), and Agrawal et al. (2013) shown in Figure 10. The analytical results fell within range of the values reported in the published literature which helped verify that the models were working correctly.

Another method of ensuring that there were no issues with the finite element model was done by analyzing the energy balance of the system. Under impact, the kinetic energy of the moving vehicle is initially dissipated into internal energy through deformations of the vehicle. After the vehicle cannot absorb anymore kinetic energy, the energy is then transferred into the pier until either the vehicle comes to rest or the pier fails. The conservation of energy is an important indicator that assures the models stability and that the kinetic energy of the vehicle is transferred effectively to internal energy within the pier. In a stable, reliable model, the energy balance should show a smooth transfer of the kinetic energy of the vehicle to internal energy in the pier all while having a constant total system energy. The hourglass energy of the system should also be kept within 10% of the total system energy to ensure the accuracy of results (Bala and Day, 2013). Presented in Figure 11 are the energy distributions for the pier undergoing impact velocities of 55, 80, and 120 kph.

www.manaraa.com

Sensitivity Analysis

A sensitivity analysis was performed to determine whether the addition of the superstructure would affect the vehicle collision response of the pier. In this analysis, the contact force time history, shear, moment, and displacement along the height of the pier were compared for both models at impact speeds of 55, 80, and 120 kph. The pier with the modeled super structure will be referred to as 900-SS and the pier without the superstructure will be referred to as 900-NS. Figure 12 shows the comparison of the two contact force time histories. The PDF for the 55 kph impact did not significantly change between the two models, however the PDF for Pier 900-NS occurred approximately 10-ms later than pier 900-SS. Under the 80 kph impact, the PDF did occur at the same time however the PDF for pier 900-NS was 12% larger than pier 900-SS. At an impact velocity of 120 kph, the time histories for the two models were shown to be identical. It is observed that as the impact velocity increases, the difference in contact force response between the two models diminishes.

The shear, moment and displacement comparison of both models are shown in Figure 13. From observations made in the field, Buth et al. (2010) established that shear failure was the governing mode of failure for piers undergoing vehicle collisions. Since shear tends to control the failure mode, the internal forces and displacements were obtained at the time of maximum shear force generated within the piers. At an impact speed of 55 kph, maximum negative and positive shear forces generated within pier 900-SS were slightly larger than pier 900-NS. Maximum negative moments occurring at the base of the piers were identical for both models. Pier 900-NS did experience a fairly larger maximum positive moment occurring at 2 m above ground surface. Also, at an approximate height of 3.8 m above the ground surface, a point of inflection is observed in the moment diagram for pier 900-SS but not for pier 900-NS. This

www.manaraa.com

difference is behavior is attributed to the change in boundary conditions at the top of the pier between the both models. Localized displacements at the location of impact were shown to be much larger for the 900-SS pier as well.

As the impact speeds increased to 80 kph, shear forces between the two models did not vary significantly. Differences between the moments and displacements began to diminish, however pier 900-SS still exhibited lower moments and larger displacements than pier 900-NS. Under a vehicle impact speed of 120 kph, the maximum values for shear, moment and displacements for both piers were almost identical. This is due to the fact that at high impact velocities, only the pier is resisting the collision forces because the duration of impact is so short compared to the natural period of the structure that all parts of the structural system does not get to respond to the abrupt excitation. This reduces the importance of the boundary conditions imposed by the superstructure. The behavior of the moments induced between the two piers however did differ. At a height of 4 m, pier 900-NS had reported positive moments while pier 900-SS had reported negative moments. From these findings, it can be concluded that while the maximum shear forces generated within both piers did not vary significantly. From these findings, it can be concluded that while the maximum shear forces generated within both piers did not vary significantly, the behavior and magnitude with respect to moment and displacements did show noticeable differences.

The next sensitivity analysis investigated the difference between a single-pier and two-pier bent system with a pier diameter of 900 mm and a hoop spacing of 150 mm. Figure 14 shows the contact force time history comparison between the two models. At an impact velocity of 55 kph, the initial peak forces between the two systems are almost identical. However at 60 ms, the single-pier bent system exhibits a secondary peak force while the two-pier system does

www.manaraa.com

not. At an increased impact velocity of 80 kph, the peak contact force the two-pier system is much higher than the latter. This can be attributed to the increase in stiffness provided by the supporting pier. At an impact speed of 120 kph, the peak contact force of the two pier system was shown to be only slightly larger than the single-pier system.

Figure 15 shows the final damage states of each model with plastic straining in the Z-direction for vehicle impact velocities of 55, 80, and 120 kph. For the 55 kph impact test, the one pier system exhibited large amounts of localized straining at the location of impact. Straining in the two pier bent system was shown to be less severe and more distributed throughout the impacted and supporting pier. Under the 80 kph impact test, both bent systems exhibited a shear failure in the impacted pier however the single-pier bent system was shown to undergo slightly more shear failure. The reason why the double-pier bent system experienced less shear failure was due to its increase in stiffness provided by the second pier. Straining in the bent towards the second pier is an indicator that the impacted pier has managed to transfer the forces up into the bent cap and towards the second supporting pier. This relieves some of the demand from the primarily impacted pier resulting in slightly less failure. Under the 120 kph impact, both bent systems exhibit the same amount of straining and failure mode. However, in the two-pier bent system, it is important to note that significant straining did not occur in the second pier. Due to the short duration of impact compared to the natural period of the two-pier bent, the entire structural system did not have enough time to respond to the loading. Hence, the first pier resists the collision alone and fails before any significant forces are transferred throughout the bent and into the second supporting pier.

Shear forces, moments, and displacements along the height of the pier for both systems were obtained at the time of maximum shear and compared in Figure 16. Time of maximum

www.manaraa.com

shear between the two bent systems was shown to differ. For the 55 kph impact case, the maximum shear force for the two-pier bent system occurred approximately 15 ms earlier than the single pier bent system. Also, the shear and moment found in the two pier bent system is slightly larger than the one pier system. Displacements within the single-pier bent system are much larger than the latter as well. This can be attributed to the inherent difference in stiffness of the two systems and the fact that due to a longer duration of impact (due to lower velocity) the two-pier system has the time to respond to the excitation as a whole structural system. As the impact velocity increases to 80 and 120 kph, the time of maximum shear between the two systems began to converge. The shear and moments between the two systems at these velocities began to converge as well. It can be concluded that the pier response with respect to the internal shear and moments does not vary significantly at high impact velocities between a single and two pier-bent systems.

From the sensitivity analyses performed, it can be concluded that the presence of a superstructure as opposed to a lumped mass placed on top of the pier affects the impact response of the pier. It can also be concluded that the effect of having a two pier bent as opposed to a single-pier bent system does not significantly affect the magnitude or distribution of internal forces or failure modes occurring within the impacted pier. In the proceeding work, all bridge pier models will consist of a single pier bent system which includes the pile foundation, pile cap, pier, and the modeled superstructure.

Parametric study

In order to investigate the factors that significantly affect a piers performance with respect to vehicle collisions, a parametric study was performed. Following a thorough study by Gomez and Alipour (2014), three major parameters of pier diameter, hoop spacing and truck

www.manaraa.com

impact velocity were shown to have the most influence on performance of the bridge piers. For this purpose, three pier diameters of 600, 900, and 1,200 mm were investigated. The varying pier diameter was chosen to be a part of the study due to the fact that it controlled the slenderness and the inertia of the pier. It is known that failure modes are dependent on the slenderness and the inertial properties of the column and strongly influence the dynamic response of the structural member.

The piers have a 1% longitudinal reinforcement ratio and are reinforced with No. 25 longitudinal bars. No. 10 hoop bars spaced at 50, 150, and 300 mm to capture the effect of transverse reinforcement on the shear capacity of the piers. The hoop spacing's are chosen as an area of interest in the parametric study as they are proven to control the degree of local shear cracking in experimental work performed by Saatchi and Vecchio (2009) on RC beam components. The natural periods for each pier size are shown in Table 1 and were obtained from an implicit Eigen analysis. The 1997 Ford F800 single unit truck (SUT) reduced model was used with impact velocities set to 55, 80, and 120 kph. In the following sections, there will be a discussion on the comparison of failure modes and internal response with respect to pier diameter, hoop spacing and impact velocity.

Failure modes

Flexural and shear failures were the two primary modes of failure observed throughout the testing. Failure of the longitudinal reinforcement and plastic hinge formation clearly indicate that the flexural strength of the structure has been exceeded. Typically, the plastic hinges formed at the base and top of the pier in addition to the location of impact. Failure mode of this nature was observed for the 600 mm piers under all test cases presented Figure 17. The same failure mode was also seen in a study performed by Tsang et al. (2008) in regards to impact response of

www.manaraa.com

slender columns. The work investigated the required velocity of a vehicle with a constant mass to cause a certain amount of damage to a column. It was stated that the kinetic energy of the vehicle would be dissipated through damage of the vehicle and flexural bending of the column. With the slender nature of the 600 mm pier, a large portion of the vehicles kinetic energy would be dissipated through bending deformations and flexural failure. For the larger diameter piers, the required energy to cause a flexural failure would be much higher than the required energy for shear failure due to their stiffer nature. This explains the shear dominated failure modes in the larger piers.

The 900 mm piers impact response ranged from experiencing no significant damage at all to shear only and shear-flexure failure modes. The piers with hoop spacing's of 50, 150 and 300 mm were able to sustain the 55 kph impact without experiencing much damage, shown in Figure 18 (a). At an impact velocity of 80 kph however, the piers with a 150 and 300 mm hoop spacing both experienced shear failure as shown in Figure 18 (b). A mixed mode of flexural and shear failure was observed for all three hoop spacing's at an impact speed of 120 kph. Diagonal cracking throughout the concrete core as well as plastic hinge formation was observed (Figure 18c). It was also observed that as the hoop spacing decreased, the amount of damage and deterioration increased, which is attributed to the lack of confinement. The confinement strength of each pier was calculated in accordance to the method developed by Mander et al. (1989) and is shown in Table 2. A strength increase ranging from 25-50 % was observed when hoop spacing decreased from 300 mm to 50 mm.

Another reason for the increased amount of deterioration observed in piers with lower transverse reinforcement is due to the shear crack control provided by the transverse reinforcement. A beam impact study performed by Saatci & Vecchio (2009) had shown that an

www.manaraa.com

increased amount of transverse reinforcement was able to control the degree of major localized cracking and deterioration of the concrete beam. The specimens with high ratios of transverse reinforcement were able to better redistribute the shear forces from the impact loads resulting in less severe and more distributed cracking along the length of the beam. Specimens with relatively lower shear reinforcement experienced larger localized shear cracks and deformations that accumulated around the point of impact.

The 1200 mm piers performed the best out of all the three pier sizes. No significant failure was observed in the 1200 mm pier at impact speeds of 55 and 80 kph; only tensile cracking of the concrete cover at the piers outer face was observed. As seen in Figure 19, shear failure only occurred at an impact velocity of 120 kph. The 1200 mm pier performed well due to its adequate stiffness allowing it to fully absorb and transfer the kinetic energy of the vehicle to the supports without causing significant structural damage. Stiffness of the pier was of great importance in resisting the impact loads.

A stiff pier is capable of absorbing the impact load and redistributing the generated forces to the support systems without failing. This can be seen in Figure 20 (a) which presents the 80 kph post impact condition of the 600 mm pier. The pier has completely failed and was unable to transfer the impact force to the supports which are indicated by the lack of straining in the footing and superstructure. Observations made from Figure 20 (b) shows that the 900 mm pier was able to redistribute the impact load down into the footing but has failed in shear before the superstructure could provide any additional resistance. The 1200 mm pier shown in Figure 20 (c) was able to resist the impact load and redistribute the forces throughout the structural system without accumulating any significant damage. Large amounts of straining can be seen in both the footing and superstructure.

www.manaraa.com

Figure 21 similarly shows the axial straining in the steel reinforcement indicating that the pier experienced a flexural failure before the supports could provide resistance. Figure 21 (a) shows excessive strains in the reinforcement for the 600 mm pier in the areas where plastic hinges have formed. The 900 mm pier shown in Figure 21 (b) shows the majority of the axial reinforcement straining located where the pier failed in shear. Minimal reinforcement straining was observed towards the top of the pier which indicates the impact forces were not able to be transferred to the superstructure. This explains the lack of straining observed in the superstructure for this pier shown in Figure 20 (b). Figure 21 (c) shows the majority of axial reinforcement straining towards the top of the 1200 mm pier. This is because the reinforcement was able assist in transferring the forces to the support system located at the superstructure.

Internal forces

Internal shear forces were obtained for all three pier sizes with a hoop spacing of 50 mm as shown in Figure 22. The maximum negative shear forces occurring at 0.5 m were shown to be much larger than the maximum positive shear occurring at 1.0 m height of the pier. This explains the tendency for the shear failure to occur at the base of the pier rather than at the location of impact. At an impact velocity of 55 kph, the shear forces generated throughout each pier do not vary significantly. However, the maximum shear in the 600 mm pier is slightly less than the shear in the other two piers. As the velocity of the impacting trucks increase, this observation becomes more visible. Under the 80 kph impact, the shear in the 600 mm pier is at least 80% smaller when compared to the other two piers and at an impact velocity of 120 kph, the difference is more than double. This is attributed to the fact that the 600 mm pier fails in flexure before any additional shear forces can be generated at impact velocities greater than 55 kph.

www.manaraa.com

From the sensitivity analysis, it was found that the kinetic energy of the impacting vehicle was the primary factor in governing the shear demand on the pier. The diameter of the pier determined the failure mode whether it be flexure, shear-flexure, or shear. Lastly, the transverse reinforcement detailing controlled the degree of local failure occurring at the point of impact at the pier because of the confinement effects and shear cracking control. It can be concluded that when designing a bridge pier for a vehicular collision event, these three factors must be accounted for the analysis and design.

Performance-Based Design

Performance-based design (PBD) is a design method implemented for structures undergoing extreme loading events such as earthquakes and is based on achieving certain performance objectives when the structure is loaded. The goal of this design approach is to achieve a balance between cost and structural performance while taking into consideration the importance of the structure. The different performance objectives, or also referred to as performance levels represent how severely the structure will be damaged when loaded. Each performance level is associated with an acceptable amount of loss resulting from the damage which includes casualties, service, and economic costs. In this design philosophy, a design based on certain performance levels that will assure safety in addition to economic considerations is required. In the context of seismic PBD, some structures such as hospitals or schools may need to have very strict performance levels which allow the structure to undergo minimal damage in order to allow for uninterrupted operations right after the event. On the other hand, targeted performance levels may be more lenient for some structures that may not be as vital to life safety while in operation. This would allow for some damage to occur but not so much that the structure would collapse. As a result, the structure would be taken out of operation after a major

www.manaraa.com

event but keeping the public or private residence safe from harm. A PBD ultimately gives flexibility to the owner allowing them to tailor their design based on the importance of the structure, location, and economic constraints.

PBD has shown to be an effective method for designing structures undergoing seismic loads. Applying the same school of thought for design of bridges under truck collisions would let the bridge owners to tailor the design requirements to the importance of the bridge as part of a larger transportation network. The benefits of adopting the PBD would consist of cost effective designs while still providing adequate protection against sudden and un-accounted for failures. This adaptive method will be able to take into account the highly dynamic nature of the loading event as well as the plasticity that is observed in the crash tests and numerical analyses but are not accounted for in the current provisions. Sharma et al. (2012) generated a framework for PBD based on the dynamic shear force capacity and demand of a column but the models developed and used were very limited in application. Agrawal et al. (2013) related damage ratios to the observed failure modes in the pier as well as its performance. However, the empirical formulations developed for design pertain strictly to the researcher's finite element model. In this study, the objective in developing a PBD for bridge piers is to create a simple intuitive method for designers that don't require the extensive use and calibration of finite element models. The finite element models generated and validated in the previous section of this study were used to implement the basis of the proposed PBD approach. Later, the concluding results were used to generate new design equations that provide the bridge designers with a new tool to consider different varying aspects of a collision without the need to create extensive finite element models

www.manaraa.com

Performance-based criteria

In order to measure the performance of each pier during the analyses, the concept of damage ratios was created in this study. There are a total of three performance levels that are associated with minor, moderate damage, and severe damage states. The failure modes associated with the minor damage state are tensile cracking of concrete and minor yielding of the longitudinal reinforcement. The moderate damage state is defined by the major yielding and plastic deformations occurring within the steel reinforcement as well as minor concrete core deterioration. Lastly, the severe damage state is assigned to a pier when plastic hinges form in the pier and/or major erosion of concrete core occurs. Examples of the provided damage states can be seen in Figure 23.

The first performance level defined is immediate serviceability which is associated with the structure experiencing minor damage. In this performance level while the structure has undergone some minor cracking and spalling, the original strength and stiffness is still retained. It is possible to restore the pier to a safe and operable condition without major repairs or closures. Life safety is the next performance level which is associated with the moderate damage state. There is still some residual strength in the structure and the structural elements responsible for sustaining gravitational loads are still functional. Closure of the bridge for immediate repairs is recommended even though there is a small probability of collapse. Repairing the structure is possible but may not be economical in some circumstances. Lastly, the final performance level is defined as collapse prevention which is linked to the severe damage state. There is minimal residual strength and stiffness in the structure. Load bearing elements are still able to support the gravitational loads without collapsing, however the structure is deemed unsafe. Immediate closure is advised and partial or full replacement of the structure is required.

www.manaraa.com

The overall objective of the study is to create a method to predict the expected amount of damage from a pier with respect to the vehicle mass, impact velocity and pier design as these three factors are shown to govern the overall performance of the pier. In order to achieve this goal, the resulting damage states of the piers observed throughout the impact simulations were quantified through an index called the damage ratios. These damage ratios are based on the kinetic energy of the vehicle, pier diameter and shear strength. The calculated damage ratios can be associated with appropriate damage states of the pier which then corresponded to certain performance levels. The expression developed to calculate the damage ratios shown below is a simple intuitive process that does not require or rely on the use of extensive finite element analyses but has been validated using the finite element models developed in the previous section.

$$Damage\ Ratio = \frac{\frac{Kinetic\ Energy\ (kJ)}{\emptyset V_C\ (kN)}}{Pier\ Diameter\ (m)} \tag{4}$$

In order to calculate the dynamic shear capacity of each pier, the method prescribed by AASHTO LRFD Bridge Design Specifications (2012) in Section 5.8.3.3 was used. The shear resistance,V_n, is specified to be calculated as the lesser of:

$$V_n = V_c + V_s + V_p \tag{5}$$

$$V_n = 0.25 f_c' b_v d_v + V_p \tag{6}$$

in which:

$$V_c = 0.0316 \beta \sqrt{f_c'} b_v d_v \tag{7}$$

$$V_s = \frac{A_v f_y d_v (cot\theta + cot\alpha) sin\alpha}{s} \tag{8}$$

www.manaraa.com

where f_c' is the unconfined compressive strength of the concrete (MPa), b_v is the effective web width taken as the diameter of the pier (mm), d_v is the effective shear depth determined using Figure 24 (mm), s is the spacing of the transverse reinforcement parallel to the longitudinal bars (mm), β is the factor indicating ability of diagonal cracked concrete to transmit tension and shear, θ is the angle of inclination of diagonal compressive stresses (degree), α is the angle of inclination of transverse reinforcement to longitudinal axis (degrees), A_v is the area of shear reinforcement within distance s (mm^2), V_p is the component in the direction of the applied shear of the effective prestressing force and is taken as 0 since no prestressing forces are used in the piers (kN). The values for β and θ were calculated by the following equations:

$$\beta = \frac{4.8}{(1 + 750\varepsilon_s)} \tag{9}$$

$$\theta = 29 + 3500\varepsilon_s \tag{10}$$

where ε_s is the net longitudinal tensile strain in the section, set to 0.006 mm/mm based on the maximum strain that would occur during a severe impact condition (Buth et al. 2010). A shear resistance factor, φ_v, of 0.9 was used to determine the nominal shear resistance of the piers.

It is known from past research performed by Asprone et al. (2009 and 2010) that concrete and steel are known to exhibit a certain degree of strength enhancement when under high rates of loading. Many factors are a function of this increase in strength such as strain rate and inertial effects. Calculating strain rate effects for material properties were needed in order to determine the dynamic shear capacity of the bridge piers.

www.manaraa.com

The unconfined compressive strength of the concrete and yield strength of the reinforcing steel were scaled using equations developed by the CEB (1988) and Malvar et al. (1998). Dynamic increase factors for each vehicle impact scenario were obtained by using the average strain rates observed in the post processing portion of the modeling. For the 55, 80, and 120 kph vehicle impacts, the average strain rates observed were 30 s^{-1}, 60 s^{-1}, and 70 s^{-1}.The concretes compressive and tensile strength DIF was calculated from the CEB (1988) expressions given by:

$$DIF_{cc} = \Upsilon_s \left(\frac{\dot{\varepsilon}}{\dot{\varepsilon}_s}\right)^{\frac{1}{3}} \qquad \begin{cases} \log(\Upsilon_s) = 6.156\alpha_s - 2 \\ \alpha_s = (5 + 9\frac{f_{cs}}{f'_c}) - 1 \end{cases} \tag{11}$$

$$DIF_{ct} = \beta \left(\frac{\dot{\varepsilon}}{\dot{\varepsilon}_s}\right)^{\frac{1}{3}} \qquad \begin{cases} \log(\beta) = 7.11\Upsilon - 2 \\ \Upsilon = (10 + 6\frac{f_{cs}}{f'_c})^{-1} \end{cases} \tag{12}$$

which were based on the dynamic tensile strength (f_{cs}), static concrete strength of 10 MPa (f'_c), static strain rate ($\dot{\varepsilon}_s$) equal to $30 \times 10^{-6}\ s^{-1}$, recorded strain rate ($\dot{\varepsilon}$) ranging from $30 \times 10^{-6} - 300\ s^{-1}$. To account for the DIF due to strain rate sensitivity of the steel reinforcement, the proposed equations developed by Malvar et al. (1998) have been used. The DIF is calculated based on the strain rate ($\dot{\varepsilon}$), α factor, and f_y which is the bar yield strength in MPa. These equations shown below are only valid for yield stresses between 290 and 710 MPa, and for strain rates between 10^{-4} and 225 s^{-1}.

$$DIF_{steel} = \left(\frac{\dot{\varepsilon}}{10^{-4}}\right)^{\alpha_{fy}} \qquad \alpha_{fy} = 0.074 - 0.040\frac{f_y}{414} \tag{13}$$

www.manaraa.com

Target performance levels with the corresponding failure modes and damage ratios are summarized in Table 3. All test cases have shown to correlate the final damage states of each pier to the corresponding failure mode(s), damage ratio and performance level. Piers that experienced minor damage had resulted in failure modes FM-1 and FM-2 which involve localized spalling of the concrete cover and tensile cracking of the concrete. Calculated damage ratios within this damage state ranged between 0 – 1.0. All piers with a damage ratio ranging from 1.0 – 1.5 were classified as a moderate damage state and experienced failure modes FM-3 and FM-4. These two failure modes were denoted by the yielding of reinforcement and shear cracking of the concrete. Any pier with a calculated damage ratio ranging from 1.5 – 2.0 was classified as severe damage. Failure modes FM-5 and FM-6 accompanied this damage state and involve the deterioration of the concrete core as well as any plastic hinge formation. Piers with a damage ratio greater than 2.0 had completely failed. Table 4 summarizes the calculated damage ratios for all test cases. This method proves to be capable in predicting the amount of damage a pier will undergo with respect to the kinetic energy of the impacting vehicle, dynamic shear capacity of the pier and diameter of the pier.

In order assess the reliability of the proposed design methodology, four additional test cases were run. The first three test cases involved an 800 mm diameter pier with a hoop spacing of 150 mm. The impacting vehicle collided with the piers at a velocity of 55, 80 and 120 kph. Before the tests were run, the damage ratios were calculated for all three cases. For the 55, 80 and 120 kph impacts, the resulting damage ratios were calculated to be 0.88, 1.80, and 3.86. Thus a minor, severe and total failure damage state would be expected for the following cases. For the fourth test case, a 1500 mm pier with a hoop spacing of 300 mm was tested under a 120

www.manaraa.com

kph impact. A damage ratio of 1.57 was calculated which just barely categorizes the damage state of the pier as severe.

Figure 25 shows the post impact conditions of the 800 mm pier at impact velocities of (a) 55, (b) 80, and (c) 120 kph. The 55 kph impact test case shows a minor damage state; there are no severe deformations or erosion of the concrete observed. Severe shear cracking and erosion of the concrete core can be seen in the base of the pier for the 80 kph impact test case thus resulting in a severe damage state. With the entire base of the pier deteriorated, total failure due to shear is observed for the 120 kph impact case. The 1500 mm pier exhibited major flexural cracking and a large longitudinal crack propagating from the superstructure down towards mid height of the pier which can be seen in Figure 26. Using equation (4), this pier was just barely categorized into the Collapse Prevention performance level with a damage ratio of 1.57. One could argue that this pier would be categorized into the life safety performance level. However, due to the severity of the cracking observed in the piers core, it is conservative to categorize the pier into a collapse prevention performance level. Predicting the performance levels using the newly proposed damage ratio index for all of the bridge piers, including the four additional test cases was shown to be a success. Therefore, equation (4) was validated to estimate the approximate damage state of a pier acting under a vehicle collision.

Based on the results from the presented work, a design approach for bridge piers subjected to vehicle impacts can be broken down into the following steps. First the performance level of the bridge is chosen by the owner in accordance to the importance of the bridge, location, and economic constraints. Next, the design vehicle and velocity is chosen in order to calculate the resulting kinetic energy. The engineer must then design the pier with the appropriate diameter and steel reinforcement detailing. Using equation (4) and the damage index

www.manaraa.com

presented in Table 3, the damage ratio for the bridge undergoing a vehicle collision must be calculated. If the damage ratio does not satisfy the respective performance level on the damage index, the design must be reiterated; the entire design process can be seen below in a simplified flow chart.

Proposed design approach

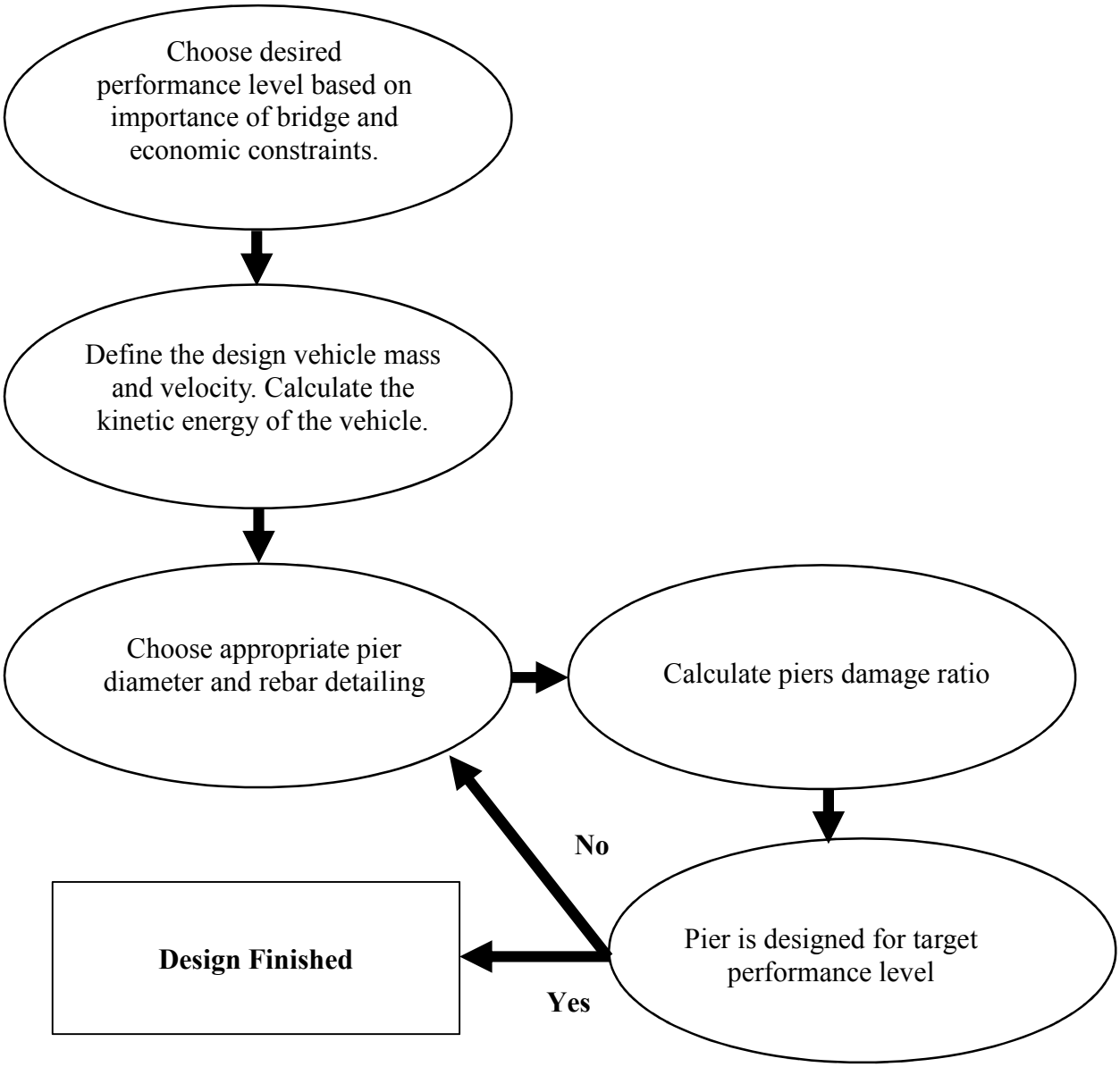

www.manaraa.com

Conclusion

From the literature review, it was found that vehicle collisions are the second leading cause of bridge failure in the United States. The ASCE rated the United States bridges a C+ for the year of 2013 and estimated that one in nine bridges were rated structurally deficient. With the current health of our bridges, they are very vulnerable to failure from vehicle collisions. Bridge failures due to collision events although rare could have a detrimental impact on the transportation network they are part of with possible rippling effects on the economy of the region they are serving. It was shown from previous published work that AASHTO's design specifications failed to capture the piers response to a vehicular collision. In response to this, a bridge pier bent consisting of the superstructure, pier, and the full foundation was modeled to study the effects different parameters such as impact velocity, pier diameter, and transverse reinforcement ratio on performance of the RC piers collided by trucks. The finite element controls, contact algorithms, and material models were initially validated by successfully replicating RC beam impact experiments. Results from the analysis were accurate when comparing the resulting contact forces, mid-span displacements, and crack profiles from the experiment. The bridge pier models were again validated by comparing contact forces and damages resulting from the impact simulations with the results of previous published work. The conservation of energy throughout each simulation were closely monitored to ensure that model was stable and providing accurate results as well.

The analyses were representative of at least level 4 AASHTP recommended analyses with some variability in the parameters for the purpose of the sensitivity analyses. A novel *damage ratio index* was proposed to estimate the level of damage different piers could experience under different kinetic energies imposed by the colliding trucks. This newly defined

www.manaraa.com

damage ratio is a function of the kinetic energy of the vehicle, pier diameter, and dynamic shear capacity of the pier. These three factors were found to significantly govern the performance of a pier to collision loadings in preliminary steps of this study. The defined damage ratio indices were then related to different damage states that defined the performance levels of the structure. Then the performance-based design philosophy, a method of design well accepted in seismic design community, was created that helps the designers and the bridge owners to tailor their design based on the importance of the structure as well as possible economic implications of the design. The proposed methodology will be a step forward in the design of safer yet more economic bridges under vehicle collisions. The proposed damage ratio index is only a function of the expected kinetic energy of the colliding vehicle (mass and velocity) and the proposed design of the pier (pier diameter and dynamic shear capacity). This performance-based design methodology is simple to implement and does not require extensive finite element models. Hence, it is a very suitable method for bridge design engineers.

Future work would entail finite element testing of vehicle collisions with different design parameters for bridge piers such as varying geometrical shapes and longitudinal reinforcement. Also, variations in impact conditions are to be considered such as using larger vehicles and increasing the impact velocity. Lastly, analyzations would be made for the bridges superstructure and foundation system in order to incorporate them into the damage index.

www.manaraa.com

Table 1. *Natural frequencies and periods of corresponding piers*

Diameter (mm)	Natural Frequency (rad/s)	Period (s)
600	**16.39**	**1.55**
900	**25.39**	**1.25**
1200	**16.15**	**1.23**

Table 2*. Confined concrete strength (MPa) with respect to pier diameter and hoop spacing*

Hoop Spacing (mm)	Pier Diameter (mm)		
	600	900	1200
50	41.7	37.2	34.9
150	32.1	30.9	30.2
300	29.4	29.2	29

Table 3. *Performance based design criteria*

Performance Level	Damage State	Failure Mode	Description	Damage Ratio
Immediate Serviceability	Minor	FM-1 FM-2	Localized spalling of concrete cover Tensile cracking of concrete	0 - 1.0
Life Safety	Moderate	FM-3 FM-4	Yielding of reinforcement Shear cracking	1.0 - 1.5
Collapse Prevention	Severe	FM-5 FM-6	Deterioration of concrete core Plastic hinge formation	1.5 - 2.0

www.manaraa.com

Table 4. *Damage ratio's for all test cases*

Pier Diameter (mm)	Hoop Spacing (mm)	55 kph	80 kph	120 kph
600	50	1.16	2.69	4.04
	150	2.41	5.56	8.26
	300	5.25	11.96	17.57
900	50	0.46	0.95	1.36
	150	0.95	2.01	2.78
	300	2.06	4.29	5.87
1200	50	0.24	0.47	0.62
	150	0.49	0.96	1.27
	300	1.05	2.04	2.67

Figure 1*. Pier support failure caused by tractor-trailer impact in Grand Junction, CO (Gallegos and McPhee 2007)*

Figure 2*. Resulting damage caused by the tractor-trailer collision with the SC Highway 150 bridge over I-85 (Kudelka 2011)*

www.manaraa.com

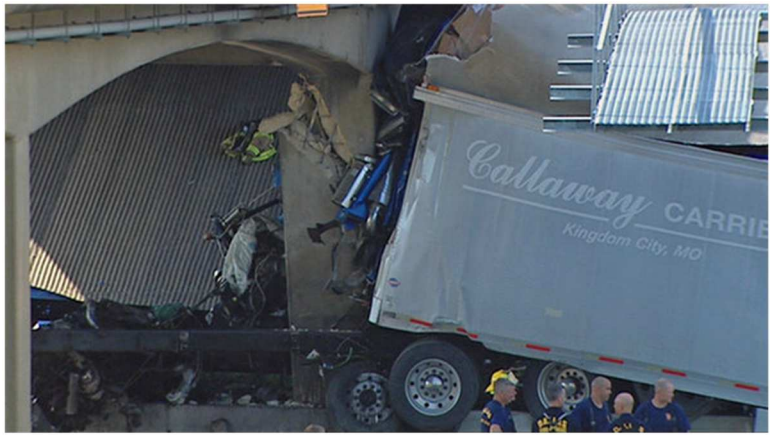

Figure 3. *Tractor-trailer collision with the I-30 bridge over Dolphin Road (Vega 2012)*

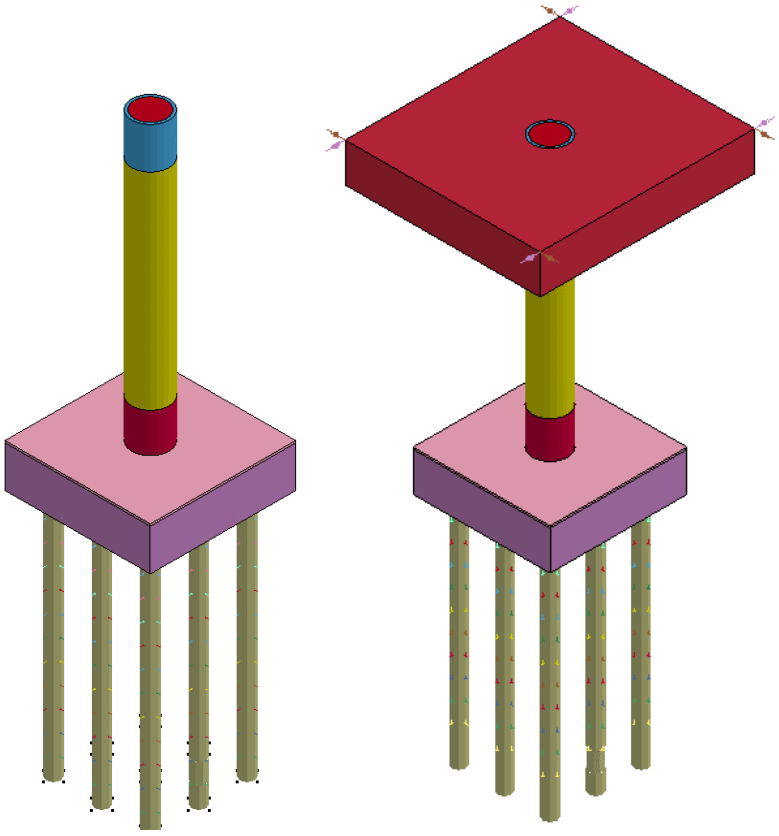

Figure 4. *FE model of pier (a) 900-NS and (b) 900-SS*

www.manaraa.com

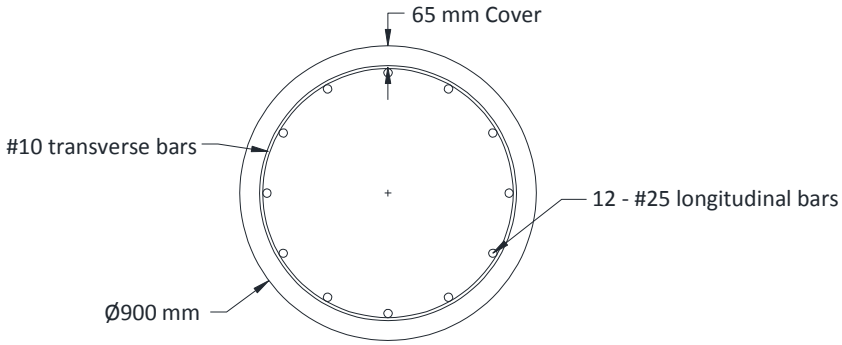

***Figure 5**. Cross sectional view of 900 mm diameter bridge pier*

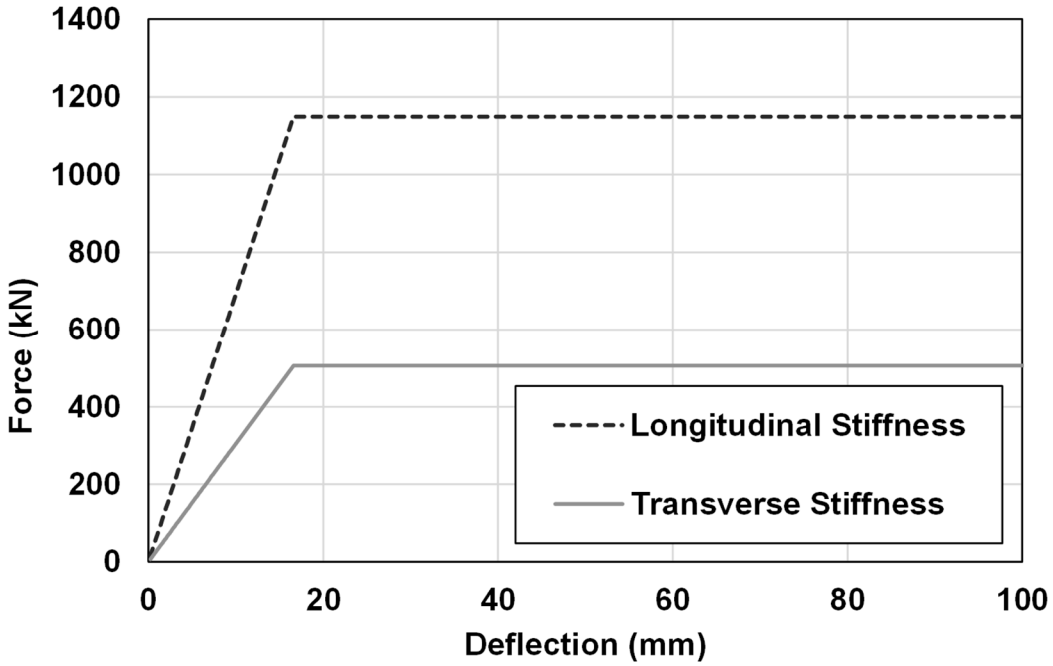

***Figure 6**. Longitudinal and transverse abutment stiffness's used for the superstructure springs*

www.manaraa.com

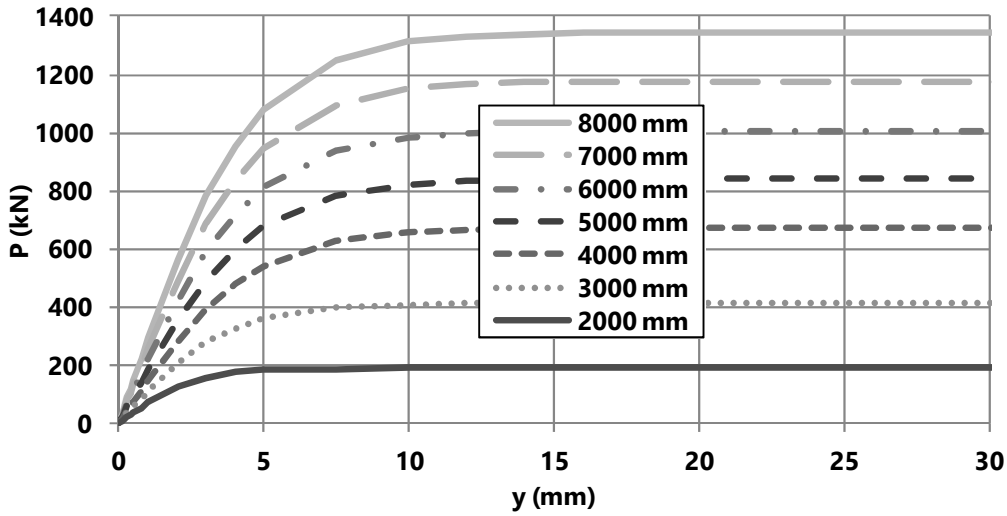

***Figure** 7. Spring stiffness p-y curves used for the soil springs*

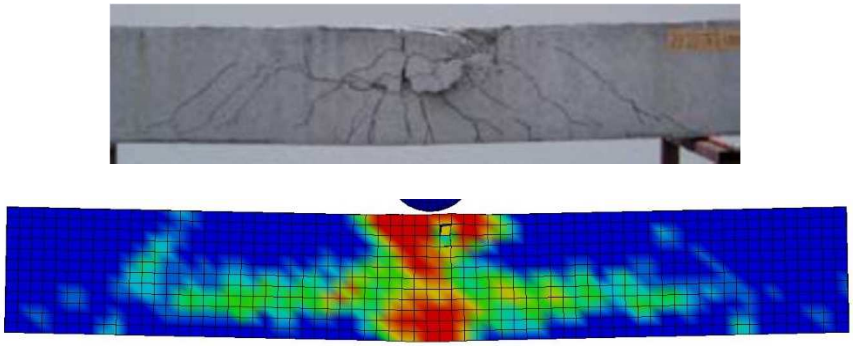

***Figure 8.** Crack profile comparison between finite element model and Fujikake et al. (2009)*

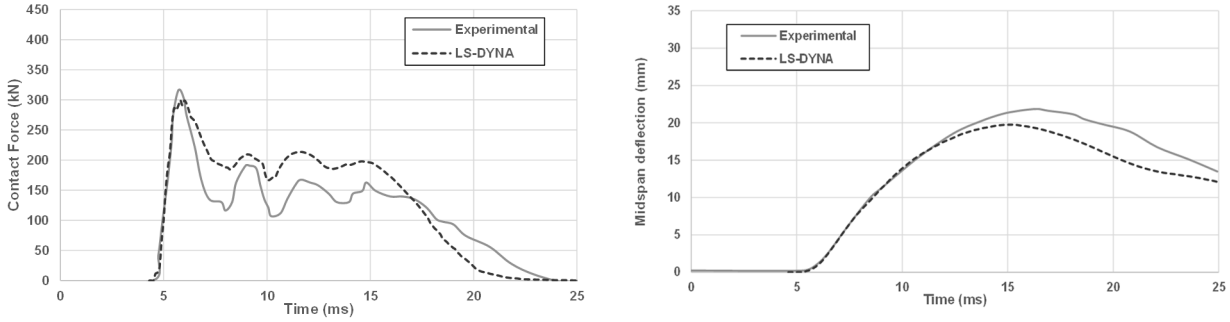

***Figure 9.** Contact force and mid-span displacement between finite element model and Fujikake et al. (2009)*

www.manaraa.com

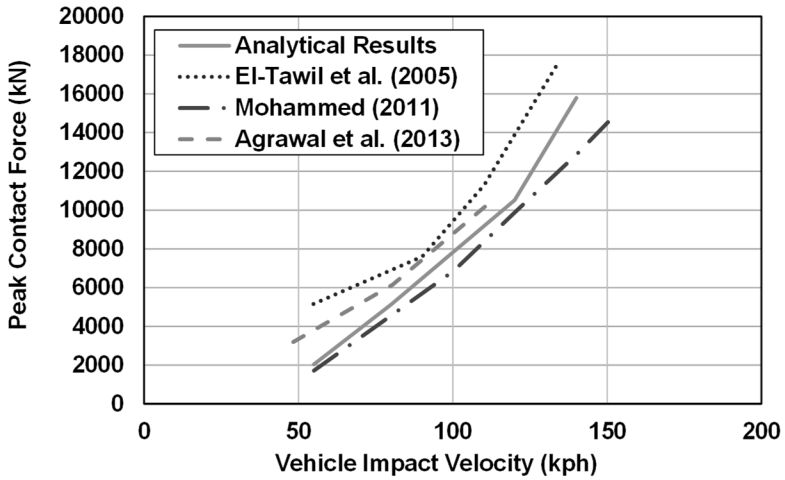

***Figure 10**. Comparison of analytical results and results from Agrawal et al. (2013), El-Tawil et al. (2005) and Mohammed (2011).*

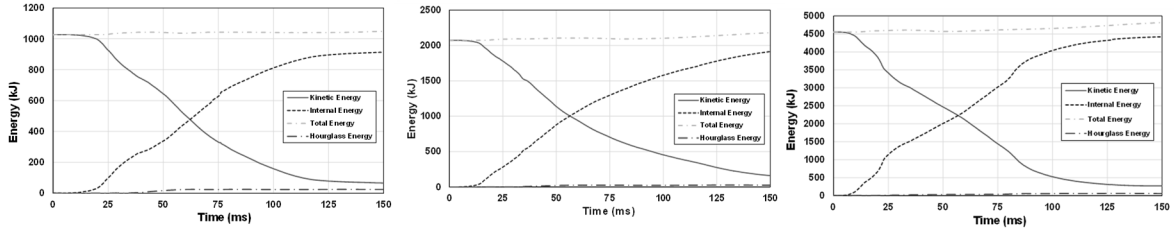

(a) 55 kph (b) 80 kph (c) 120 kph

Figure 11. Energy balance of the 900 mm pier with a hoop spacing of 50 mm

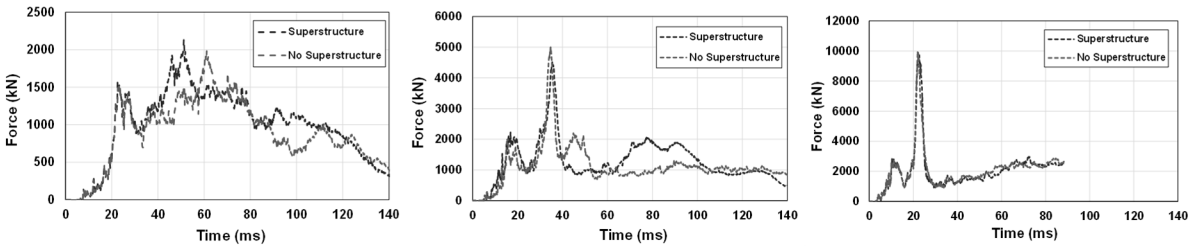

(a) 55 kph (b) 80 kph (c) 120 kph

***Figure 12**. Contact force time histories for pier 900-NS and 900-SS at impact velocities of (a) 55, (b) 80, and (c) 120 kph*

www.manaraa.com

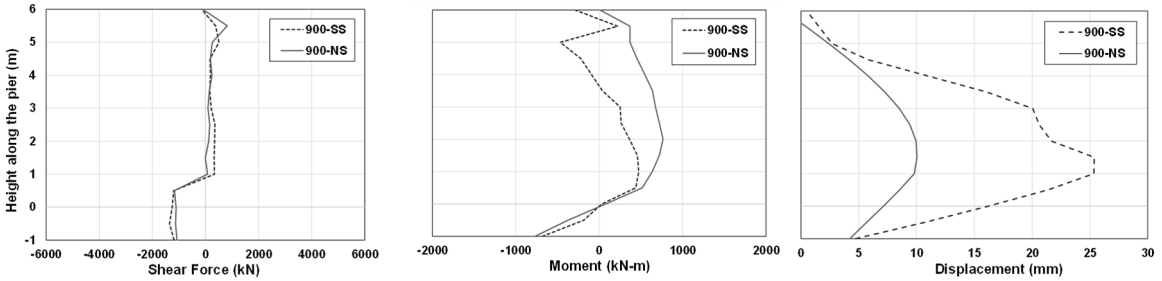

(a) V = 55 kph, Time=0.533 ms

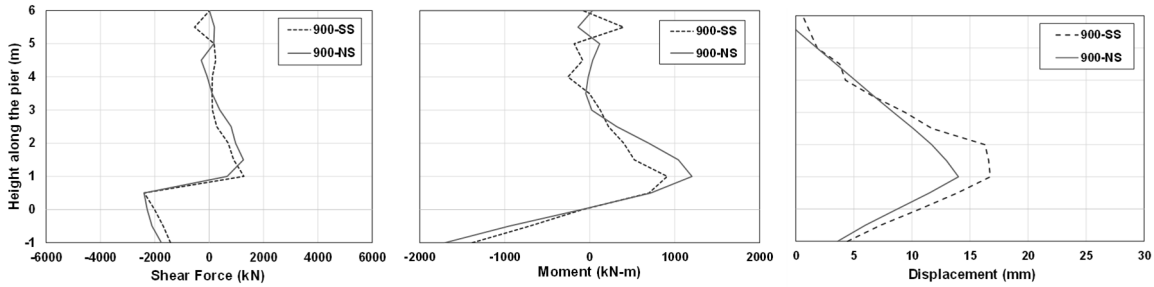

(b) V = 80 kph, Time = 0.355 ms

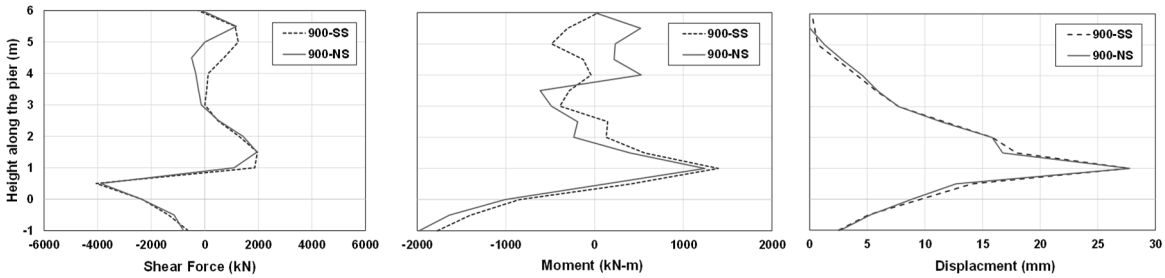

(c) V = 120 kph, Time = 0.227 ms

Figure 13. *Shear, moment and displacement of piers at time of maximum shear at impact velocities of (a) 55, (b) 80, and (c) 120 kph*

www.manaraa.com

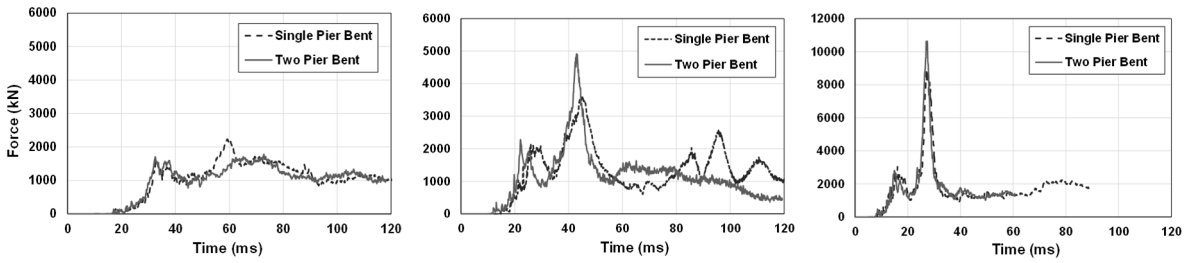

Figure 14. *Contact force time histories for pier 900-NS and 900-SS at impact velocities of (a) 55, (b) 80, and (c) 120 kph*

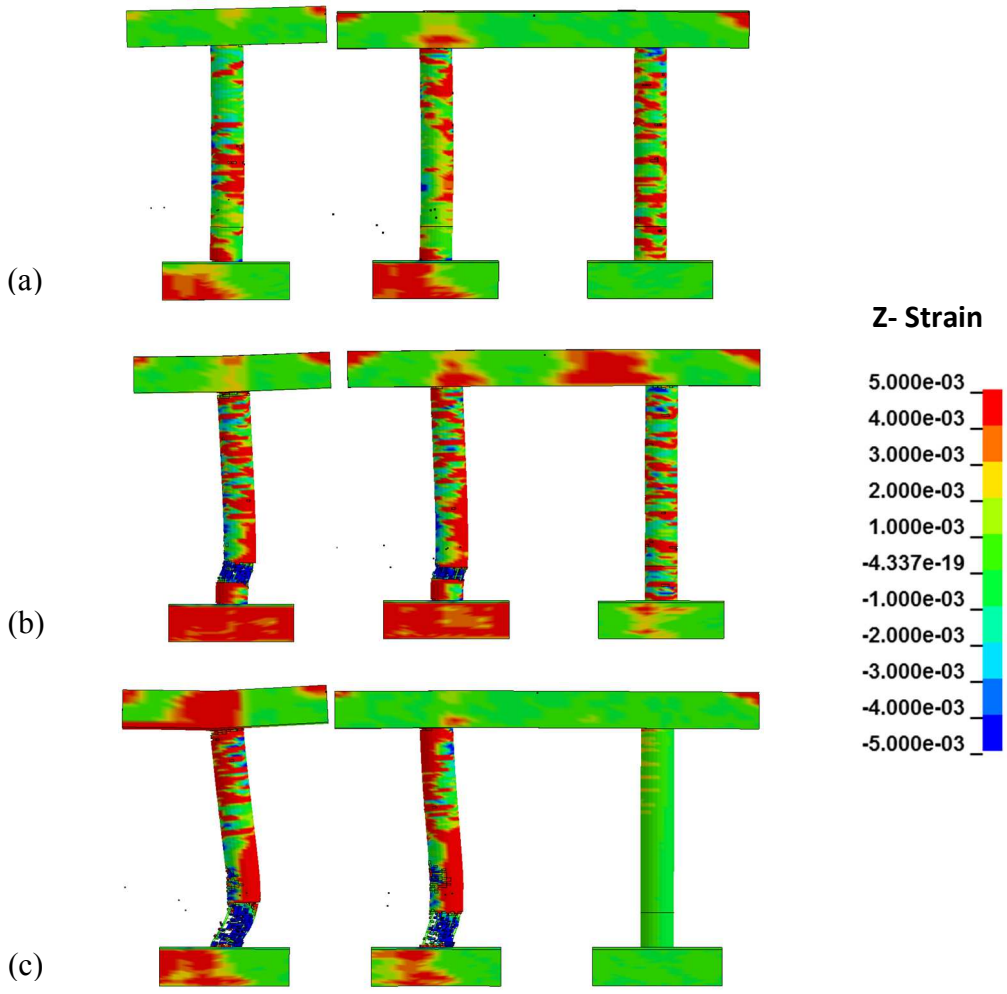

Figure 15. *Strain contours in the Z-direction of the single pier and double pier bent system for impact velocities of (a) 55, (b) 80, and (c) 120 kph*

www.manaraa.com

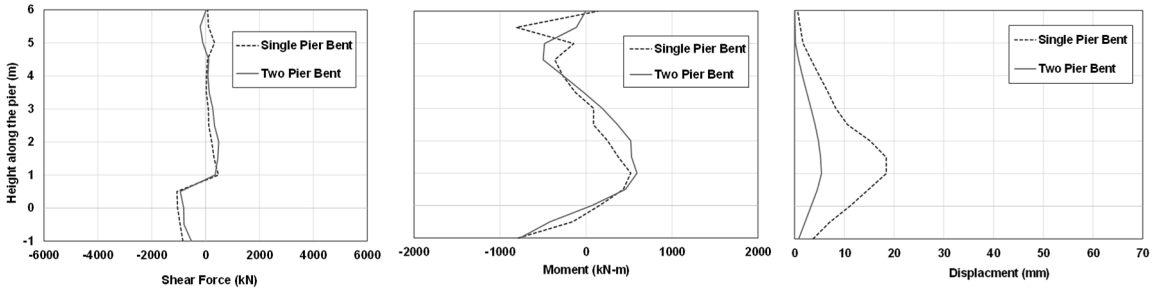

(a) 55 kph

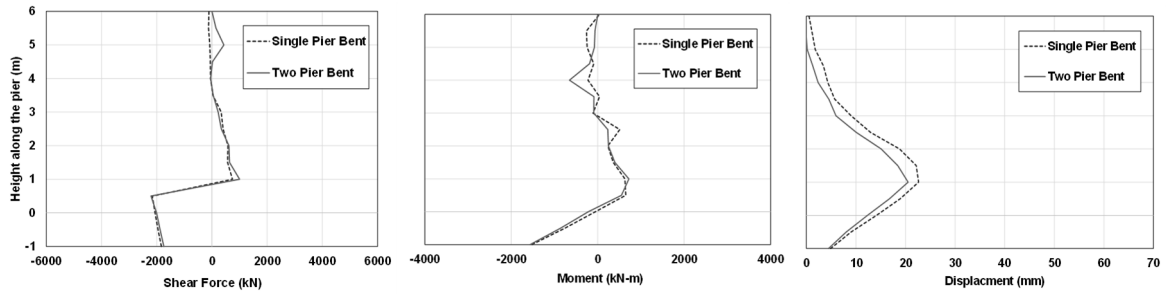

(b) 80 kph

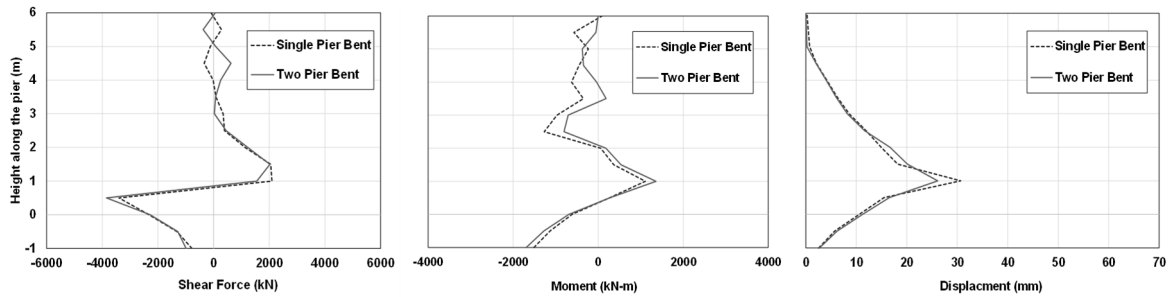

(c) 120 kph

Figure 16. *Shear, moment, and displacement along the height of the pier at time of maximum shear for vehicle impact velocities of (a) 55, (b) 80, and (c) 120 kph*

www.manaraa.com

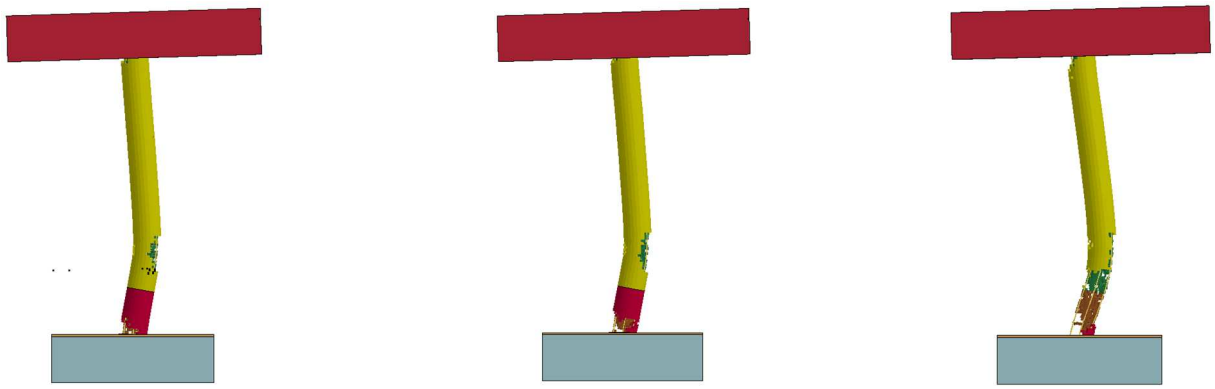

(a) 55 kph

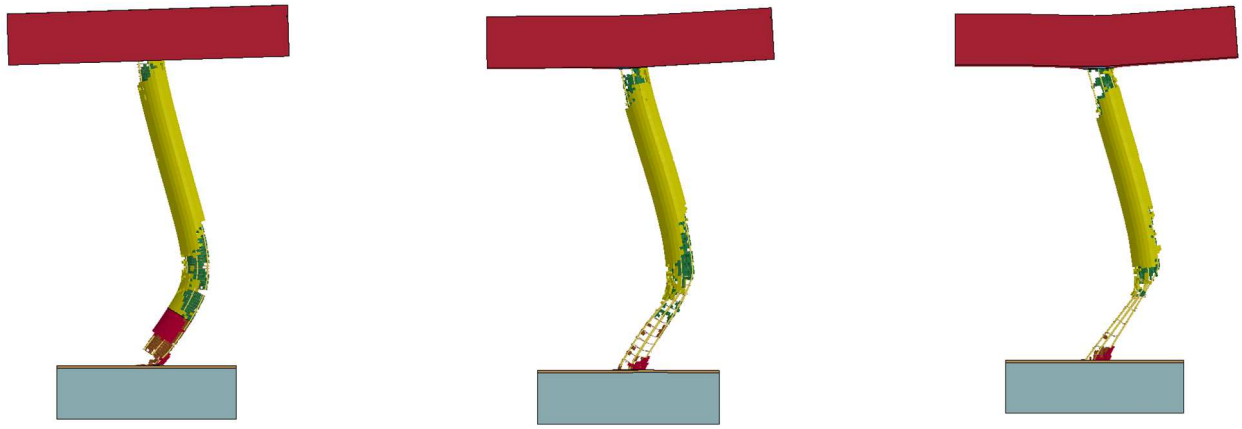

(b) 80 kph

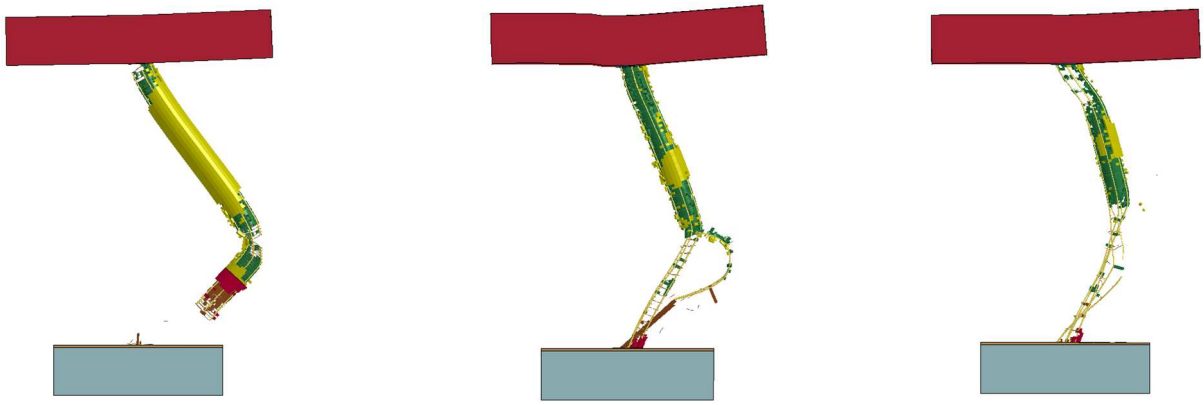

(c) 120 kph

Figure 17*. 600 mm pier post impact response at various impact velocities with hoop spacing's of 50 (left), 150 (center), and 300 mm (right)*

www.manaraa.com

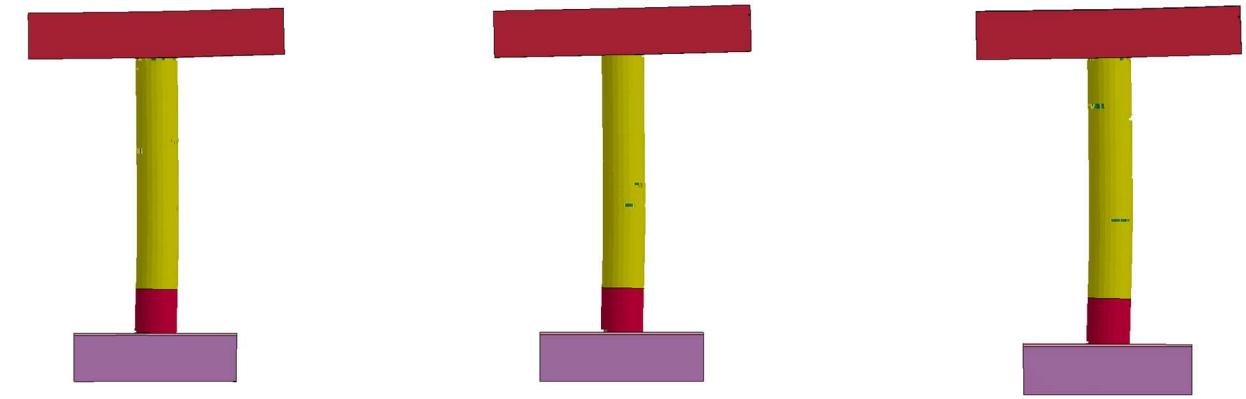

(a) 55 kph

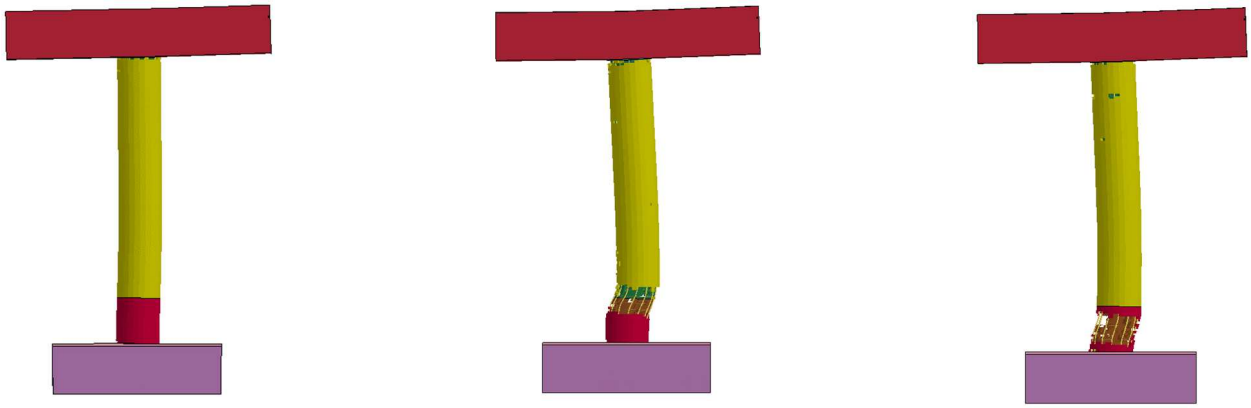

(b) 80 kph

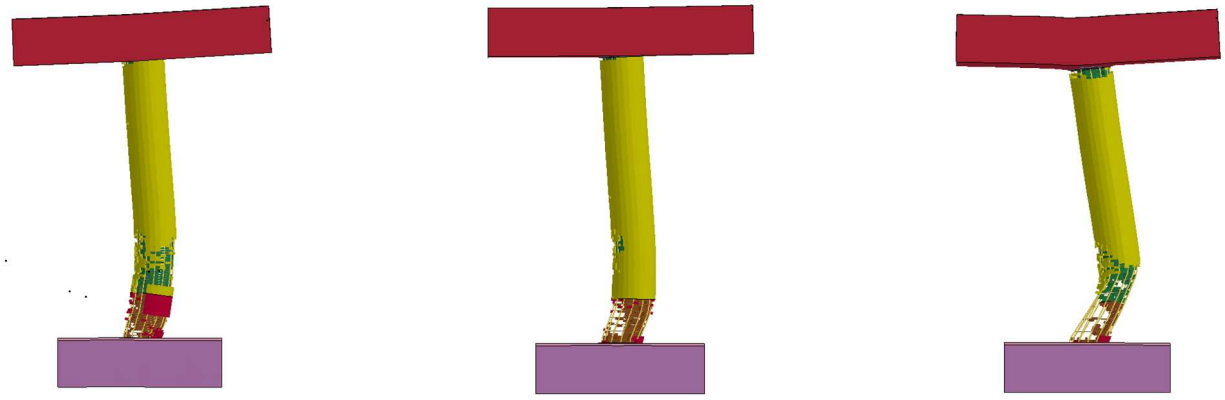

(c) 120 kph

Figure 18 *900 mm pier post impact response at various impact velocities with hoop spacing's of 50 (left), 150 (center), and 300 mm (right)*

www.manaraa.com

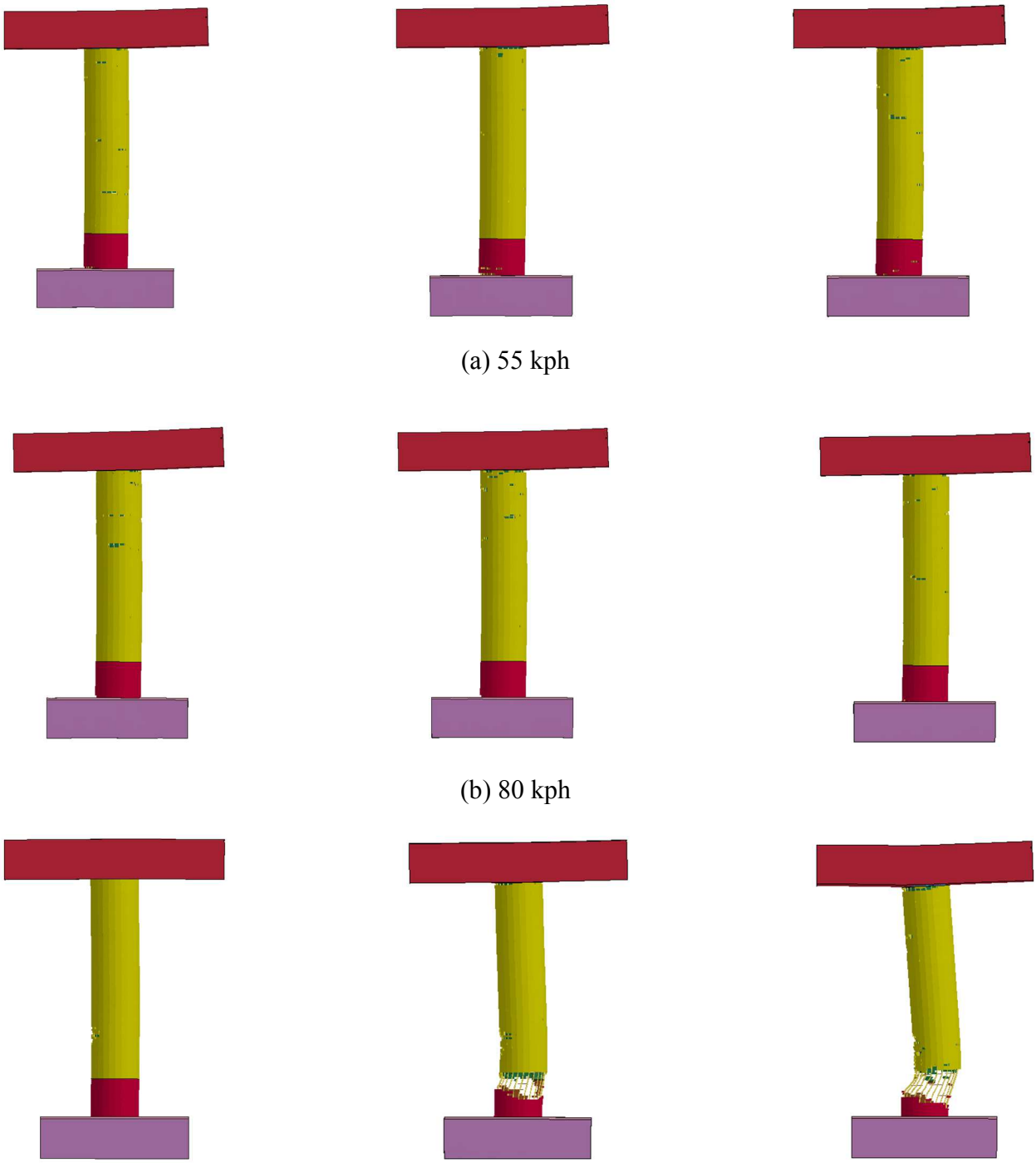

(a) 55 kph

(b) 80 kph

(c) 120 kph

Figure 19. *1200 mm pier post impact response at various impact velocities with hoop spacing's of 50 (left), 150 (center), and 300 mm (right)*

www.manaraa.com

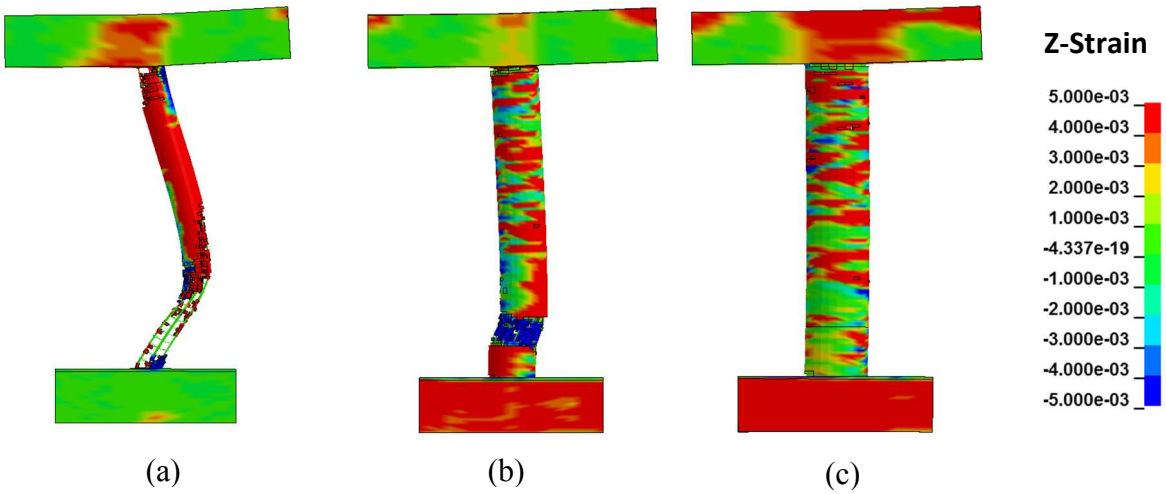

Figure 20 *Plastic strain in Z-direction post 80 kph impact of (a) 600 mm, (b) 900 mm and (c) 1200 mm diameter pier*

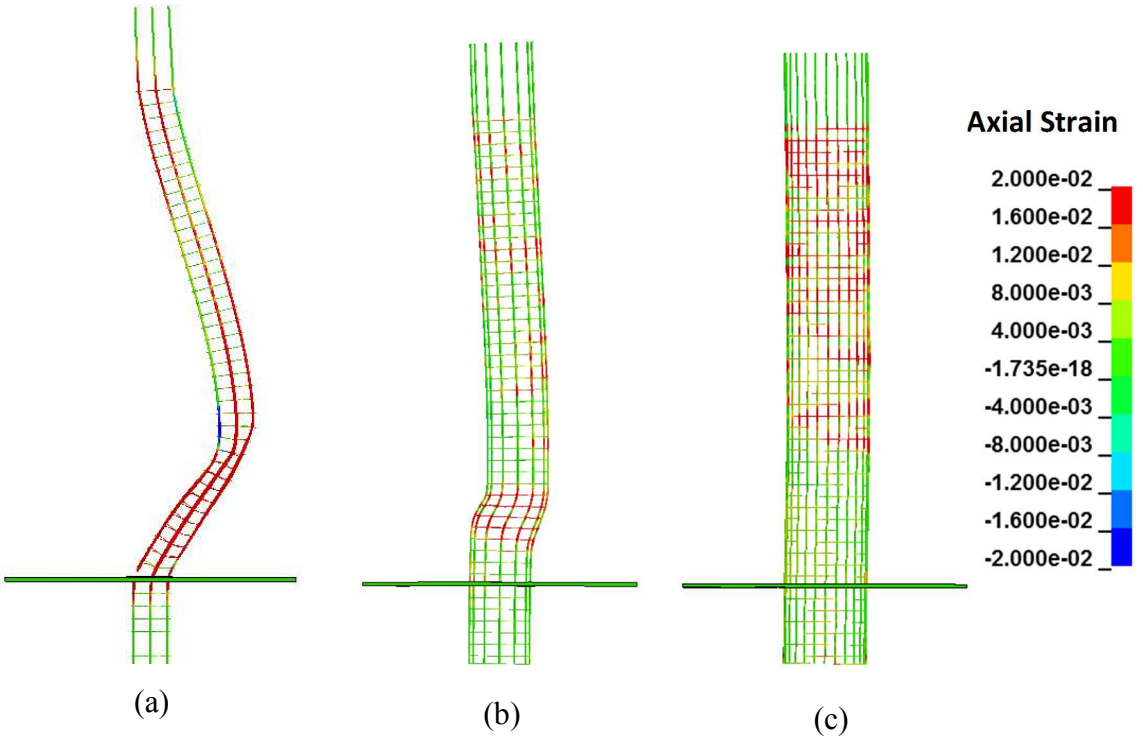

Figure 21*. Axial strain of steel reinforcement for the (a) 600, (b) 900, and (c) 1200 mm pier with a hoop spacing of 50 mm at an impact velocity of 80 kph*

www.manaraa.com

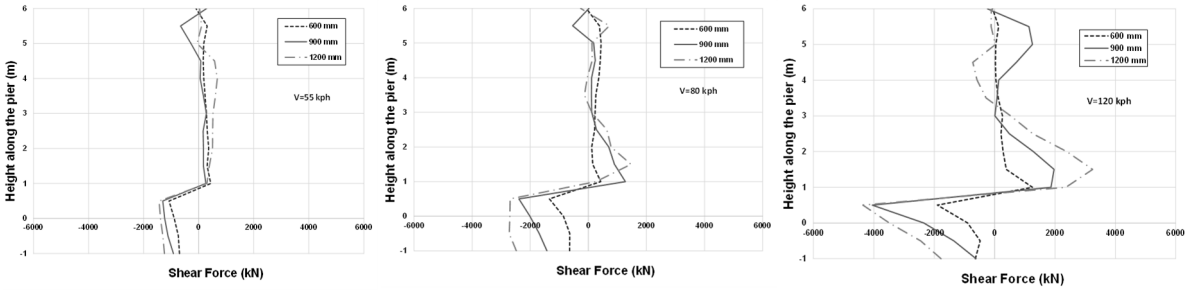

(a) (b) (c)

Figure 22. *Max shear forces along the length of the pier at impact velocities of (a) 55 (b) 80 and (c) 120 kph*

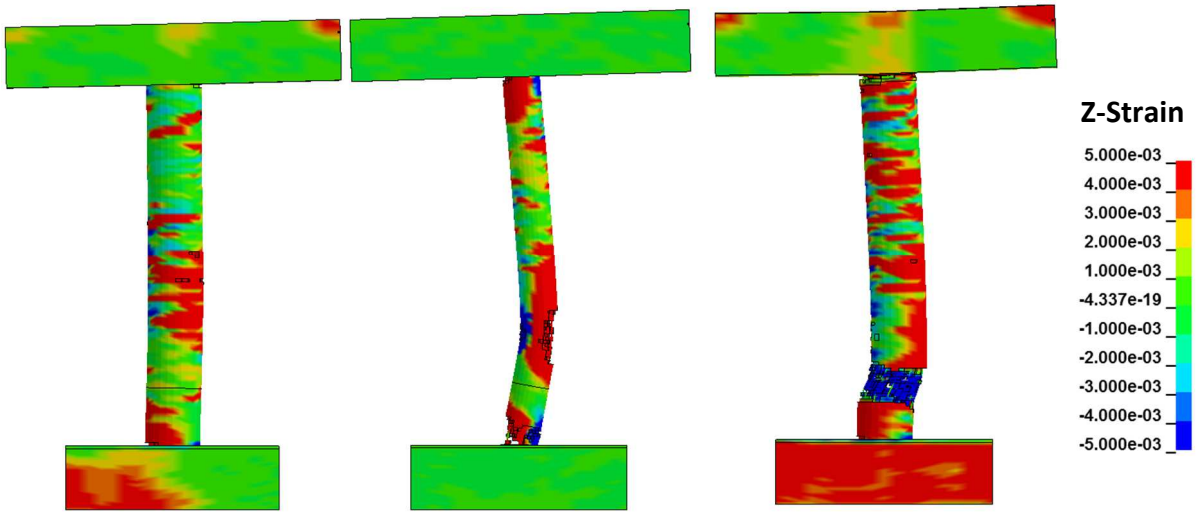

(a) (b) (c)

Figure 23. *Piers representing damage states of (a) minor damage, (b) moderate damage, and (c) severe damage*

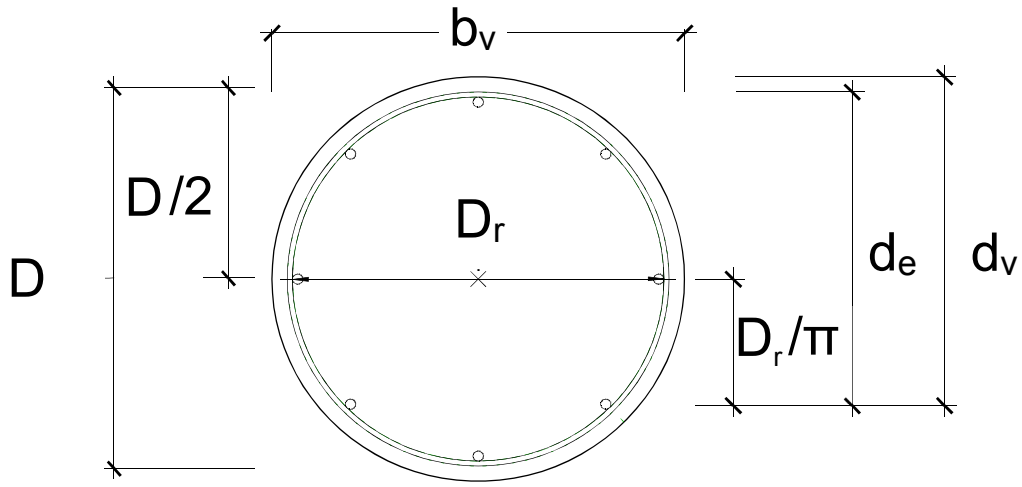

Figure 24. *Design section for circular piers (AASHTO 2012)*

www.manaraa.com

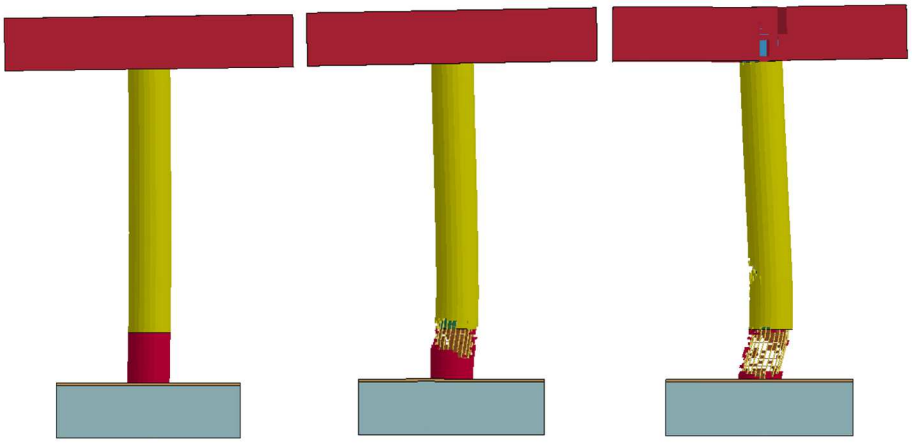

Figure 25. *Final damage states for the 800 mm pier at impact velocities of (a) 55, (b) 80, and (c) 120 kph*

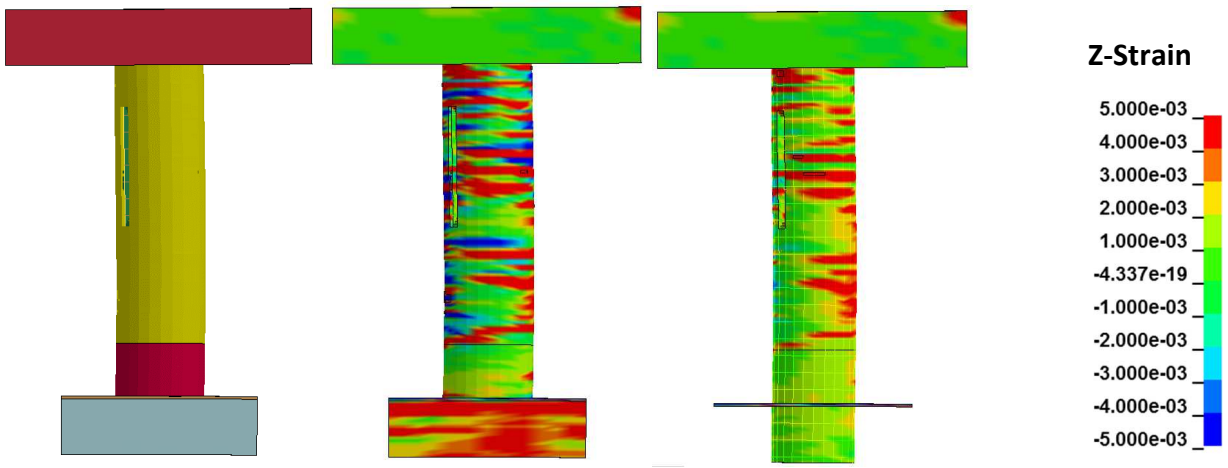

Figure 26. *Final damage state for the 1500 mm pier showing the strain contours of the (a) entire pier, and (b) the pier core*

www.manaraa.com

References

1. AASHTO, *AASHTO LRFD Bridge Design Specifications,* Sixth Edition, American Association of State Highway and Transportation Officials, Washington, D.C., 2012.

2. Agrawal, A. K., and Chen, C. (2008). "Bridge Vehicle Impact Assessment." Project #C-07-10, University Transportation Research Consortium, New York Department of Transportation.

3. Agrawal, A. K., Liu, G., and Alampalli, S. (2013) "Effects of Truck Impacts on Bridge Piers." *Advanced Materials Research*, 639-640, pp. 13-25.

4. API (2005). "Recommended Practice for Planning, Designing and Constructing Fixed Offshore Platforms – Working Stress Design." American Petroleum Institute, 70-71

5. ASCE. (2013). "Report Card for America's Infrastructure." American Society of Civil Engineers. <http:// http://www.infrastructurereportcard.org/executive-summary> (June 6, 2015)

6. American Society of Civil Engineers. (2007). *Seismic rehabilitation of existing buildings* (Vol. 41, No. 6). ASCE Publications.

7. Asprone, D., Cadoni, E., and Prota, A. (2009) "Experimental analysis on tensile dynamic behavior of existing concrete under high strain rates." *ACI Structural Journal,* 106.1, pp. 106-113.

8. Asprone, D., Cadoni E., and Prota A. (2009) "Tensile high strain-rate behavior of reinforcing steel from an existing bridge." *ACI Structural Journal,* 106.4, pp. 523-529

9. Tabiei, A., "Contact in LSDYNA", course notes." (2014)

10. Bala, S., & Day, J. (2012). General Guidelines for Crash Analysis in LS-DYNA.*Livermore Software Technology Corporation*.

11. Buth, E., Brackin, M. S., Williams, W. F., and Fry, G. T. (2010). "Analysis of Large Truck Collisions with Bridge Piers: Phase 1, Report of Guidelines for Designing Bridge Piers and Abutments for Vehicle Collisions." Texas Transportation Institute, Texas A & M University System, College Station, Texas.

12. Buth, E., Brackin, M. S., Williams, W. F., and Fry, G. T. (2011). "Collision Loads on Bridge Piers: Phase 2. Report of Guidelines for Designing Bridge Piers and Abutments for Vehicle Collisions." Texas Transportation Institute, Texas A & M University System, College Station, Texas.

www.manaraa.com

13. Caltrans. (2013). Seismic Design Criteria, Version 1.7. Caltrans, Sacramento, CA

14. Comité Euro-International du Béton, "Concrete Structures under Impact and Impulsive Loading", CEB Bulletin 187, Lausanne, Switzerland, August 1988.

15. Cook, W. (2014). Bridge Failure Rates, Consequences, and Predictive Trends. Chopra, A. (2011). "Dynamics of Structures: Theory and Application to Earthquake Engineering." 4th ed. Prentice Hall, Boston, MA

16. El-Tawil, S., Severino, E., and Fonseca, P. (2005). "Vehicle Collision with Bridge Piers." *Journal of Bridge Engineering,* 10(3), 345-353.

17. EN, B. (1991). 1-1: 2002 Eurocode 1: Actions on structures—General actions—Densities, self-weight, imposed loads for buildings BS EN 1991-1-3: 2003.*Eurocode 1: Actions on structures—General actions—Snow loads*.

18. EN, B. (1991). 1-7: 2006: Eurocode 1: Actions on Structures: Part 1-7: General actions-Accidental actions. *British Standards Institution, London*.

19. Fujikake, K., Li, B., and Soeun, S. (2009). "Impact Response of Reinforced Concrete Beam and Its Analytical Evaluation." *Journal of Structural Engineering*, 135(8), 938–950.

20. Furtado, M. N., and A. Alipour. (2014) "Estimation of direct and indirect losses in transportation networks due to seismic events." *Transportation Research Board 93 rd Annual Meeting, Washington, DC*.

21. Gallegos, D., and McPhee, M. *Two Truckers Die in Fiery I-70 Crash*. The Denver Post, 15 August 2007. Web. 8 November 2013. < www.denverpost.com/ci_6628365>

22. Gomez, N. L., Alipour, A. (2014). "Study of Circular Reinforced Concrete Bridge Piers Subjected to Vehicular Collisions." *Structures Congress 2014*, 577-587
.

23. Gomez, N. L., AuYeung S. J., and Alipour, A. (2015) "Performance Assessment of Bridges with Different Bent Configurations under Vehicle Collision." *Transportation Research Board 94th Annual Meeting*. No. 15-5581.

24. Hallquist, J. O. (2006). LS-DYNA theory manual. *Livermore software Technology corporation*, *3*.

25. Hallquist, J. O. (2007). LS-DYNA keyword user's manual. *Livermore Software Technology Corporation*, *970*.

www.manaraa.com

26. Harik, I. E., Shaaban, A. M., Gesund, H., Valli, G. Y. S., and Wang, S. T. (1990). "United States Bridge Failures, 1951–1988." *Journal of Performance of Constructed Facilities,* 4(4), 272-277.

27. Kudelka, B. (2011). "SCDOT Crews Respond After Fiery Crash Shuts Down I-85." *The Connector*, 2(14).

28. Malvar, L. J., & Crawford, J. E. (1998). *Dynamic increase factors for concrete*. NAVAL FACILITIES ENGINEERING SERVICE CENTER PORT HUENEME CA. Malvar, L. J., and Crawford, J. E. (1998). "Dynamic Increase Factors for Steel Reinforcing Bars." Ft. Belvoir: Defense Technical Information Center.

29. Mander, J., Priestley, M., and Park, R. (1988). "Theoretical Stress-Strain Model for Confined Concrete." *Journal of Structural Engineering*, 114(8), 1804-1826.

30. Mohammed, T. (2011). "Reinforced Concrete Structural Members Under Impact Loading." Doctoral dissertation. University of Toledo, Toledo, OH.

31. Murray, Y. D. (2007). "Users manual for LS-DYNA Concrete Material Model 159." *Report No. FHWA-HRT-05-062*. USA: Federal Highway Administration, US Department of Transportation; 2007.

32. Ross Jr, H. E., Sicking, D. L., Zimmer, R. A., & Michie, J. D. (1993).*Recommended procedures for the safety performance evaluation of highway features* (No. 350). Saatci, S., & Vecchio, F. J. (2009). Effects of shear mechanisms on impact behavior of reinforced concrete beams. *ACI structural Journal*, *106*(1), 78-86.

33. Sha, Y., & Hao, H. (2013). Laboratory tests and numerical simulations of barge impact on circular reinforced concrete piers. *Engineering structures*, *46*, 593-605.

34. Sharma, H., Hurlebaus, S., & Gardoni, P. (2012). Performance-based response evaluation of reinforced concrete columns subject to vehicle impact.*International Journal of Impact Engineering*, *43*, 52-62.

35. Smoke, G. (2012). "SC-150 Bridge Replacement After Damage." *2012 South Carolina Highway Engineers Conference*. Columbia Metropolitan Convention Center, Columbia, SC.

36. Tsang, H. H., & Lam, N. T. (2008). Collapse of reinforced concrete column by vehicle impact. *Computer-Aided Civil and Infrastructure Engineering*, *23*(6), 427-436.

www.manaraa.com

37. Vega, C. *Race to Repair Damaged I-30 Overpass*. WFAA, 11 June 2012. WFAA. Web. 23 October 2013. http://www.wfaa.com/news/local/Truck-hits-overpass-on-I-30-in-Dallas-158372365.html

38. Wardhana, K., & Hadipriono, F. C. (2003). Analysis of recent bridge failures in the United States. *Journal of Performance of Constructed Facilities*, *17*(3), 144-150.

www.manaraa.com

CHAPTER IV SUMMARY AND CONCLUSIONS

Summary

Inadvertent collisions of vehicles with bridge piers can lead to extensive damage to the structural members of the bridge and could lead to total collapse. The aftermath of this extreme loading event has a major effect on the surrounding communities and business's by disrupting traffic flow due to the repairs needed. Past work has shown that a bridge pier subjected to a vehicle collision behaves differently when compared to being loaded by a static point load recommended by AASHTO (2012). The finite element software LS-DYNA was used to conduct the analyses in this study. The preceding report outlines different methods of validating and developing finite element models that simulate vehicle collisions with bridge piers.

It was shown in Chapter II that LS-DYNA could accurately model the impact behavior of RC members using certain finite element controls and material models. Material model 159 and 24 could capture the behavior of concrete and steel reinforcement when applied under dynamic loads. The automatic surface to surface contact algorithm could adequately model the contact between two impacting segments. Stiffness based hourglass controls were proven to suppress hourglass deformations within the elements while not over stiffening the entire model. The analyses also revealed that longitudinal reinforcement controls the degree of local failure experienced within a RC beam while the transverse reinforcement is mainly used to prevent localized severe shear cracks and punching shear failure.

Chapter III reveals that the vehicle models obtained from the NCAC can efficiently simulate vehicle collisions with the bridge pier models developed, all while providing reliable results. From the sensitivity analyses, it was concluded that the addition of a superstructure to the finite element model did noticeably affect the impact behavior with respect to internal shear,

www.manaraa.com

moment and displacements as opposed to the original model that did not have a superstructure. Also, the impact response of the pier within a single and double bent system did show some noticeable differences in the impact response at a low velocity of 55 kph. The behavior between the two models however did quickly converge as the impact velocity increased to 80 and 120 kph. The kinetic energy of the vehicle was the governing factor for the shear demand imposed on the pier. Pier diameter governed the overall mode of failure whether it be shear, flexure or a combination of the two. Transverse reinforcement controlled the amount of local damage the pier experienced due to confinement effects. A novel damage ratio index that related the kinetic energy of the colliding vehicle, the pier geometry (diameter), and the pier structural characteristics (dynamic shear capacity) was proposed. The different levels of the damage ratio were shown to correlate with different damage states (minor, moderate, and severe). The performance-based design philosophy which is shown to be an effective method for seismic designed structures was adopted to design the bridges for three performance levels. The proposed approach will no longer neglect the effects of vehicles with different colliding speeds or the capacity of the collided piers in the design of bridge piers under collision loads. It provides a feasible, yet more accurate approach for the bridge designers to tailor their design for the specific conditions that each bridge will be exposed to considering all the economic and societal impacts of bridge failure in their design.

Conclusion

The preceding report has established that LS-DYNA was able to provide accurate and reliable results in impact simulations. A promising performance based design method for bridge piers subjected to vehicle collisions has been proposed that eliminates the need for finite element analyses. Implementation of the proposed performance based design approach would give

www.manaraa.com

engineers the ability to design bridge piers to withstand a certain amount of damage based on expected colliding vehicle mass, velocity, dynamic shear capacity, and pier diameter. This would result in more economical and safer designs. Future work would involve additional testing that includes an even larger variety of pier designs as well as include analyses regarding the superstructure and foundation damage states.

www.manaraa.com